Supplementary Material for:

Oudemansin and 9-methoxystrobilurin derivatives with antimalarial activity from cultures of the basidiomycete *Favolaschia minutissima*: assignments of the absolute configurations of the isoprene-derived units

Somporn Palasarn[a], Thapanee Pruksatrakul[a], Wilunda Choowong[a], Natthawut Wiriyathanawudhiwong[b], Thitiya Boonpratuang[b], Panida Surawatanawong[c], Chawanee Thongpanchang[a], Masahiko Isaka[a,*]

[a] *National Center for Genetic Engineering and Biotechnology (BIOTEC), National Science and Technology Development Agency (NSTDA), 111 Thailand Science Park, Phahonyothin Road, Klong Luang, Pathumthani 12120, Thailand*

[b] *National Biobank of Thailand, National Science and Technology Development Agency (NSTDA), 111 Thailand Science Park, Phahonyothin Road, Klong Luang, Pathumthani 12120, Thailand*

[c] *Department of Chemistry and Center of Excellence for Innovation in Chemistry, Faculty of Science, Mahidol University, Bangkok 10400, Thailand*

Fig. S1 Structures of the compounds isolated from cultures of *Favolaschia minutissima* TBRC-BCC 19434.

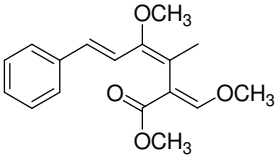

9-methoxystrobilurin A (128 mg)

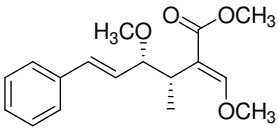

oudemansin A (**7**, 240 mg)

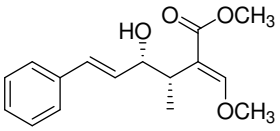

noroudemansin A (**8**, 2.0 mg)

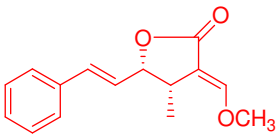

γ-lactone derivative **6** (33 mg)

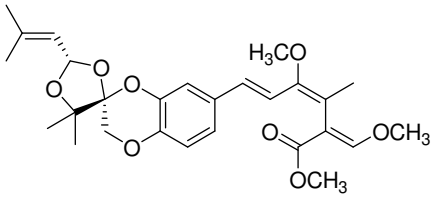

9-methoxystrobilurin E (**9**, 760 mg)

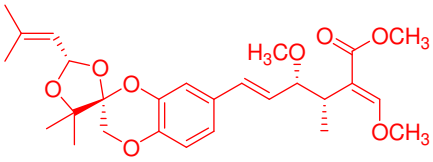

oudemansin E (**1**, 10.2 mg)

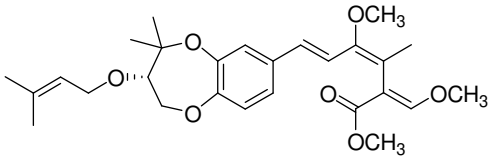

9-methoxystrobilurin G (**11**, 680 mg)

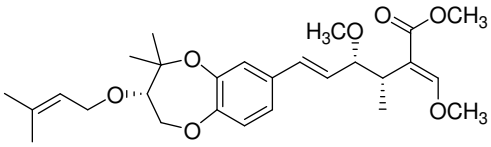

oudemansin G (82 mg)

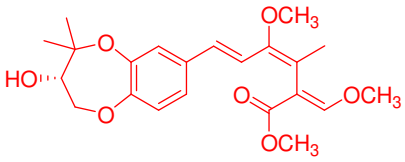

9-methoxystrobilurin I (**5**, 29 mg)

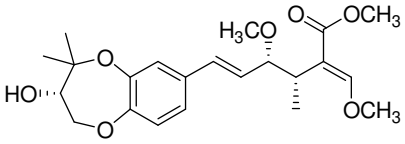

oudemansin I (**10**, 10.0 mg)

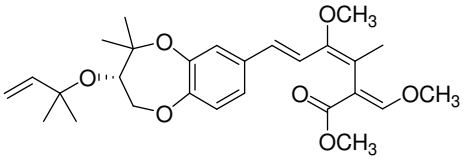

9-methoxystrobilurin K (150 mg)

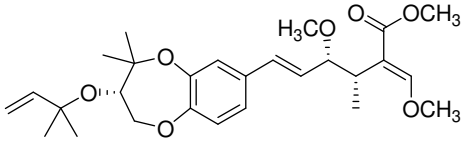

oudemansin K (10.6 mg)

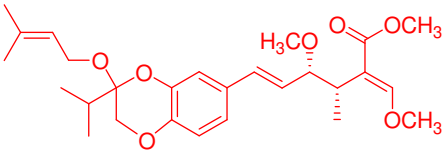

oudemansin M (**2**, 2.5 mg)

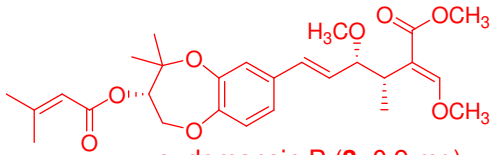

oudemansin P (**3**, 0.9 mg)

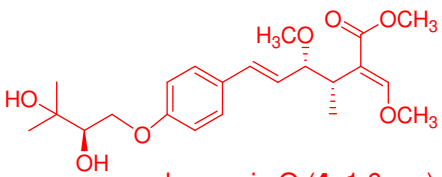

oudemansin Q (**4**, 1.6 mg)

Fig. S2 ^{1}H NMR spectrum of oudemansin E (**1**) ($CDCl_3$, 500 MHz)

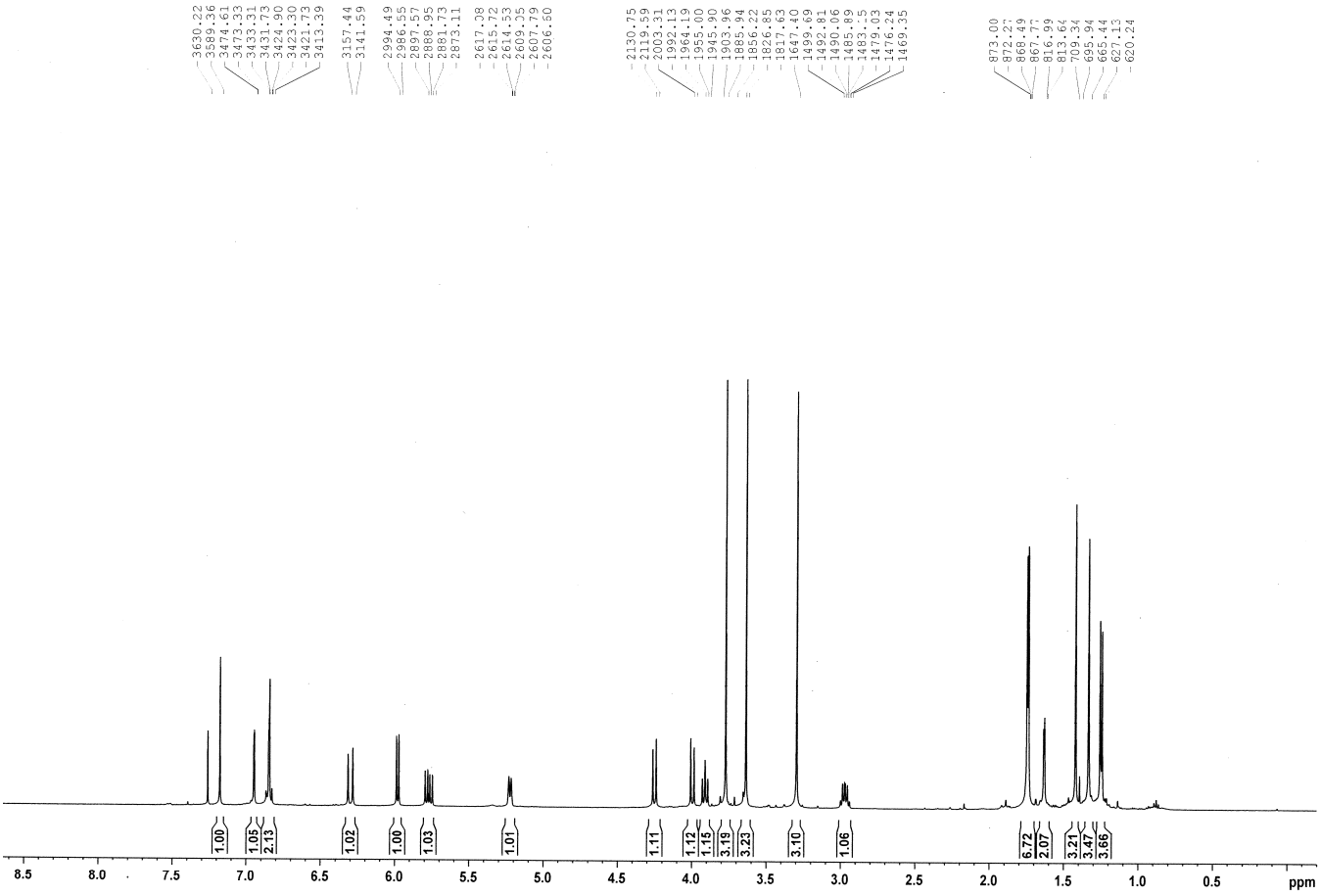

Fig. S3 ^{13}C NMR spectrum of oudemansin E (**1**) ($CDCl_3$, 125 MHz)

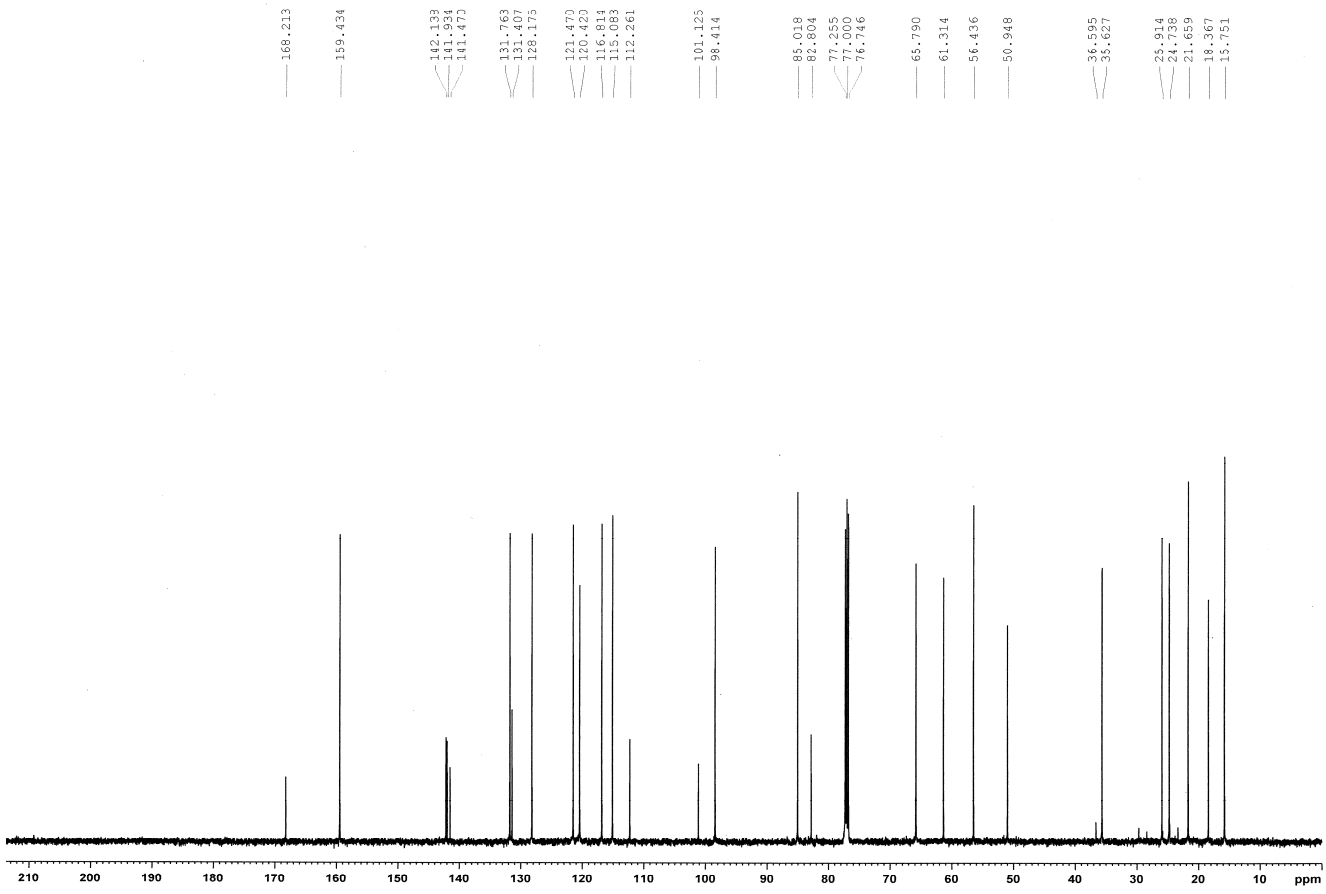

Fig. S4 DEPT-135 spectrum of oudemansin E (**1**) ($CDCl_3$, 125 MHz)

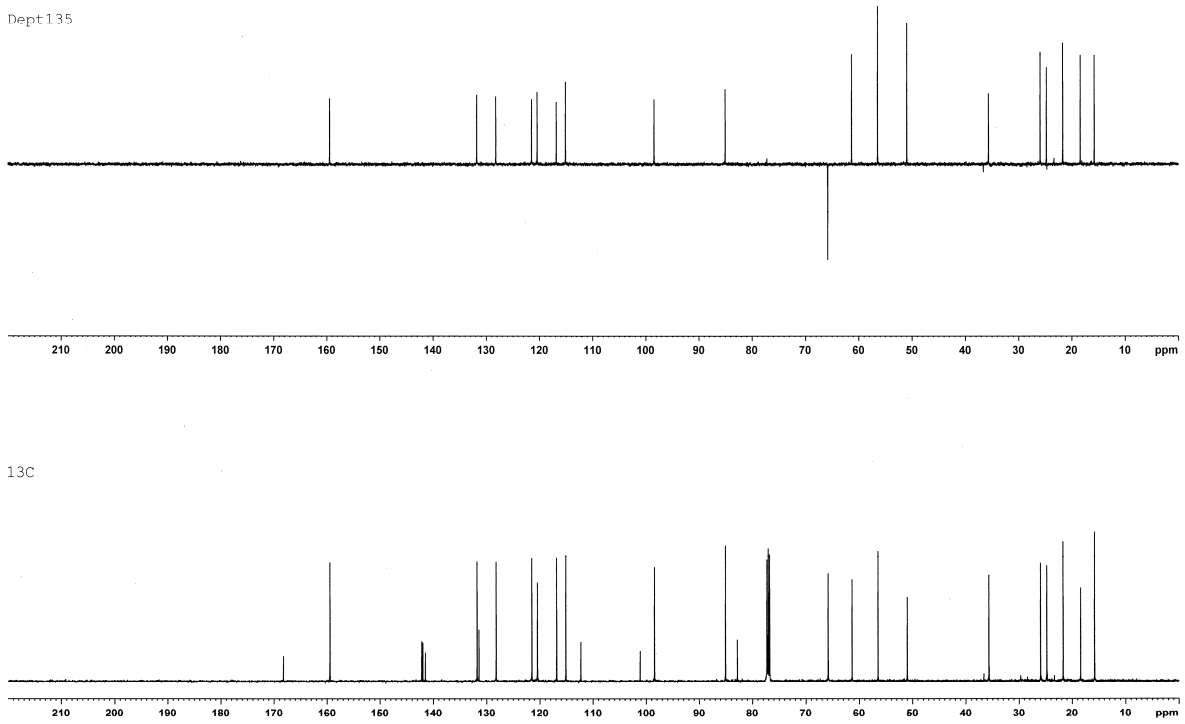

Fig. S5 COSY spectrum of oudemansin E (**1**) ($CDCl_3$, 500 MHz)

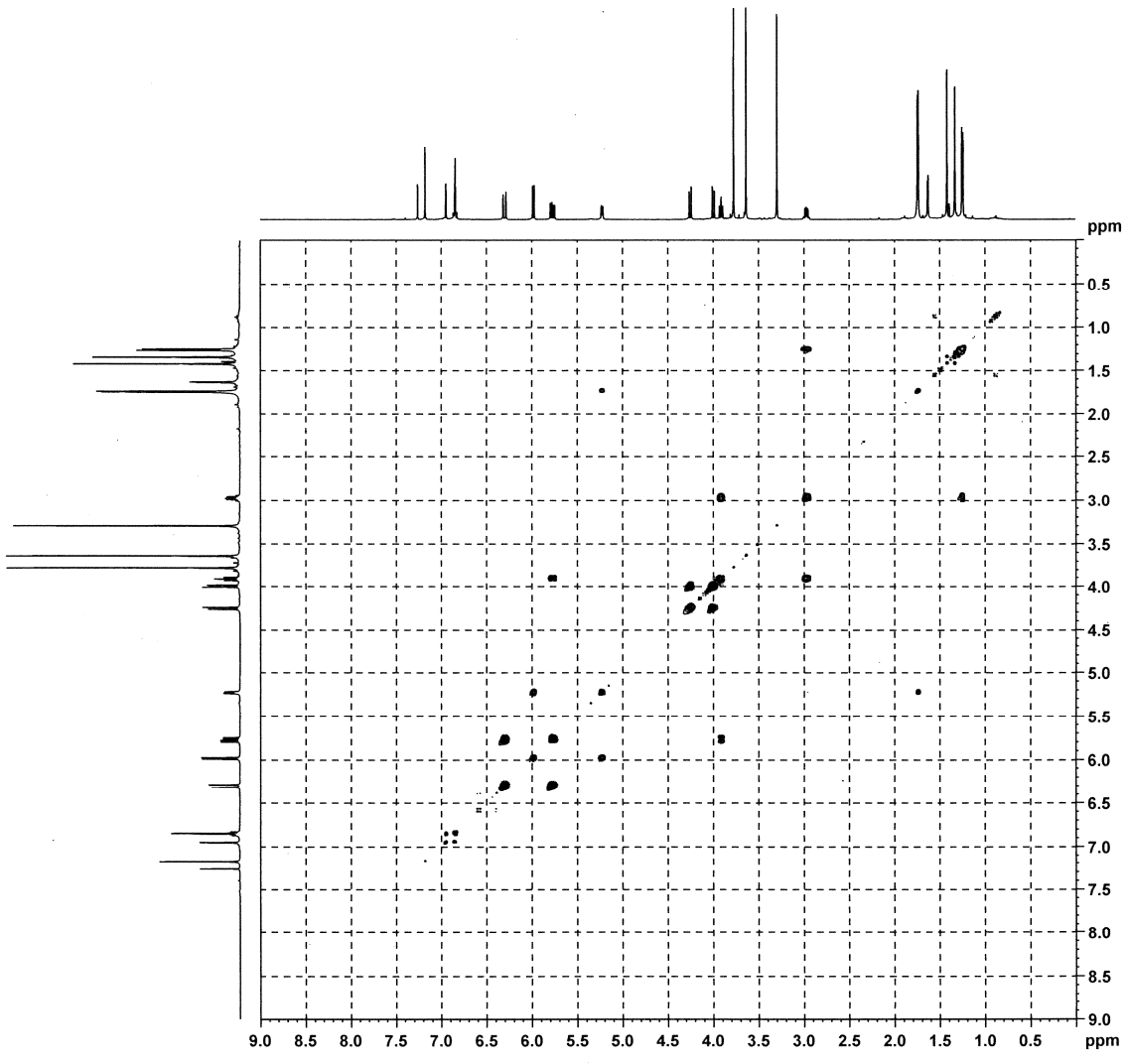

Fig. S6 HSQC spectrum of oudemansin E (**1**) ($CDCl_3$, 500 MHz)

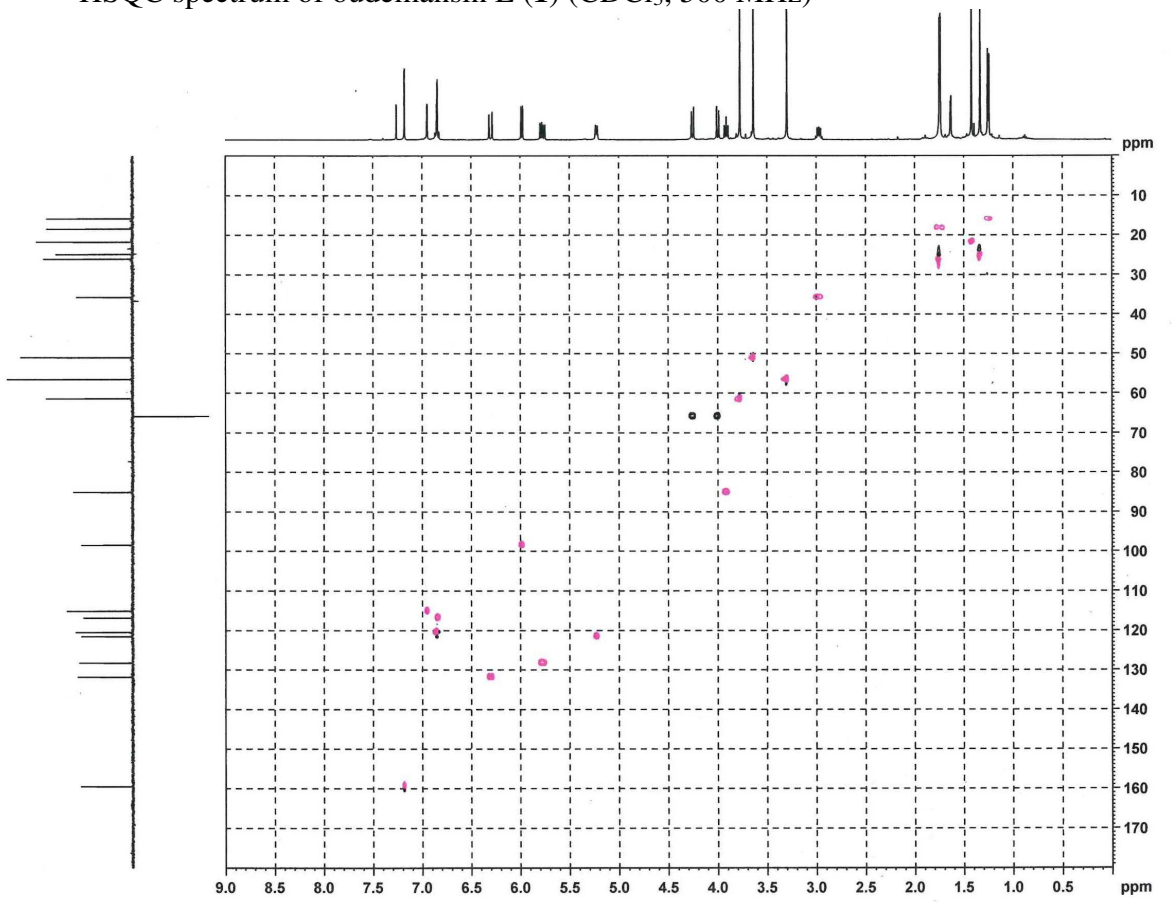

Fig. S7 HMBC spectrum of oudemansin E (**1**) ($CDCl_3$, 500 MHz)

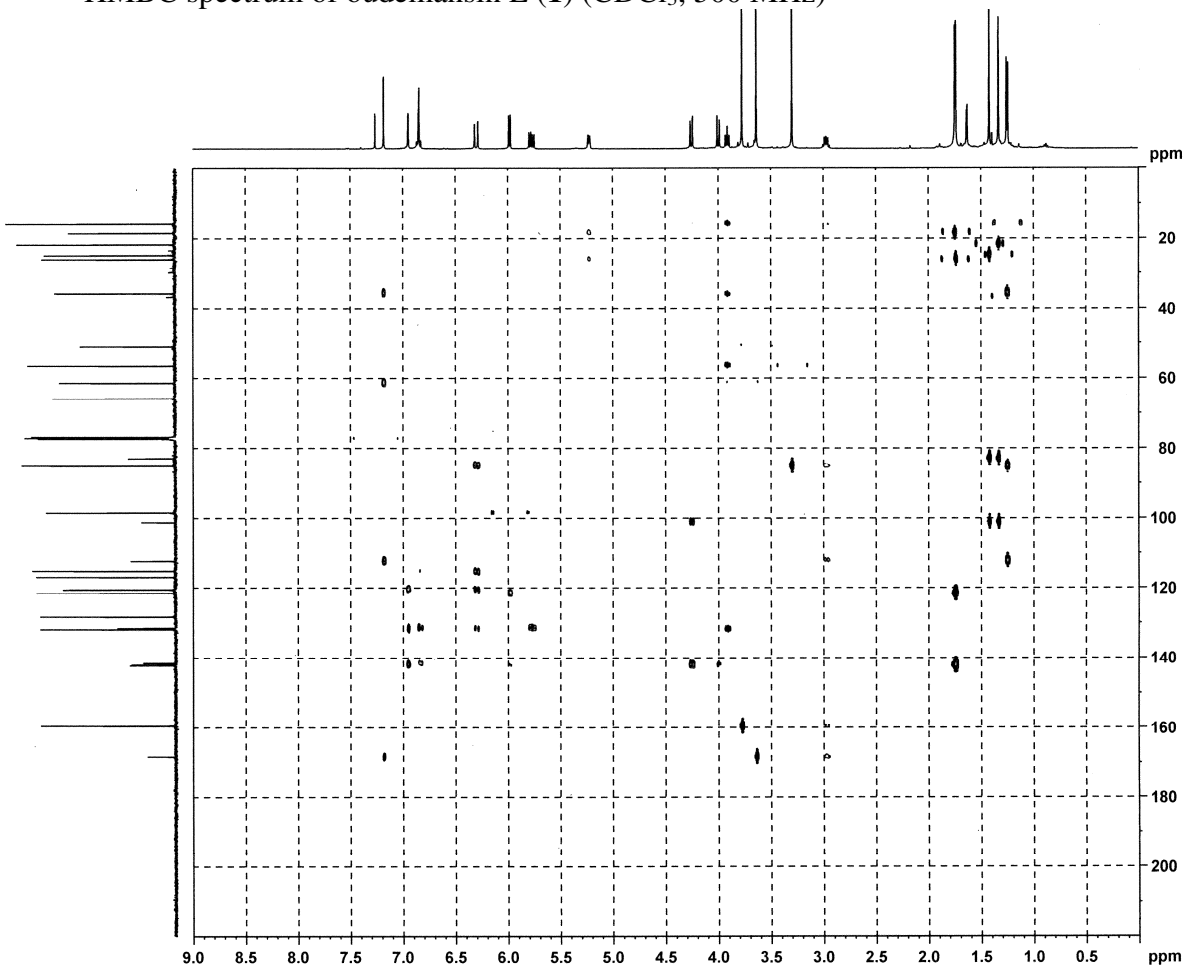

Fig. S8 NOESY spectrum of oudemansin E (**1**) ($CDCl_3$, 500 MHz)

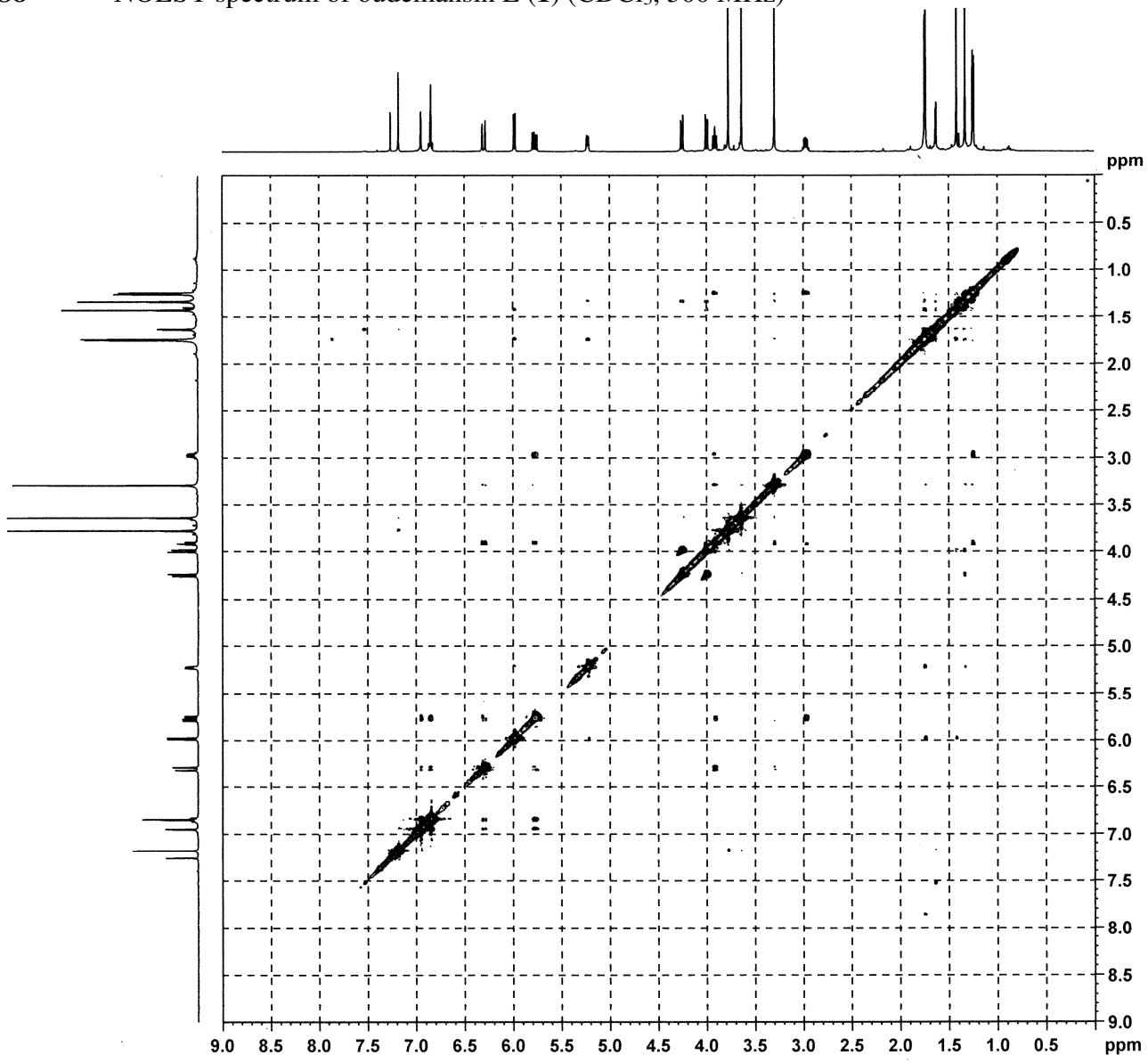

Fig. S9 HRESIMS of oudemansin E (**1**) (positive ion mode)

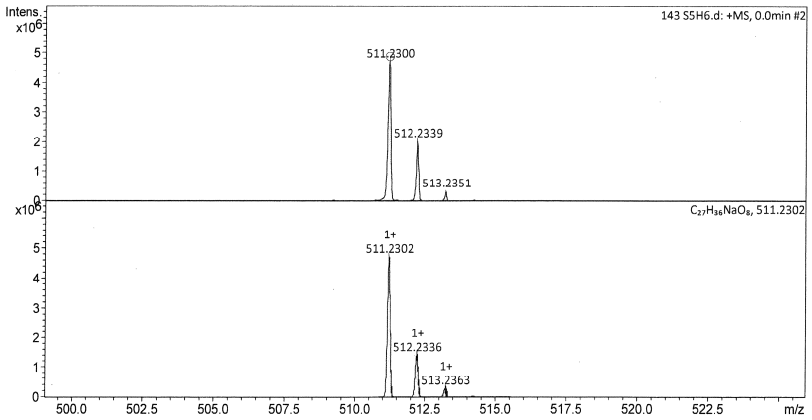

Fig. S10 ^{1}H NMR spectrum of oudemansin M (**2**) ($CDCl_3$, 400 MHz)

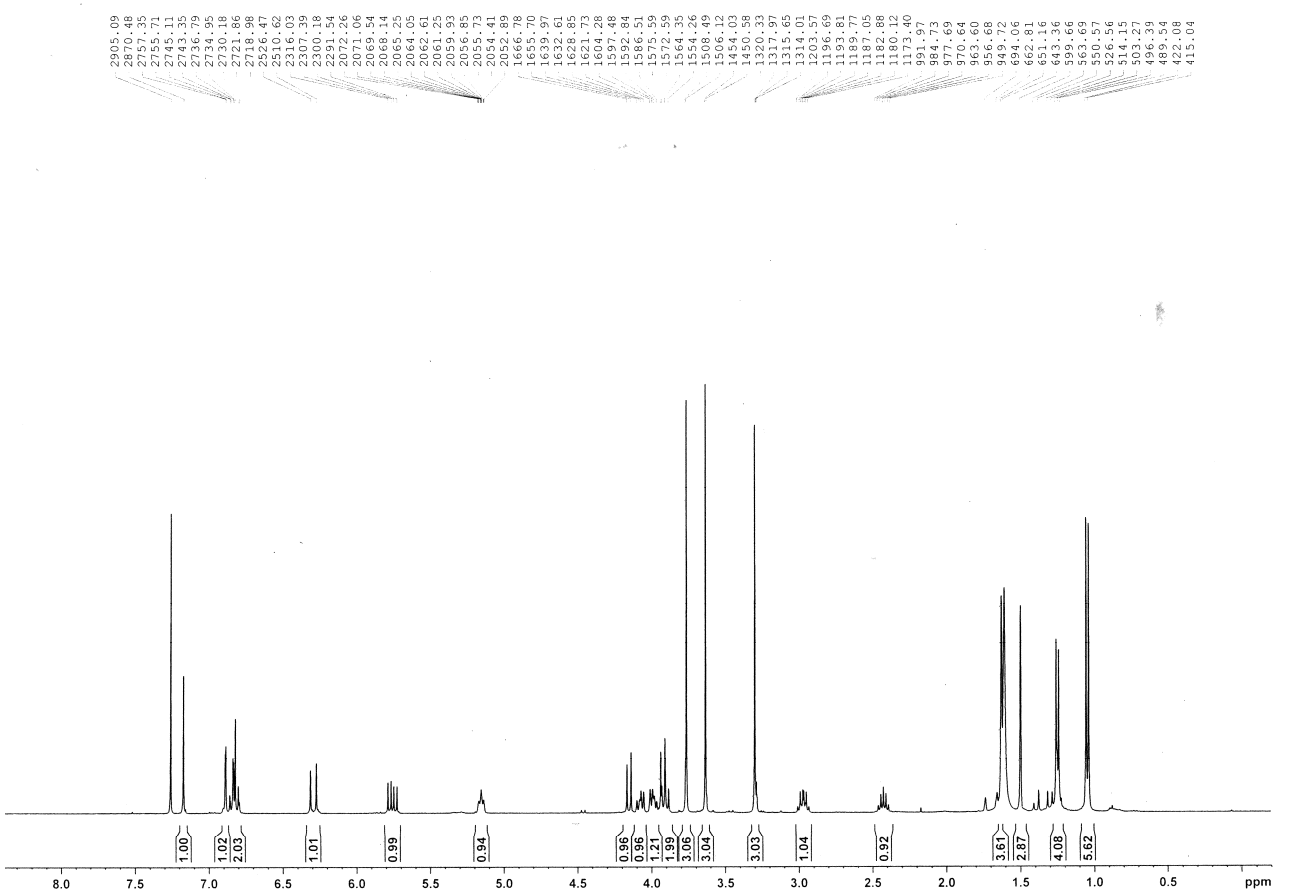

Fig. S11 ^{13}C NMR spectrum of oudemansin M (**2**) ($CDCl_3$, 100 MHz)

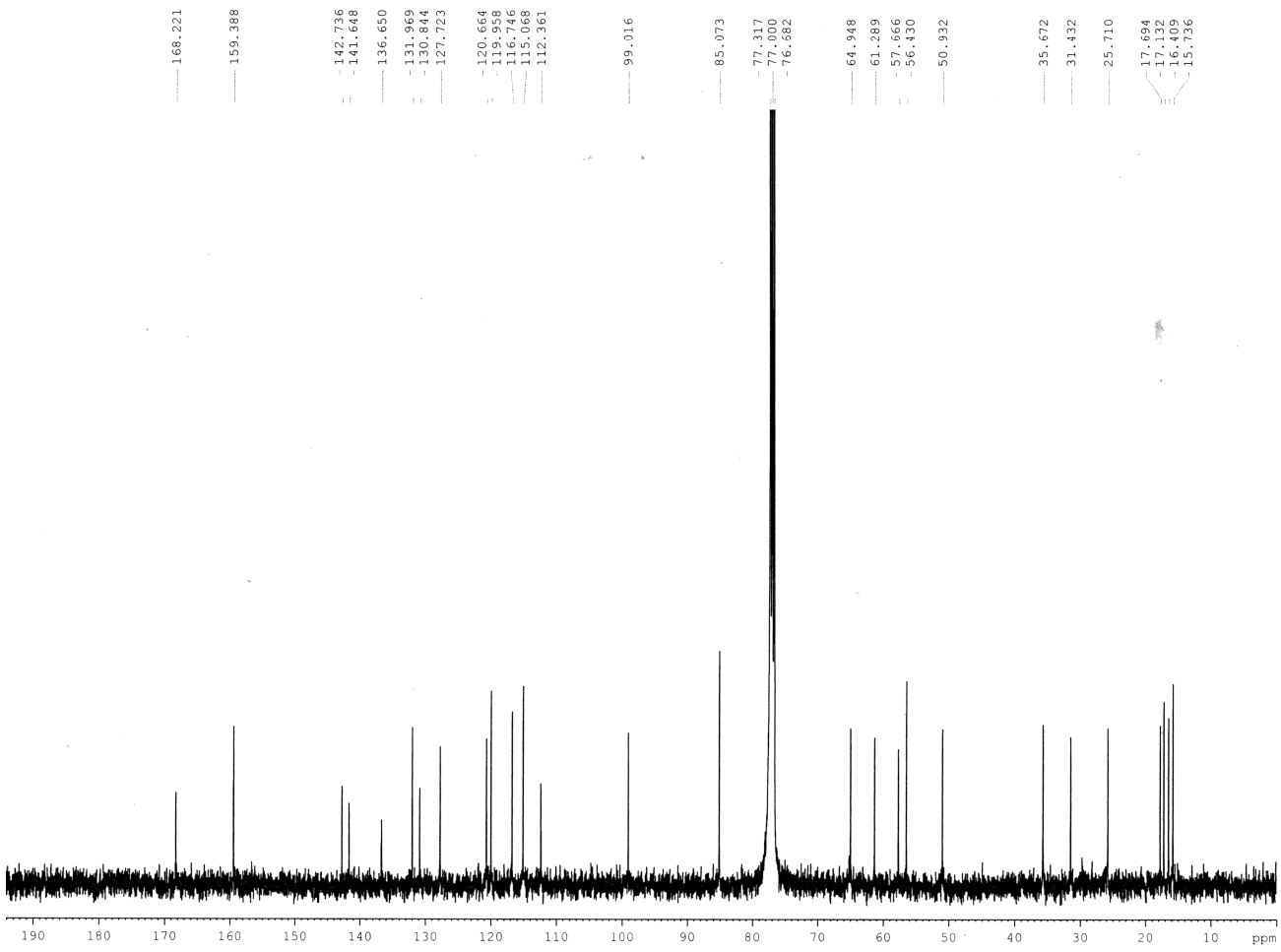

Fig. S12 DEPT-135 spectrum of oudemansin M (**2**) ($CDCl_3$, 100 MHz)

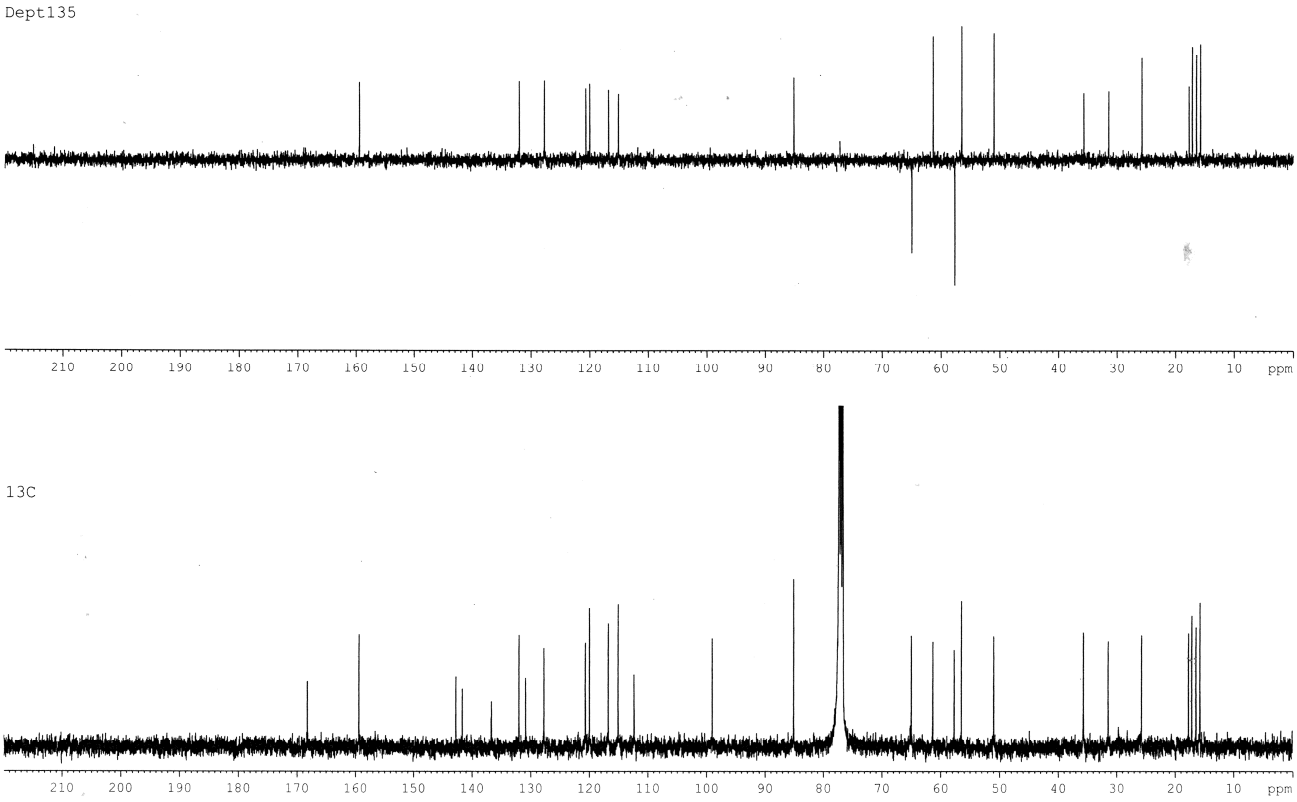

Fig. S13 COSY spectrum of oudemansin M (**2**) ($CDCl_3$, 400 MHz)

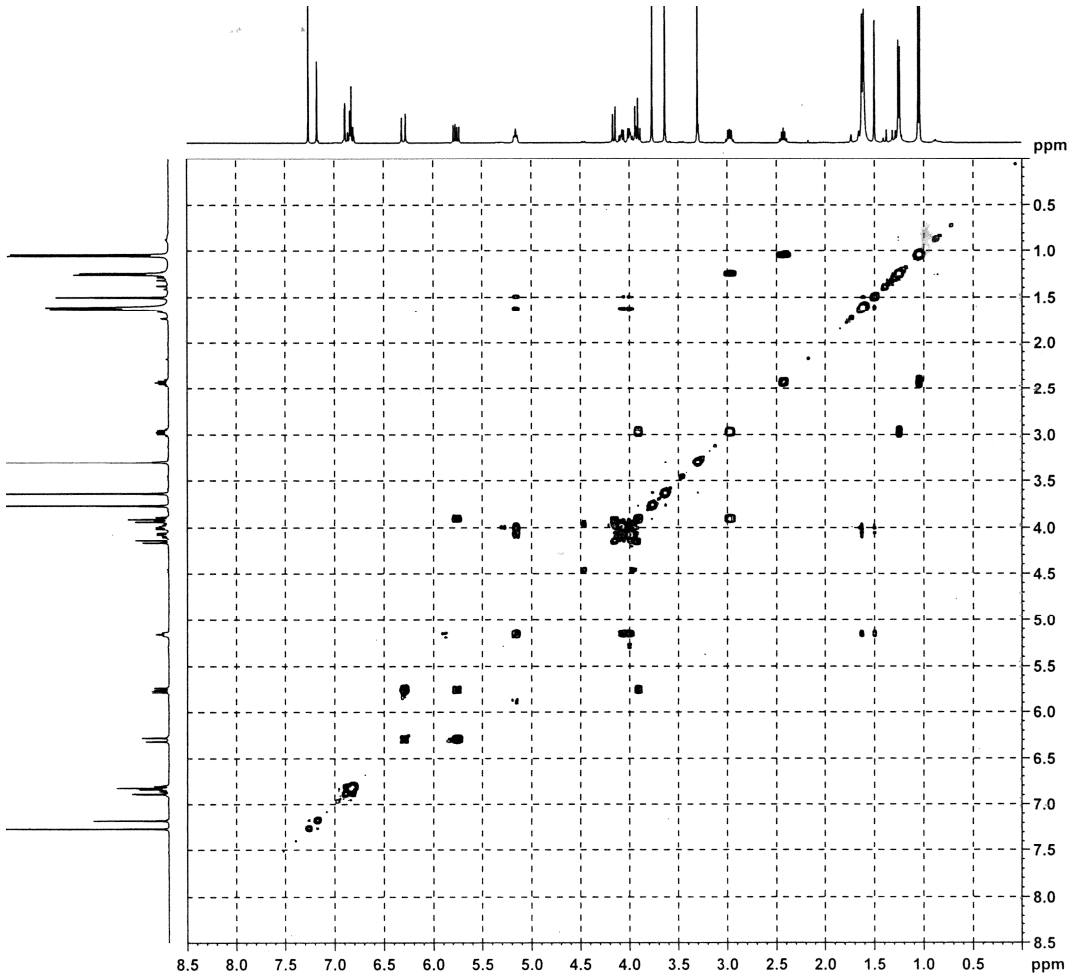

Fig. S14 HMQC spectrum of oudemansin M (**2**) ($CDCl_3$, 400 MHz)

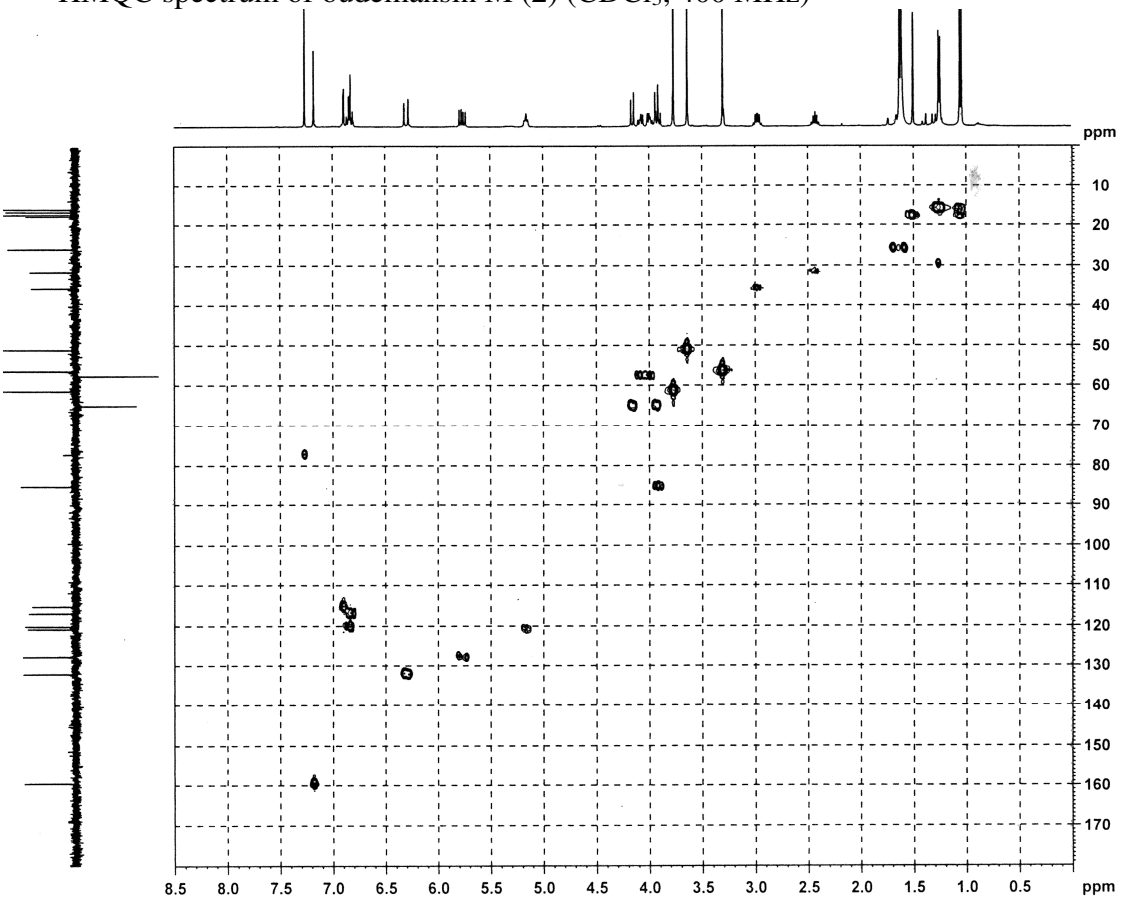

Fig. S15 HMBC spectrum of oudemansin M (**2**) ($CDCl_3$, 400 MHz)

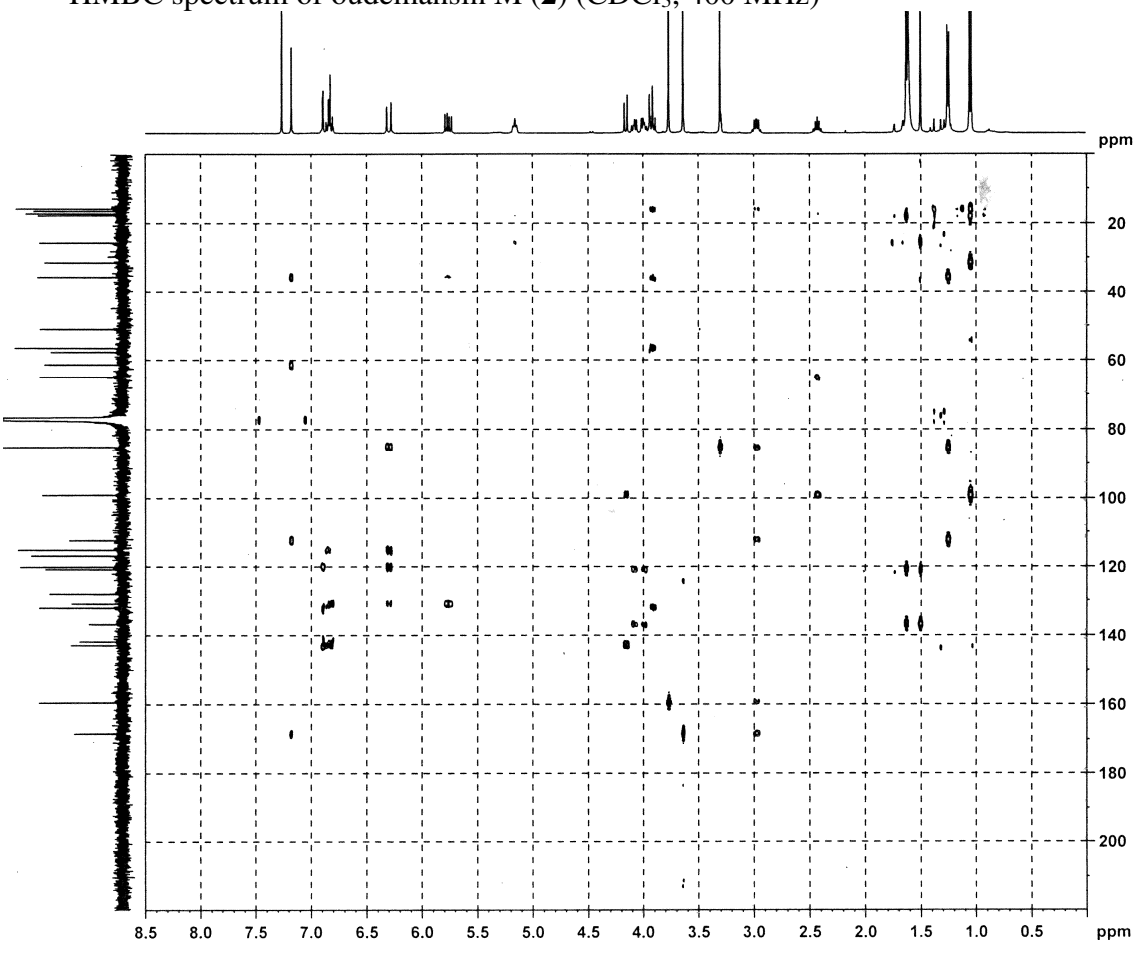

Fig. S16 NOESY spectrum of oudemansin M (**2**) ($CDCl_3$, 400 MHz)

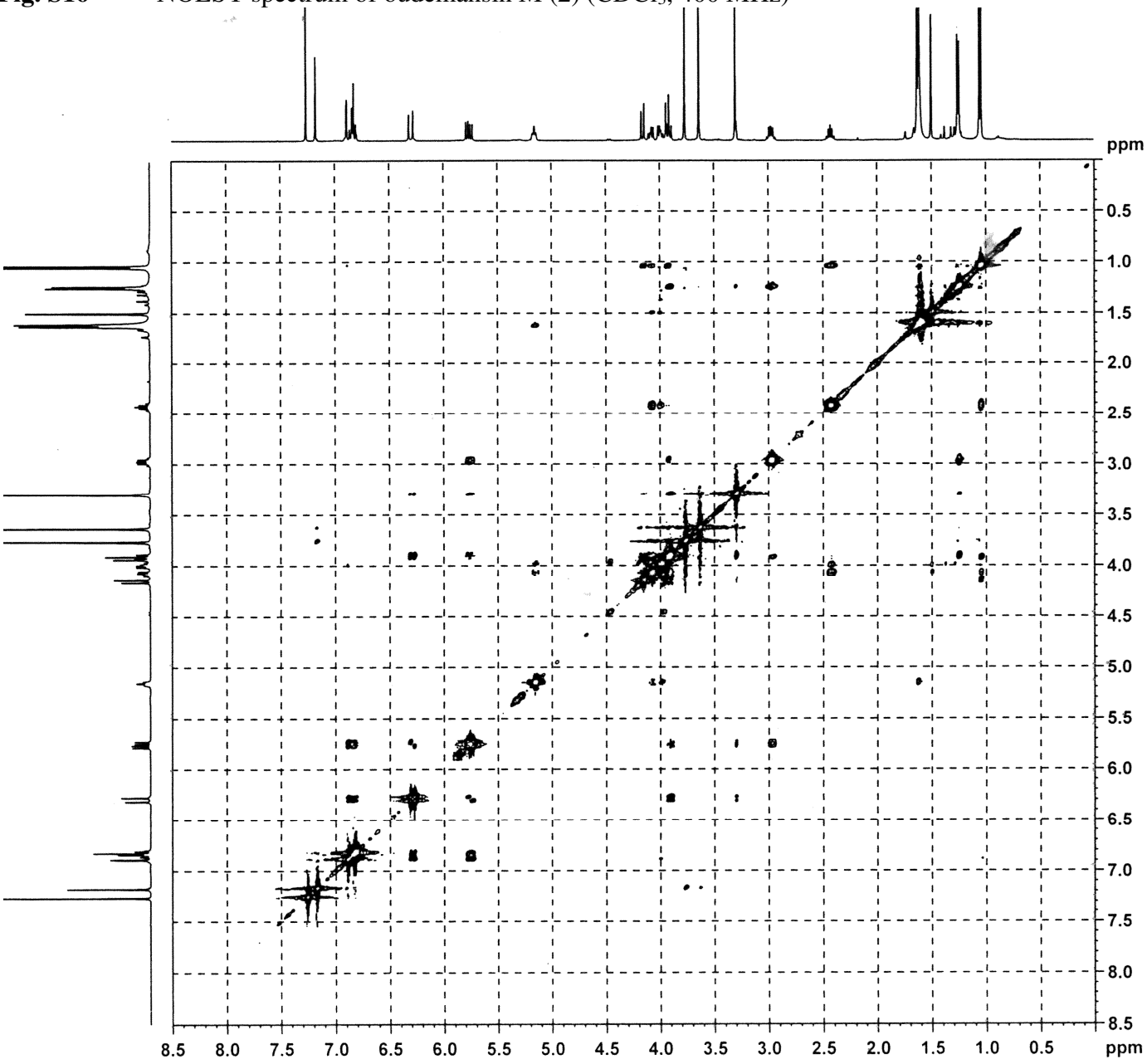

Fig. S17 HRESIMS of oudemansin M (**2**) (positive ion mode)

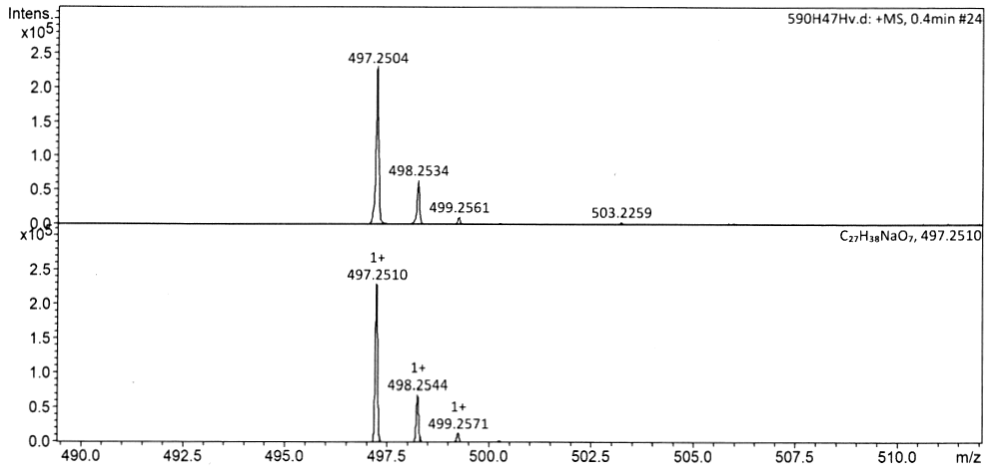

Fig. S18 ^{1}H NMR spectrum of oudemansin P (**3**) ($CDCl_3$, 400 MHz)

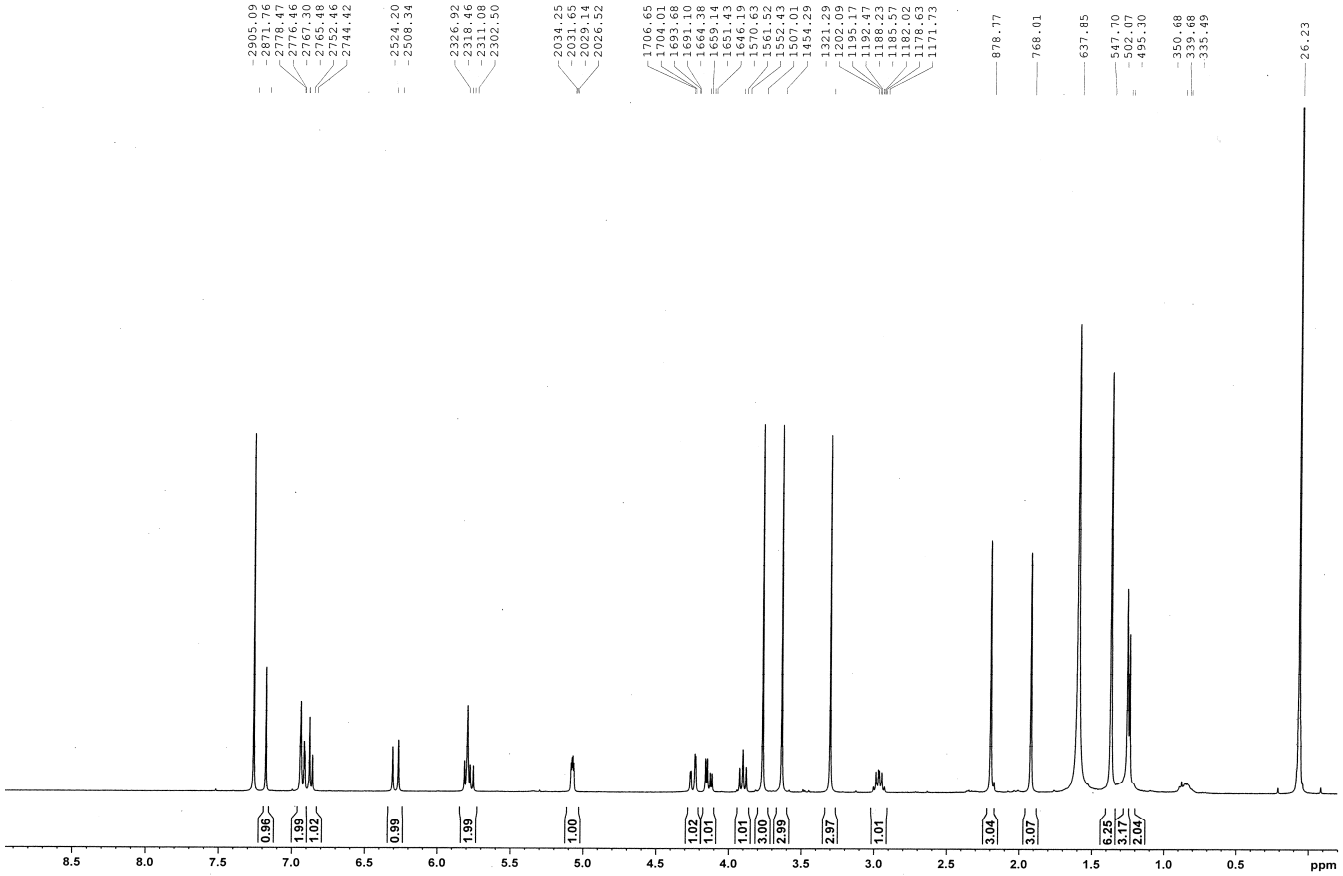

Fig. S19 ^{13}C NMR spectrum of oudemansin P (**3**) ($CDCl_3$, 100 MHz)

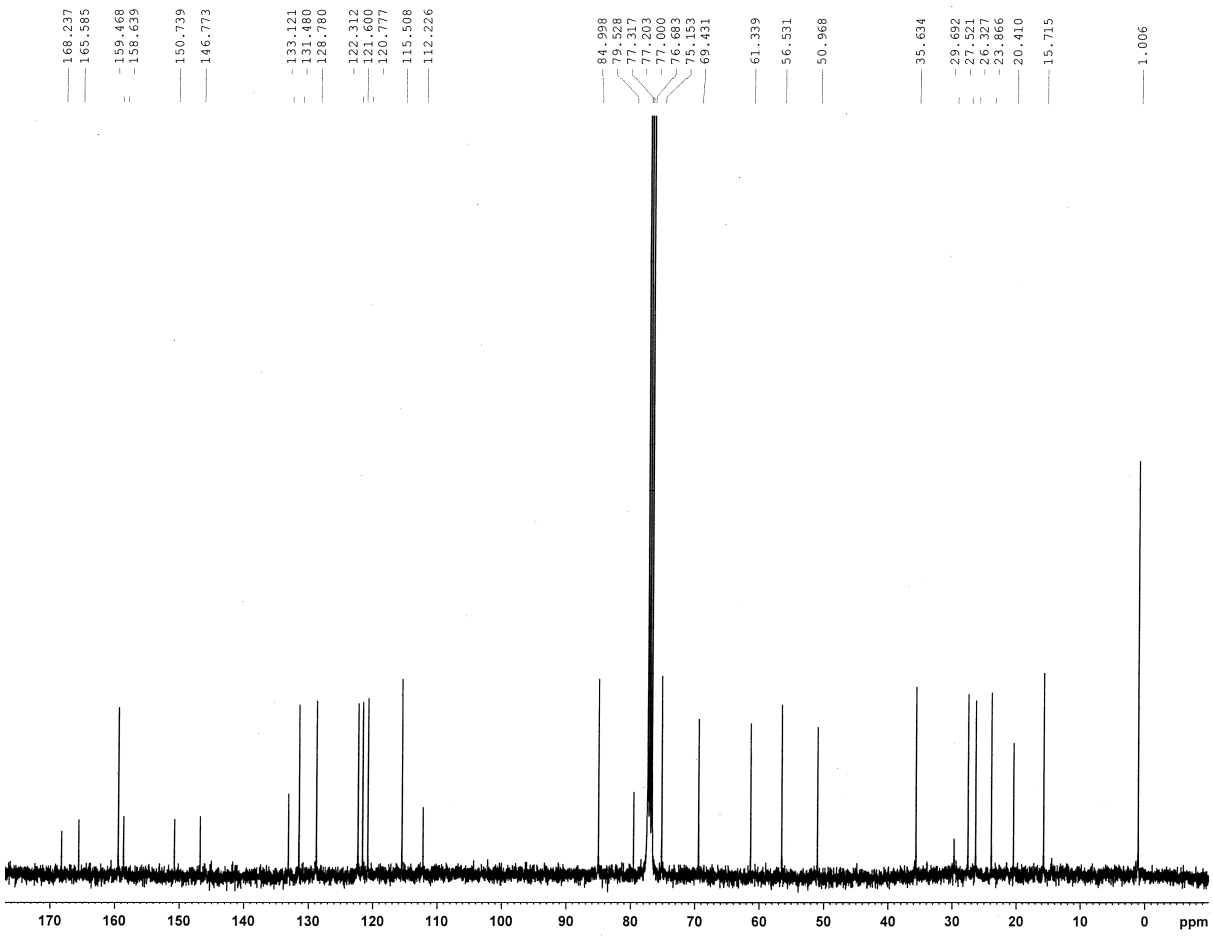

Fig. S20 DEPT-135 spectrum of oudemansin P (**3**) ($CDCl_3$, 100 MHz)

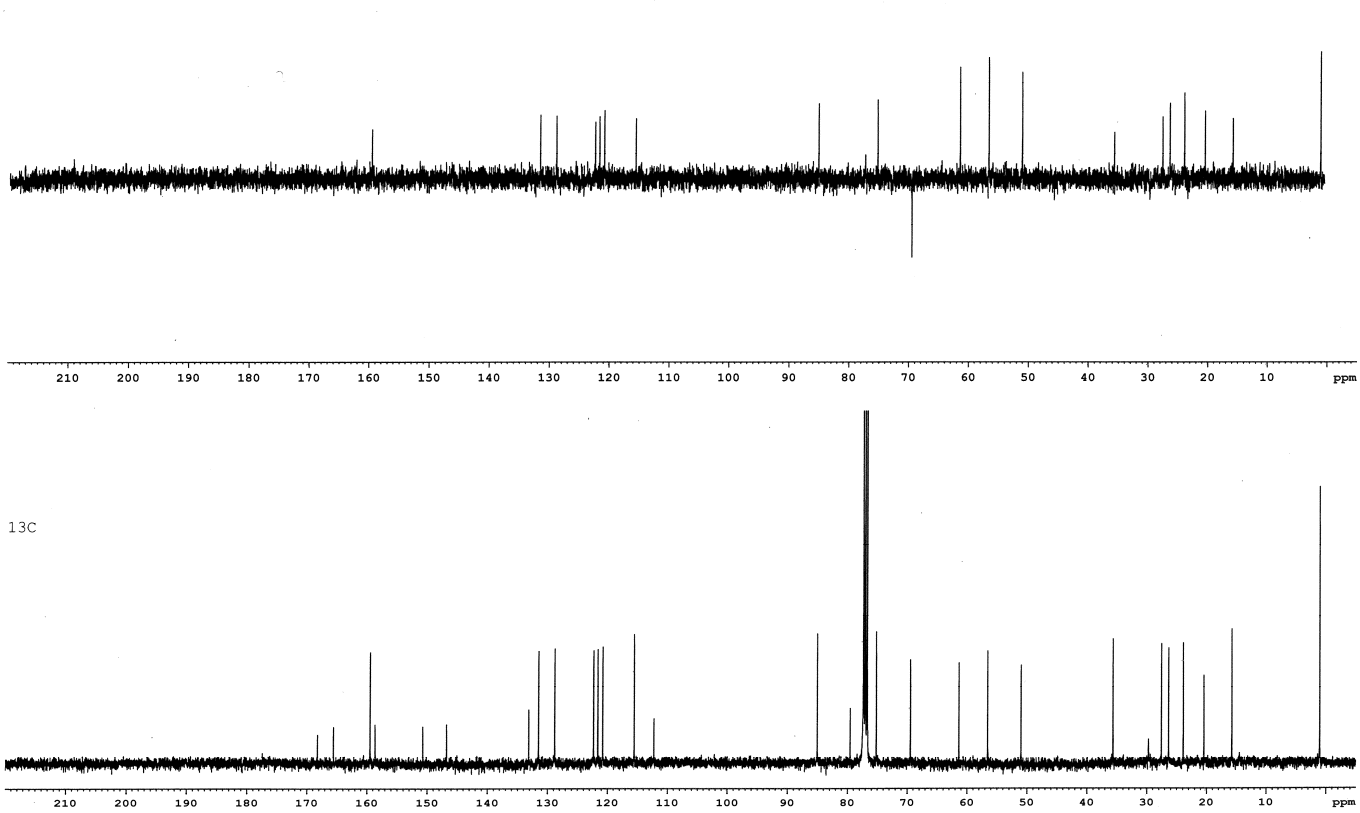

Fig. S21 COSY spectrum of oudemansin P (**3**) ($CDCl_3$, 400 MHz)

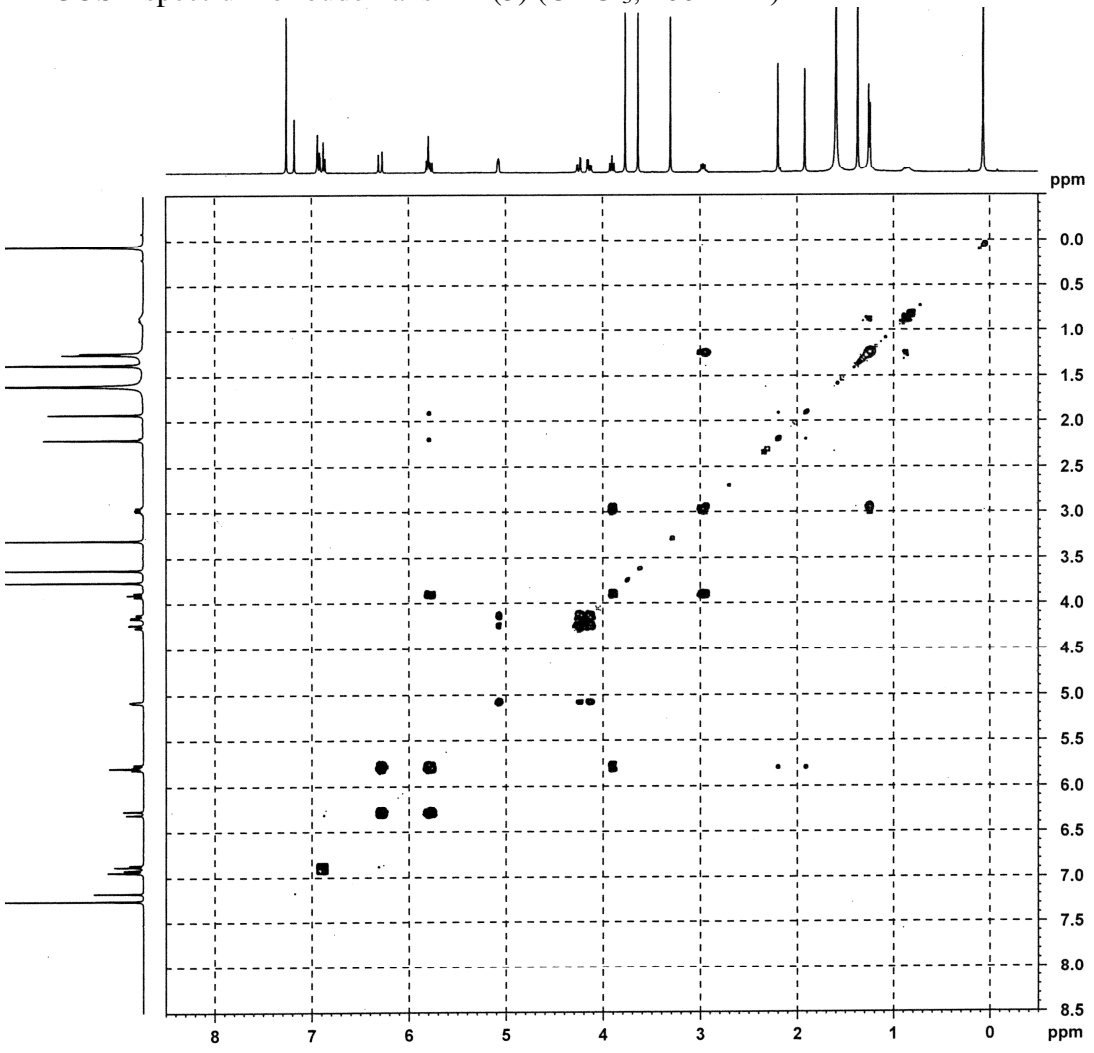

Fig. S22 HMQC spectrum of oudemansin P (**3**) ($CDCl_3$, 400 MHz)

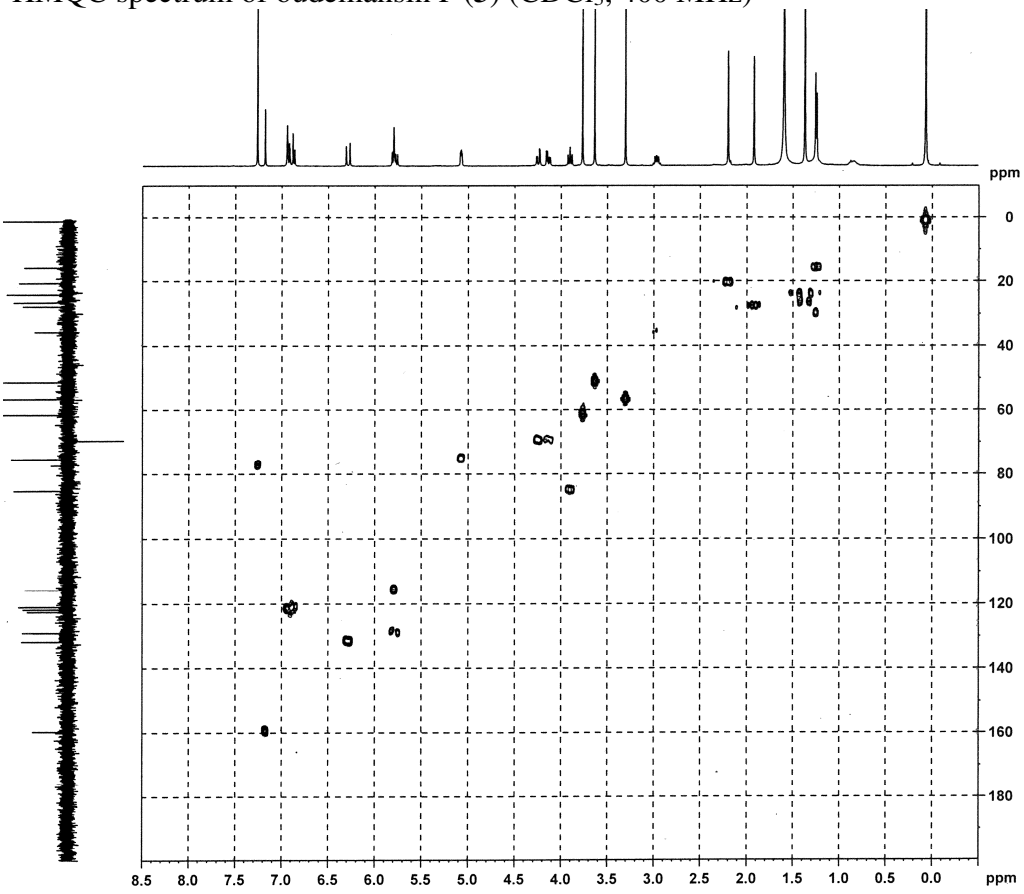

Fig. S23 HMBC spectrum of oudemansin P (**3**) ($CDCl_3$, 400 MHz)

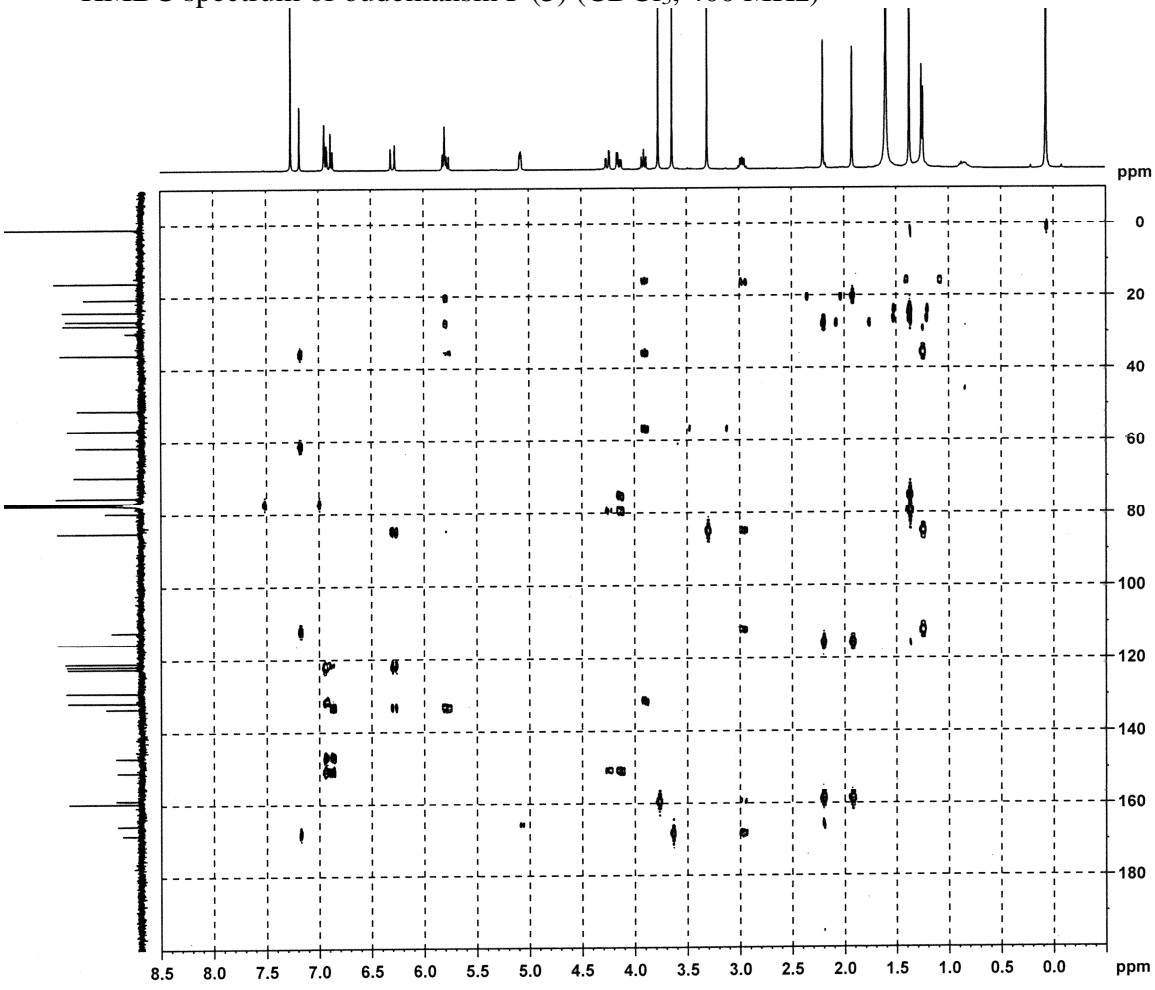

Fig. S24 NOESY spectrum of oudemansin P (**3**) ($CDCl_3$, 400 MHz)

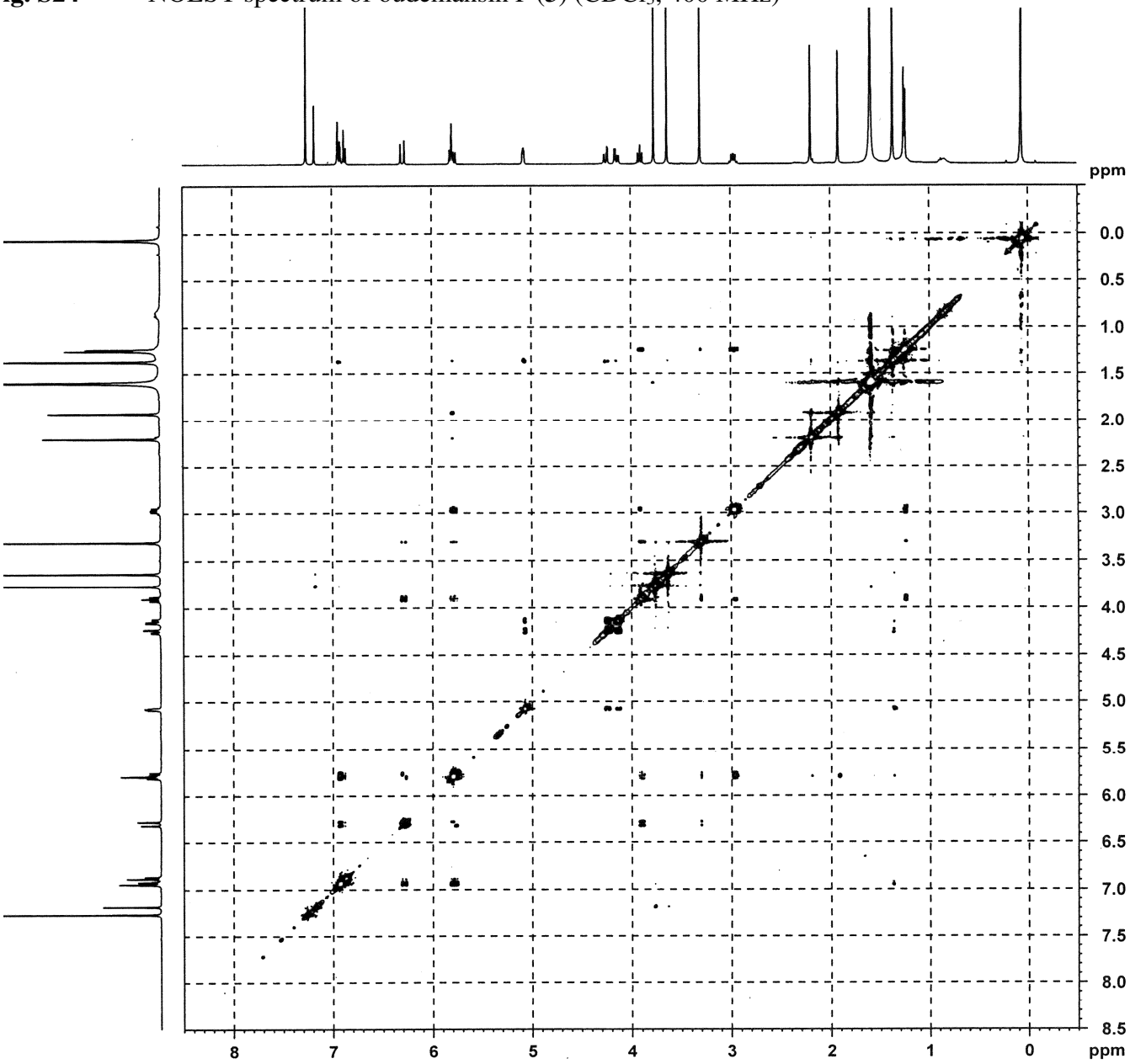

Fig. S25 HRESIMS of oudemansin P (**3**) (positive ion mode)

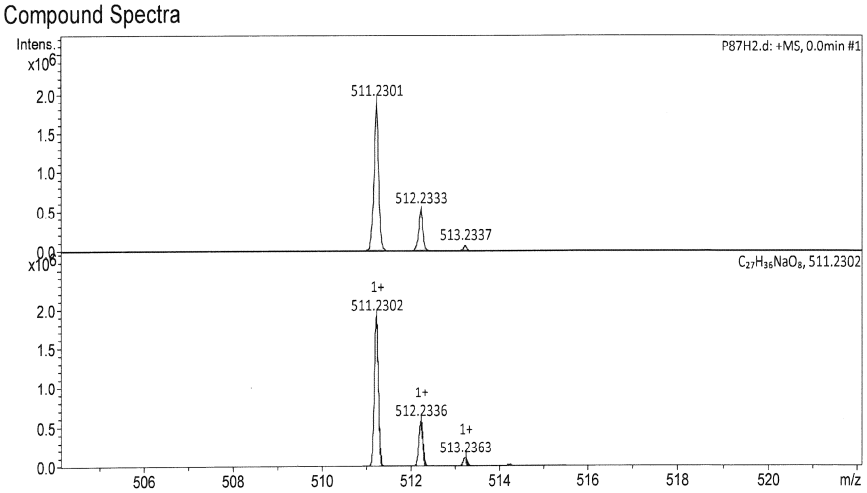

Fig. S26 ^{1}H NMR spectrum of oudemansin Q (**4**) ($CDCl_3$, 400 MHz)

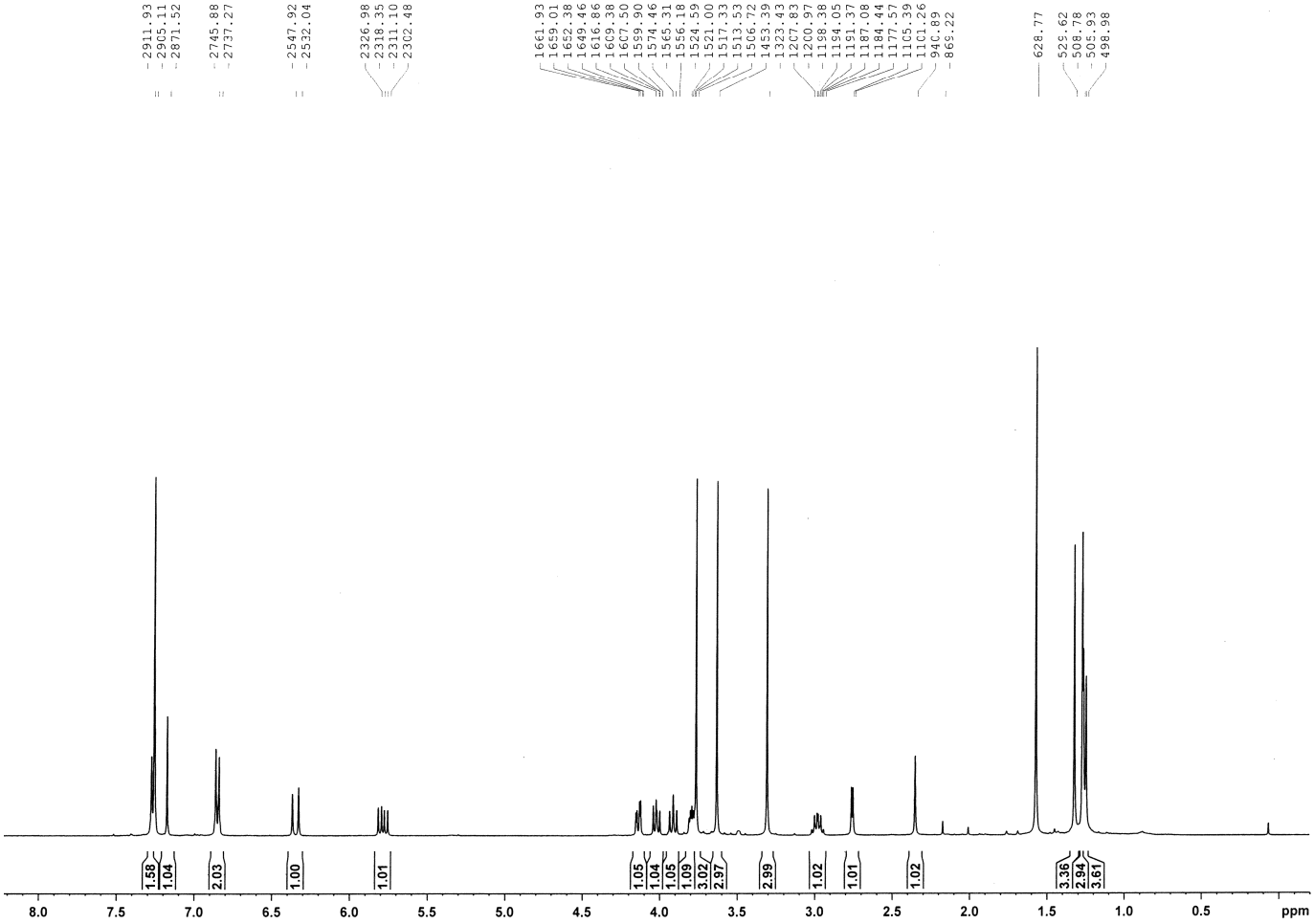

Fig. S27 ^{13}C NMR spectrum of oudemansin Q (**4**) ($CDCl_3$, 100 MHz)

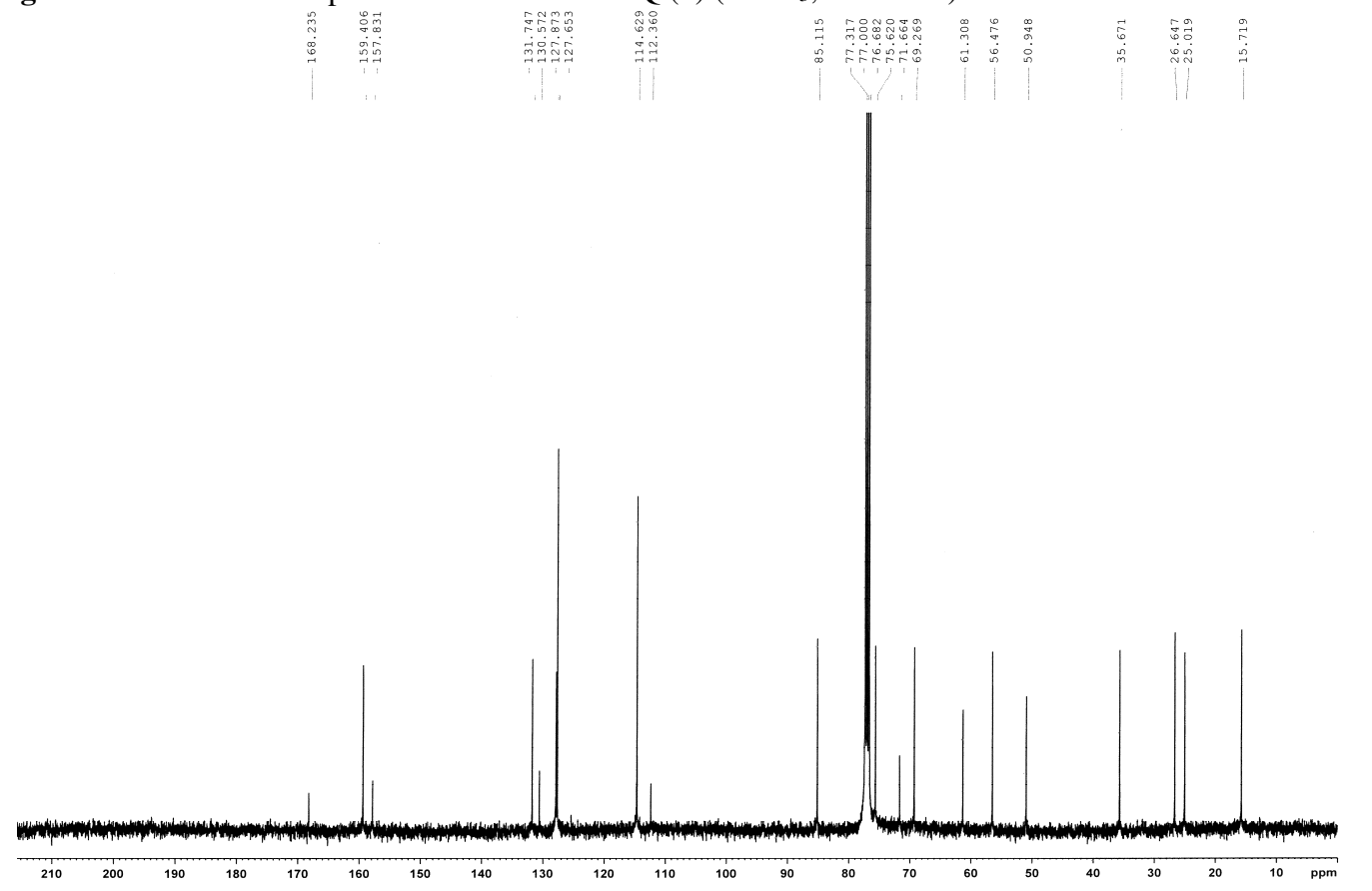

Fig. S28 DEPT-135 spectrum of oudemansin Q (**4**) ($CDCl_3$, 100 MHz)

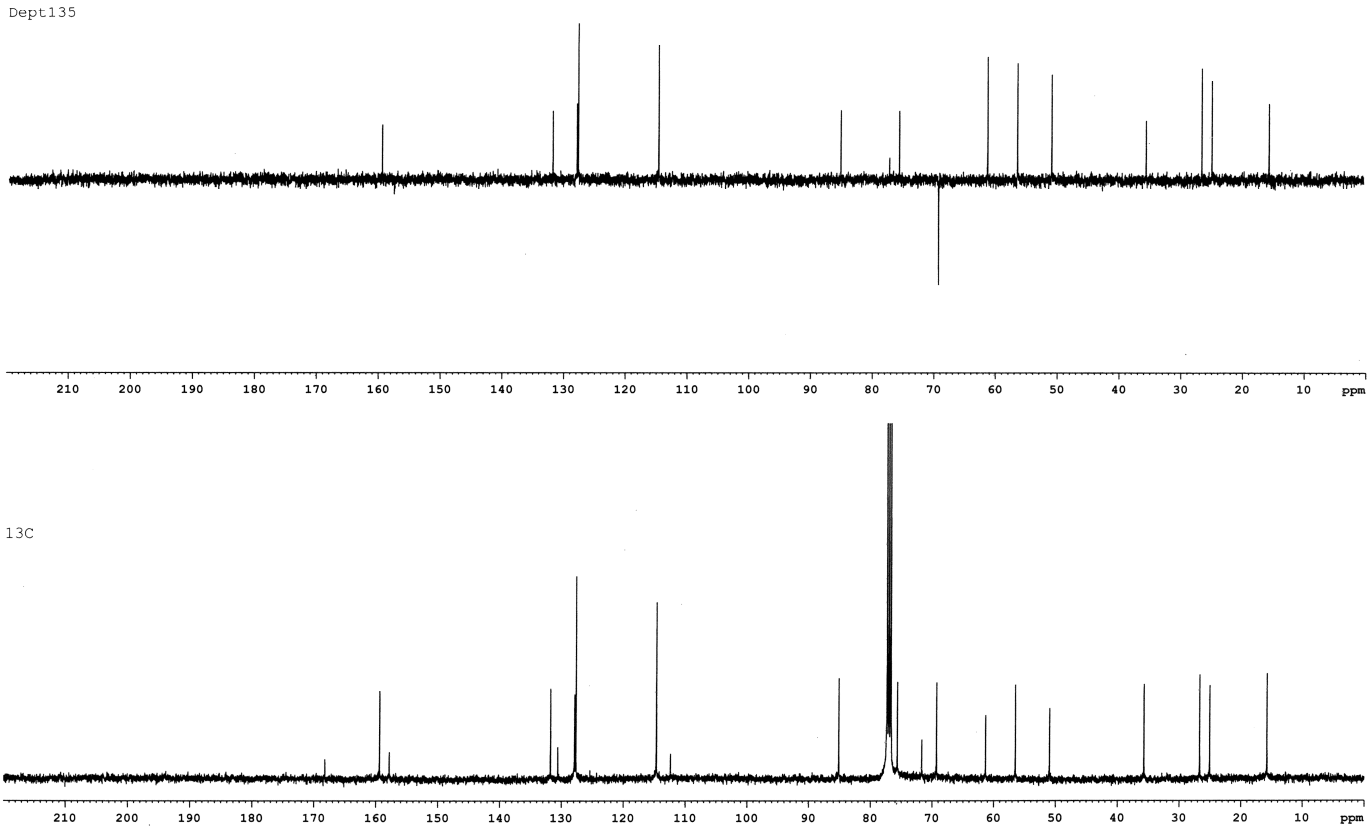

Fig. S29 COSY spectrum of oudemansin Q (**4**) ($CDCl_3$, 400 MHz)

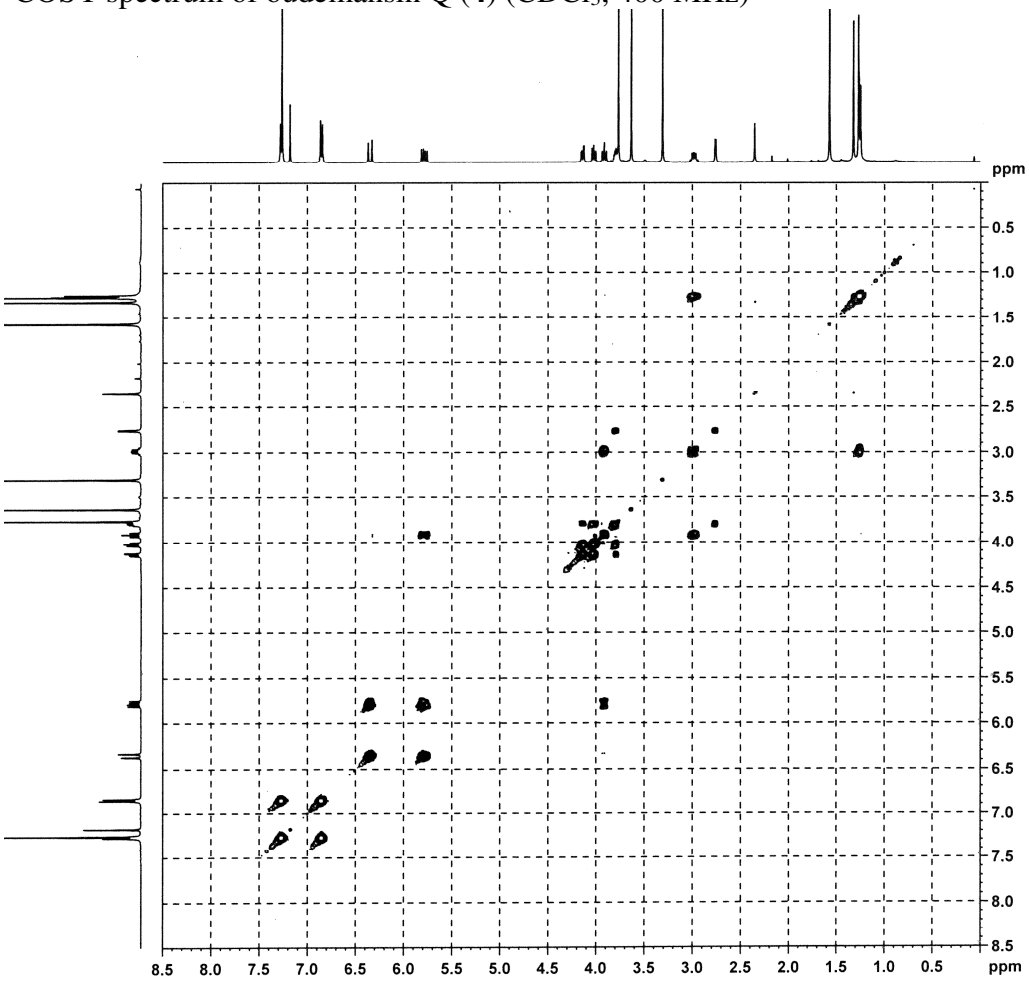

Fig. S30 HMQC spectrum of oudemansin Q (**4**) ($CDCl_3$, 400 MHz)

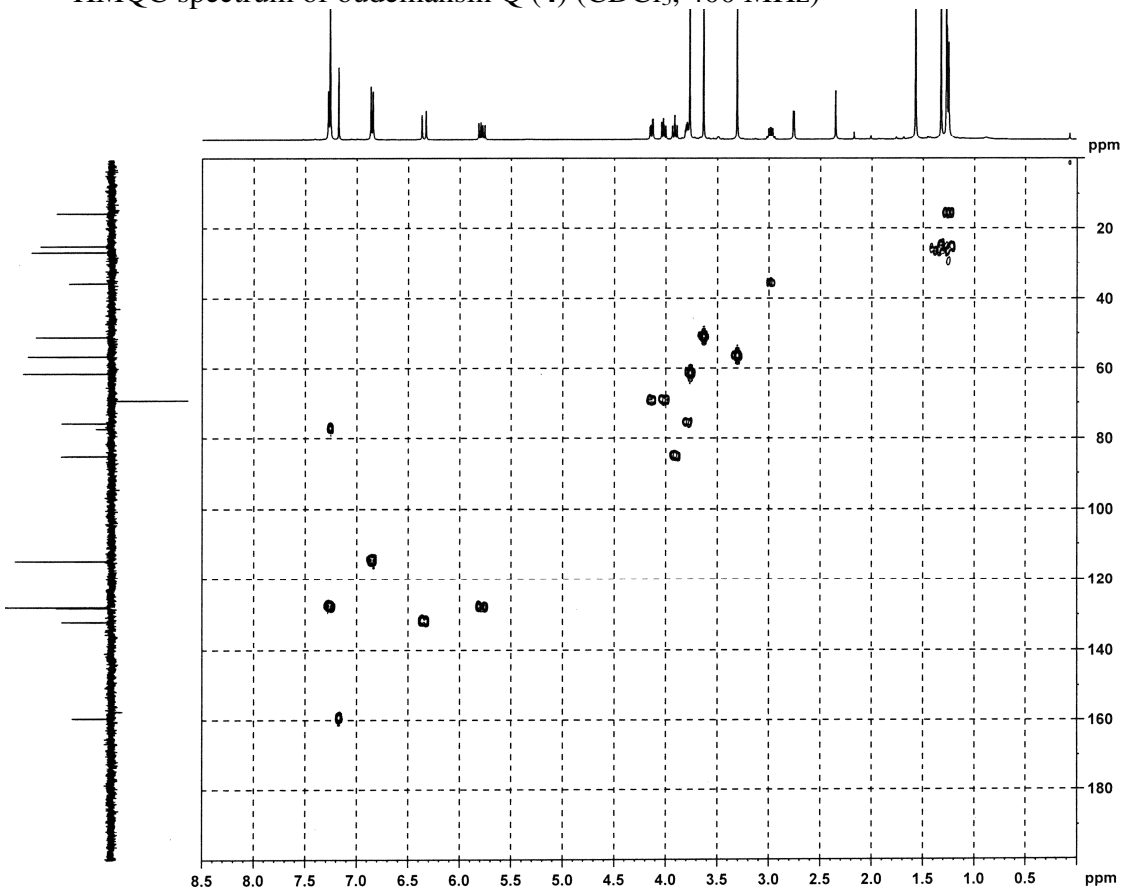

Fig. S31 HMBC spectrum of oudemansin Q (**4**) ($CDCl_3$, 400 MHz)

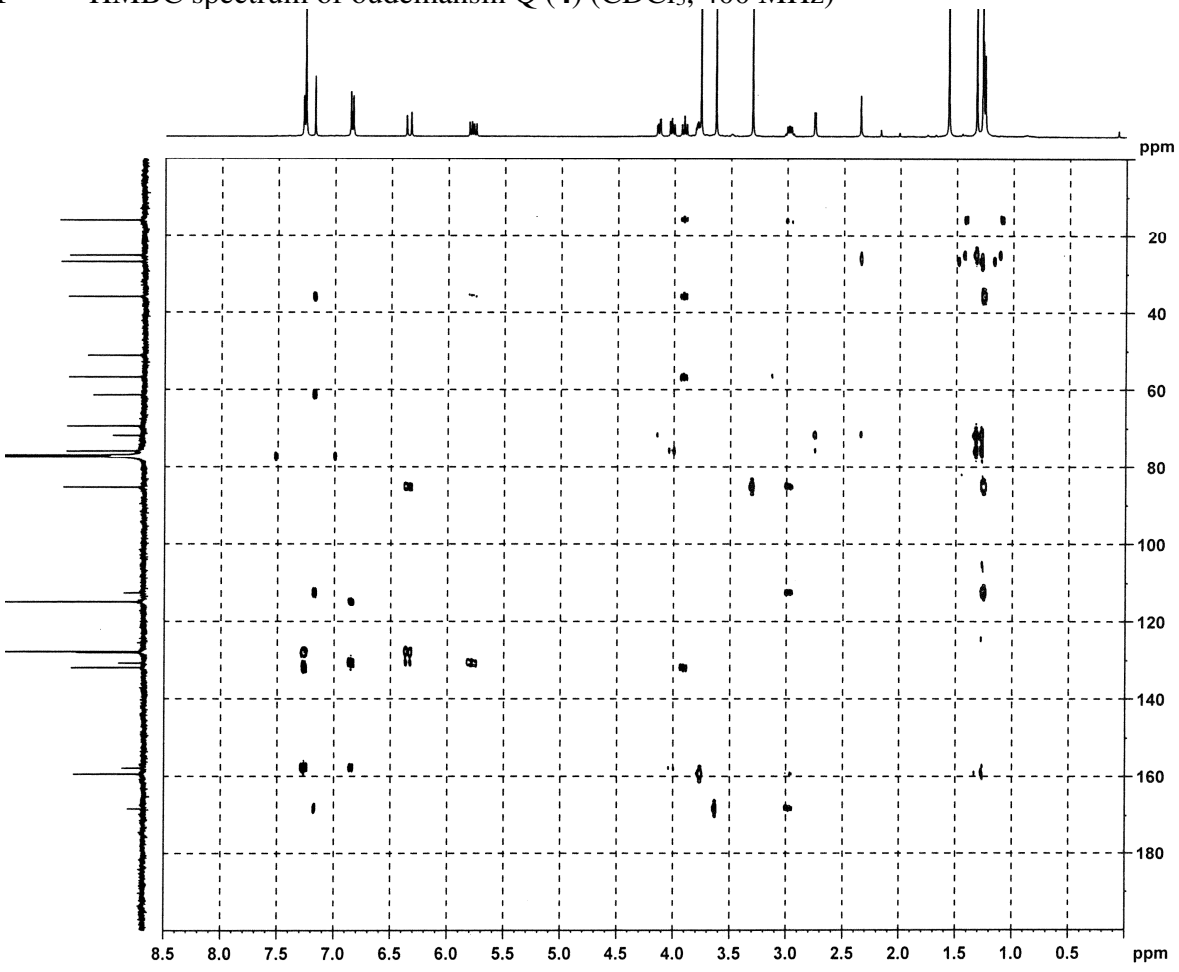

Fig. S32 NOESY spectrum of oudemansin Q (**4**) ($CDCl_3$, 400 MHz)

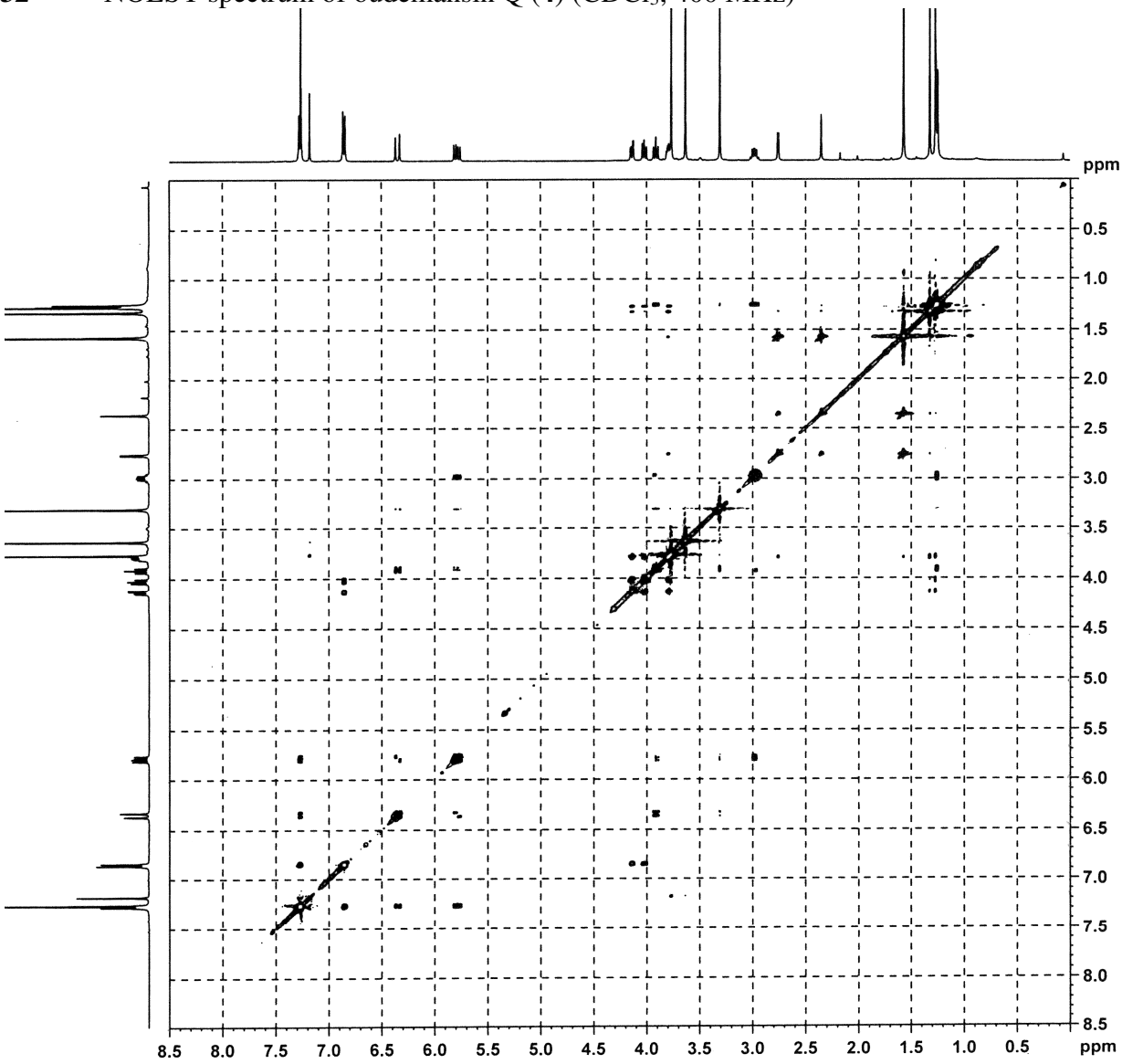

Fig. S33 HRESIMS of oudemansin Q (**4**) (positive ion mode)

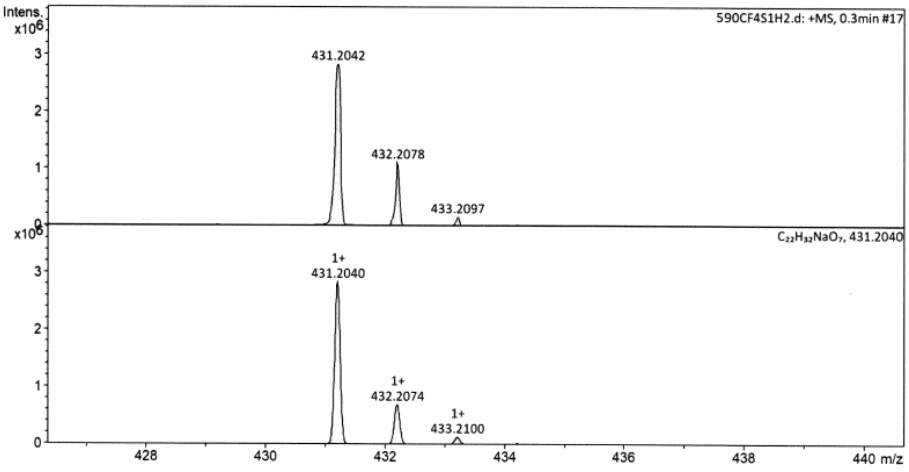

Fig. S34 ^{1}H NMR spectrum of 9-methoxystrobilurin I (**5**) ($CDCl_3$, 500 MHz)

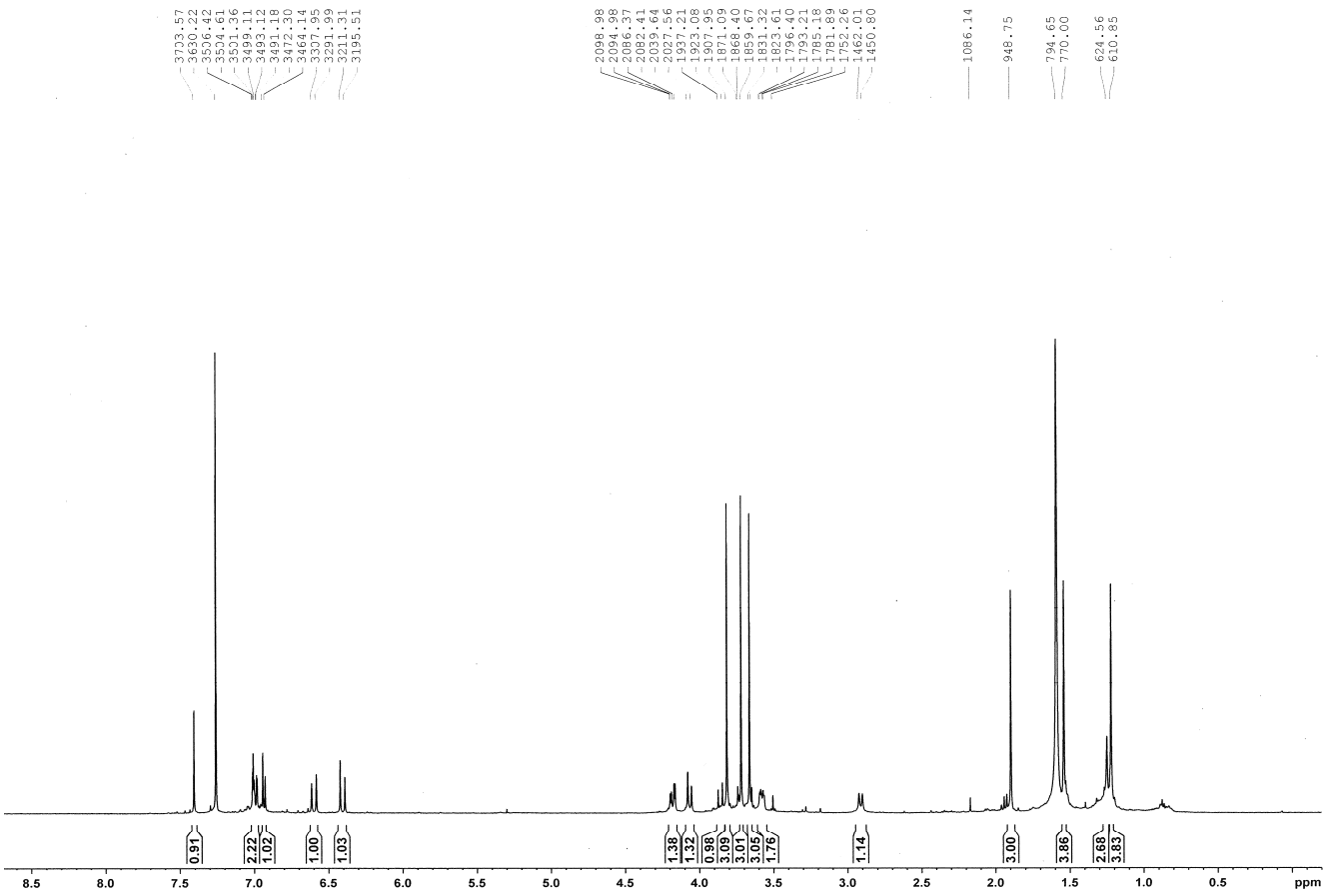

Fig. S35 ^{13}C NMR spectrum of 9-methoxystrobilurin I (**5**) ($CDCl_3$, 125 MHz)

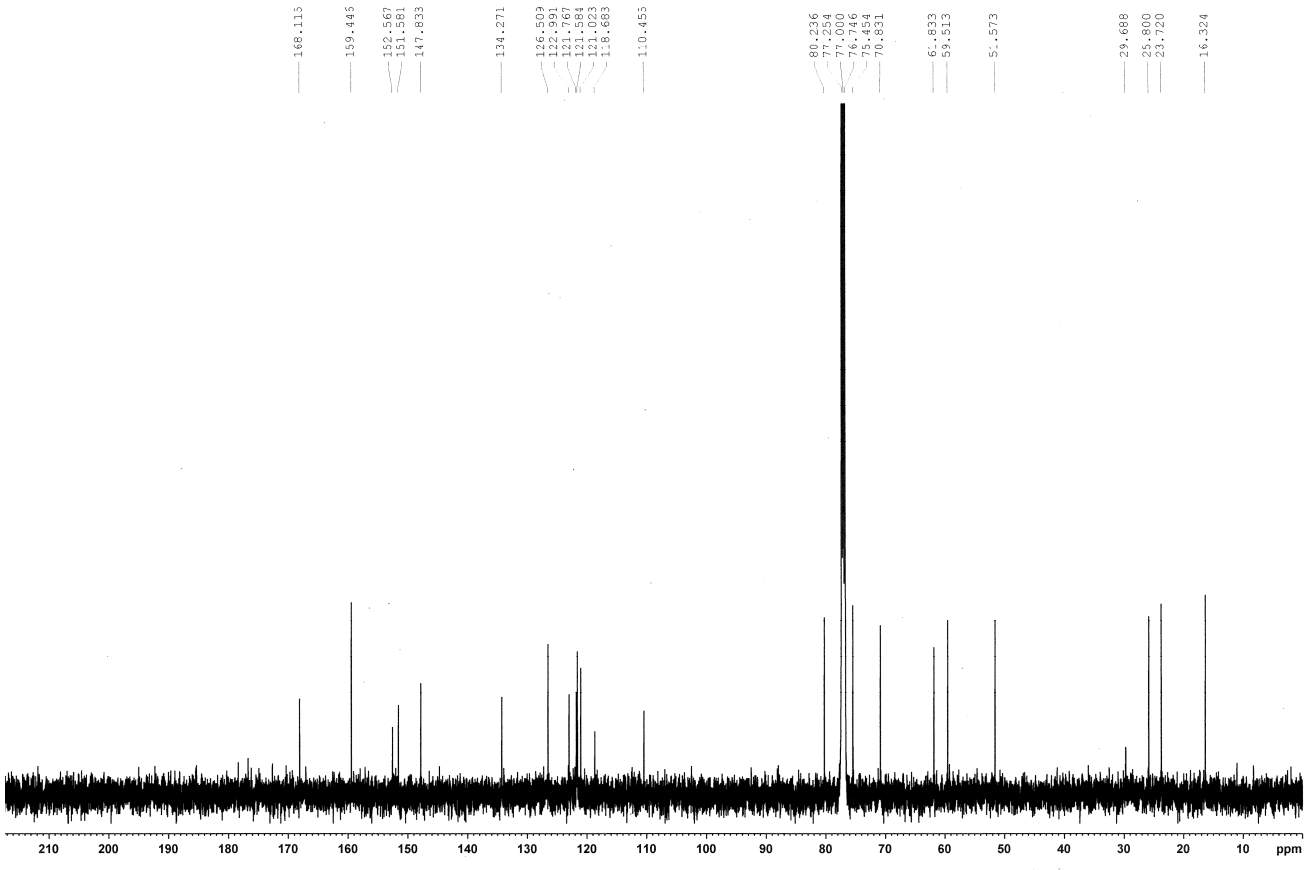

Fig. S36 DEPT-135 spectrum of 9-methoxystrobilurin I (**5**) ($CDCl_3$, 125 MHz)

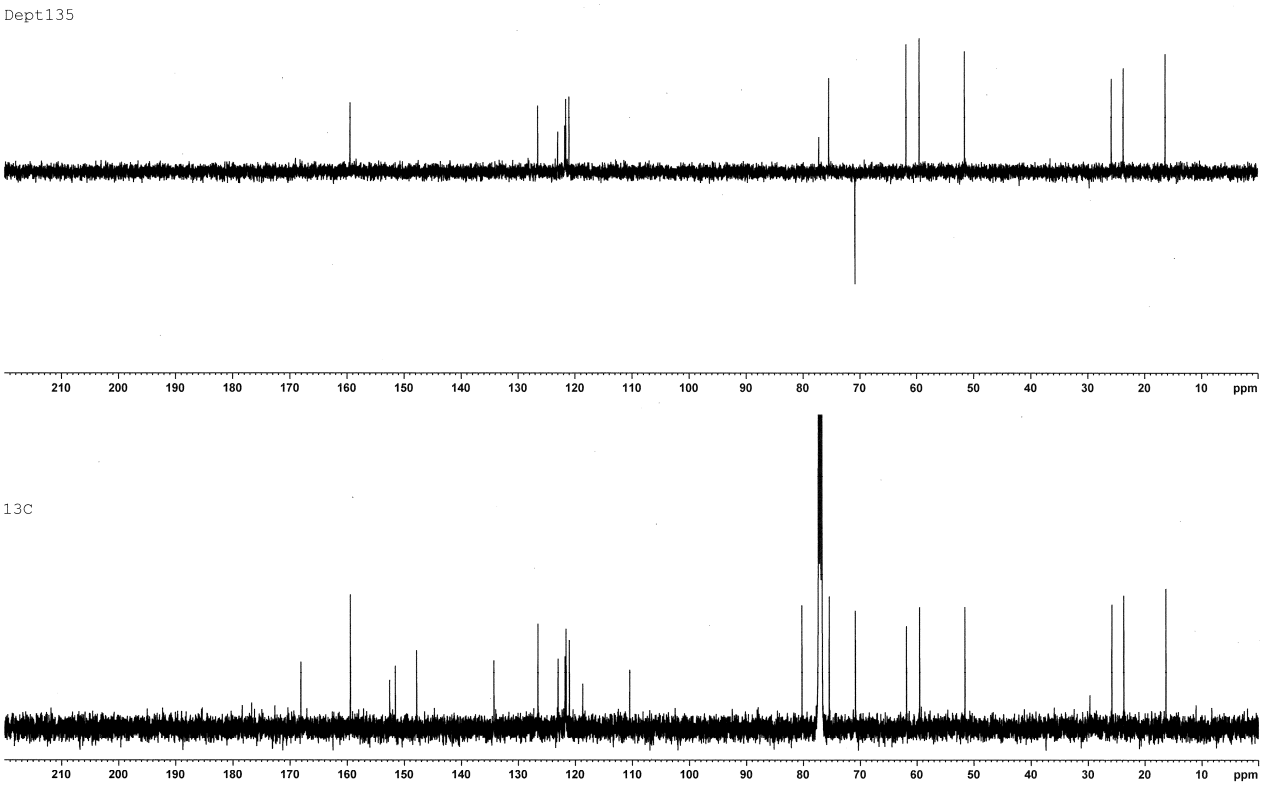

Fig. S37 COSY spectrum of 9-methoxystrobilurin I (**5**) ($CDCl_3$, 500 MHz)

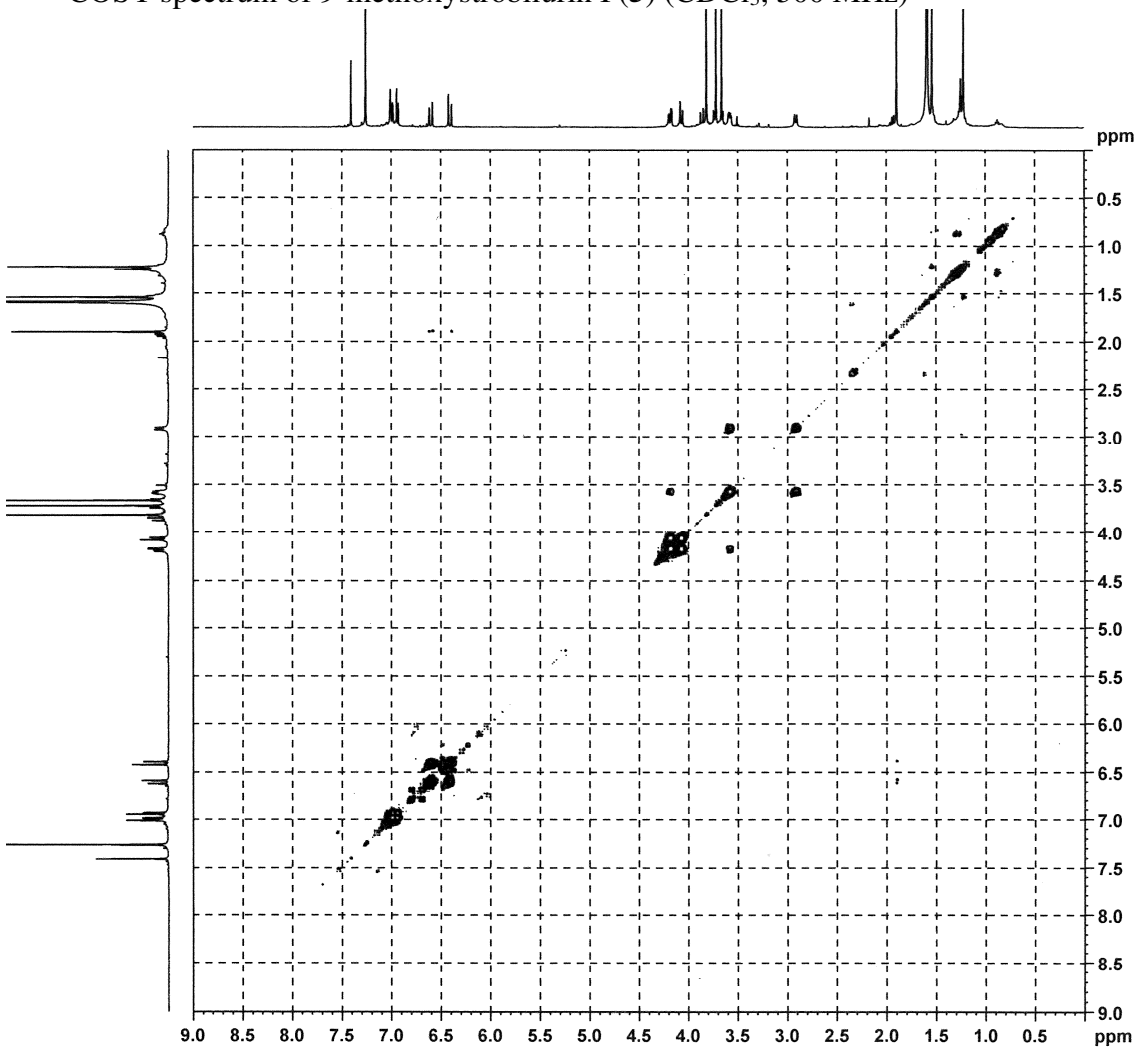

Fig. S38 HSQC spectrum of 9-methoxystrobilurin I (**5**) ($CDCl_3$, 500 MHz)

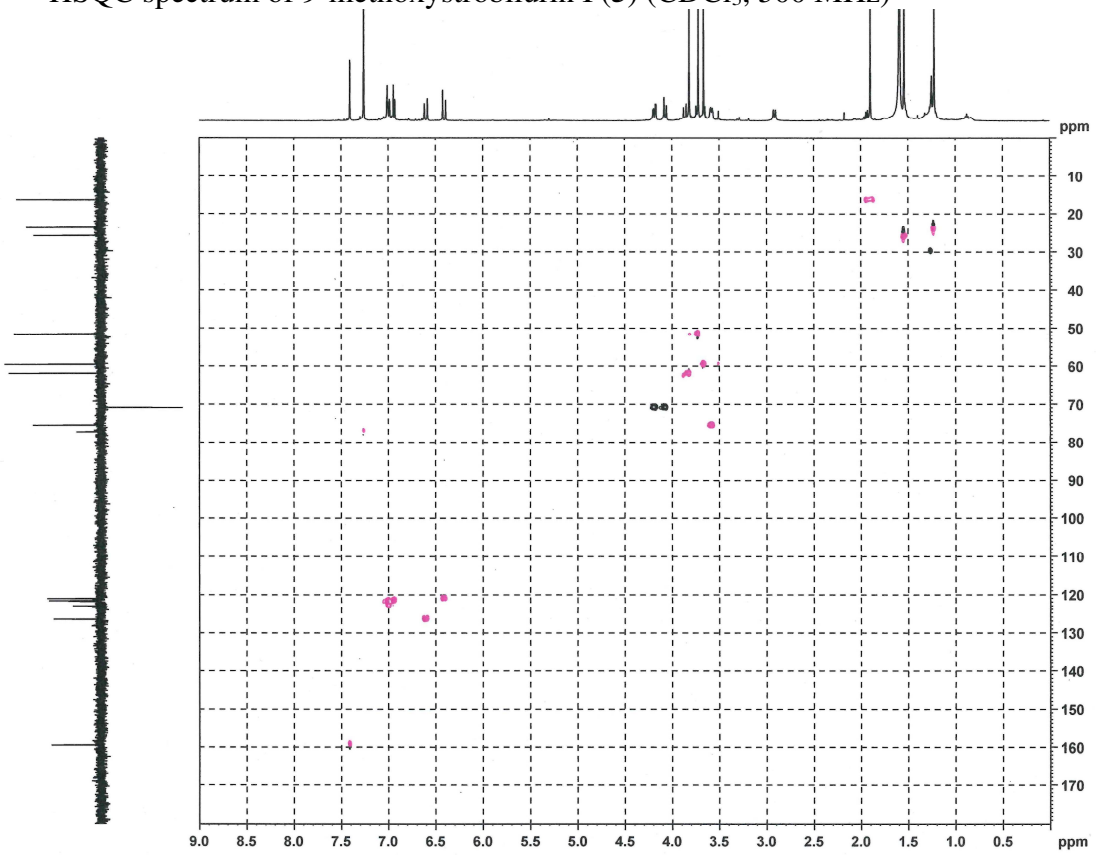

Fig. S39 HMBC spectrum of 9-methoxystrobilurin I (**5**) ($CDCl_3$, 500 MHz)

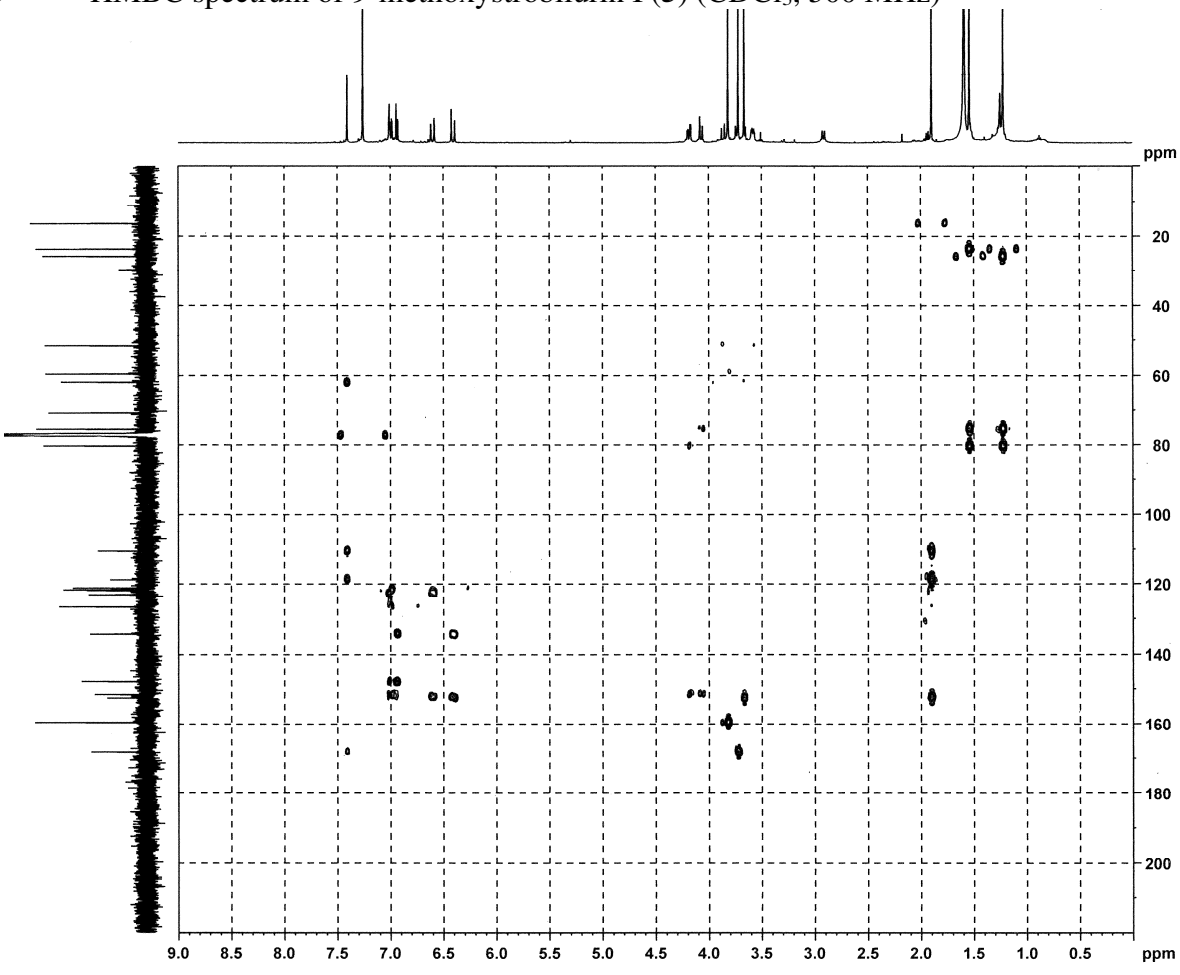

Fig. S40 NOESY spectrum of 9-methoxystrobilurin I (**5**) ($CDCl_3$, 500 MHz)

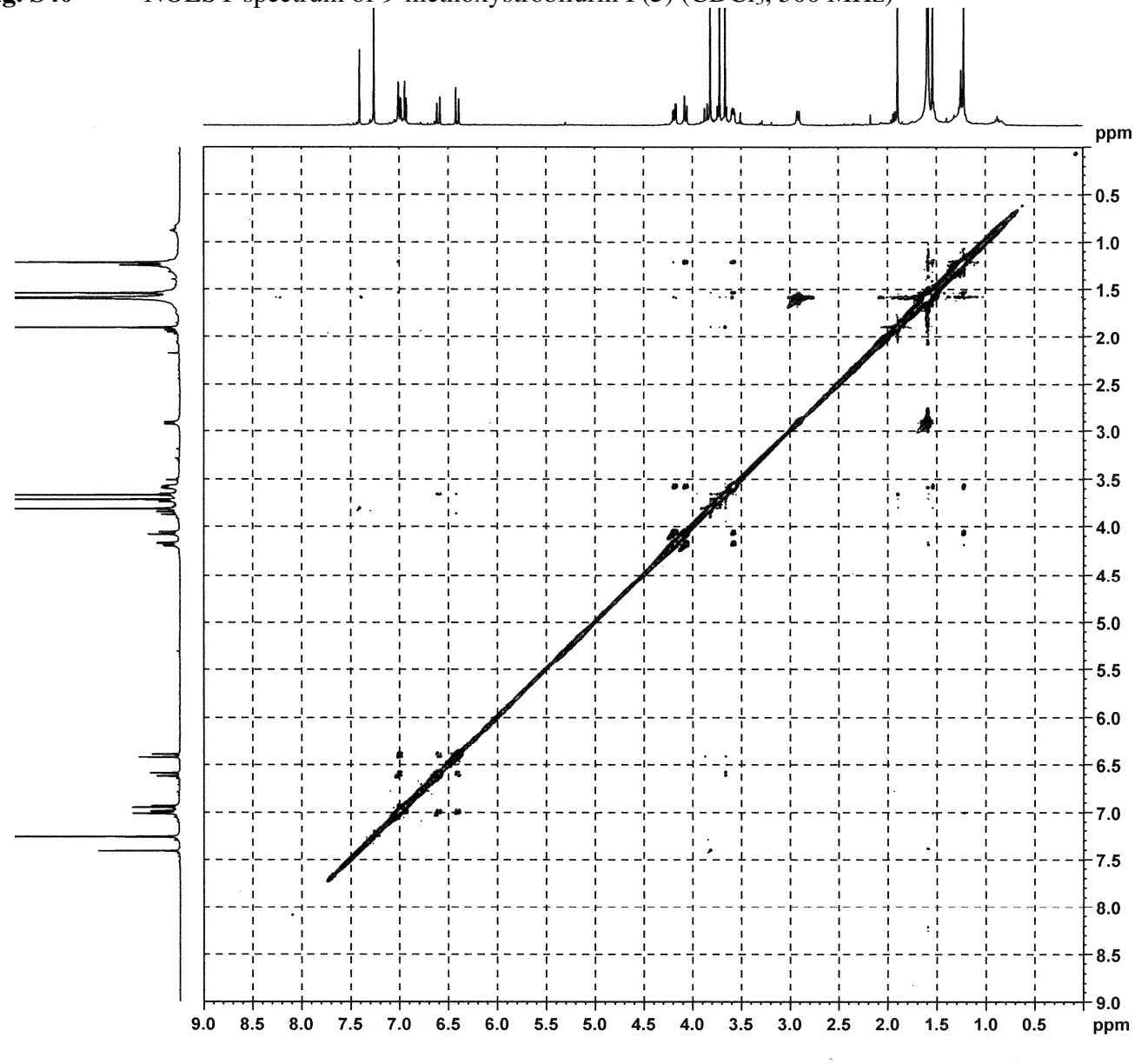

Fig. S41 HRESIMS of 9-methoxystrobilurin I (**5**) (positive ion mode

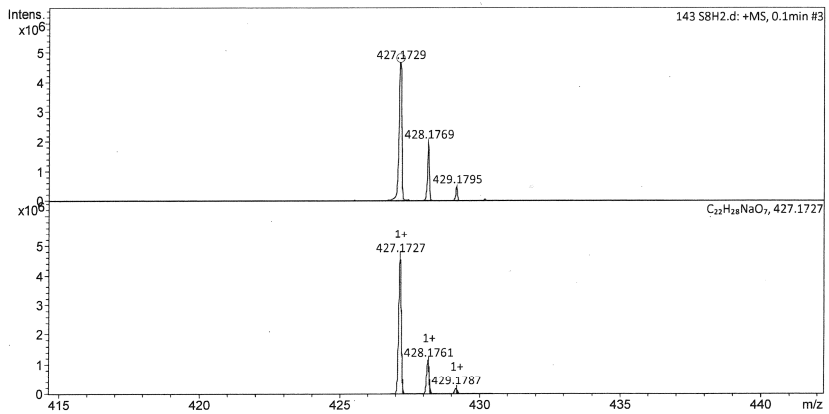

Fig. S42 ^{1}H NMR spectrum of **6** ($CDCl_3$, 400 MHz)

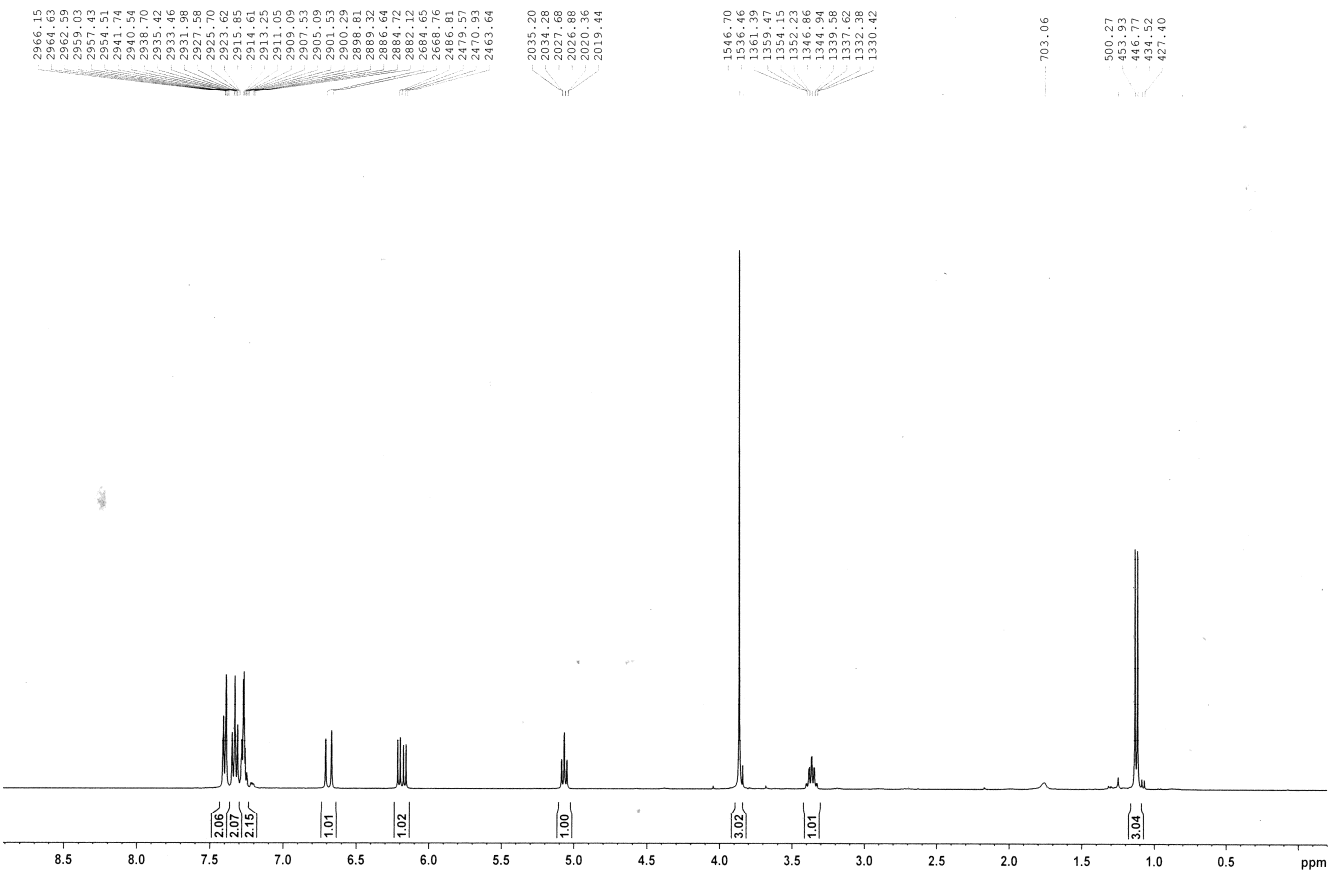

Fig. S43 ^{13}C NMR spectrum of **6** ($CDCl_3$, 100 MHz)

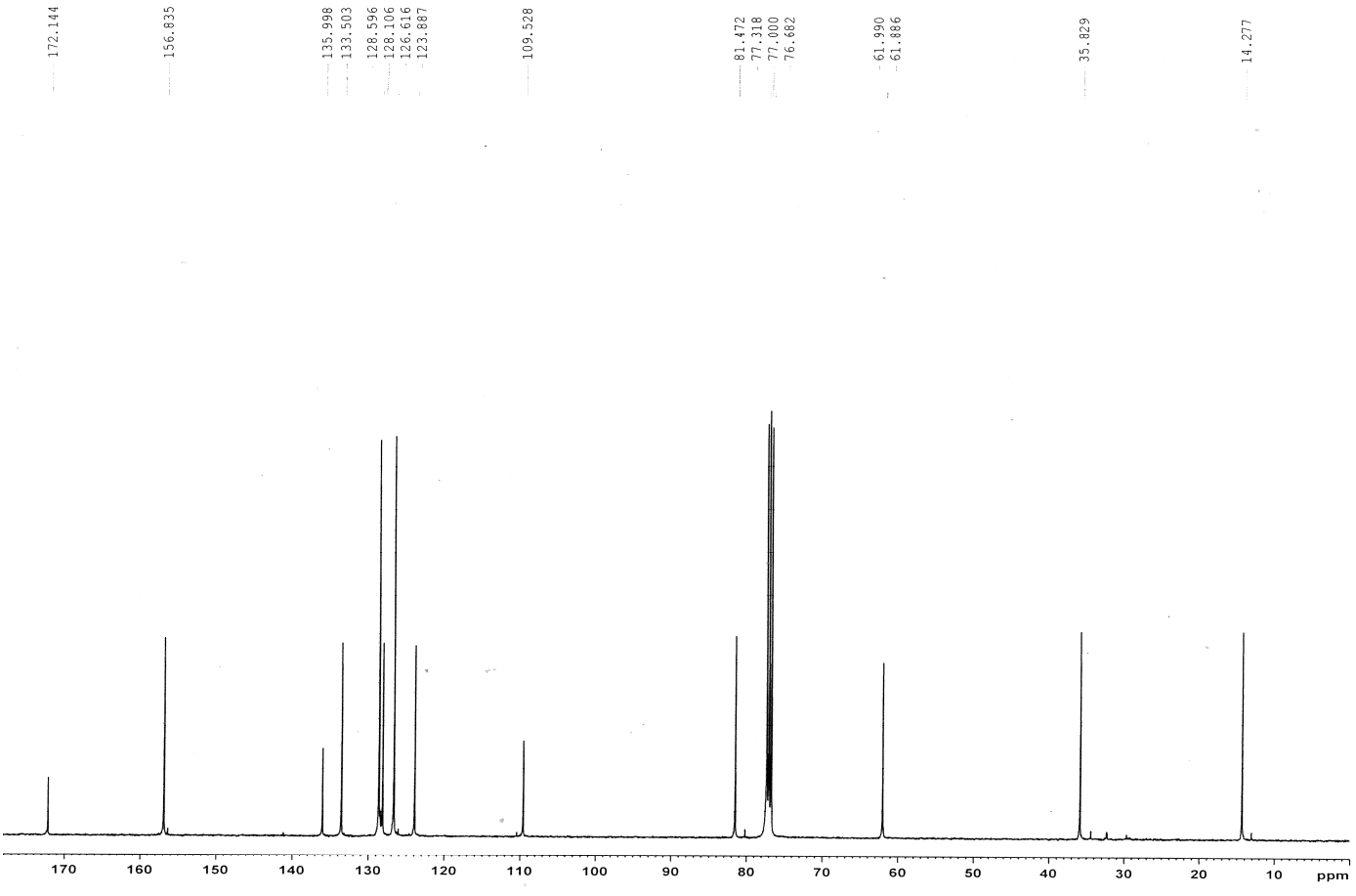

Fig. S44 DEPT-135 spectrum of **6** ($CDCl_3$, 100 MHz)

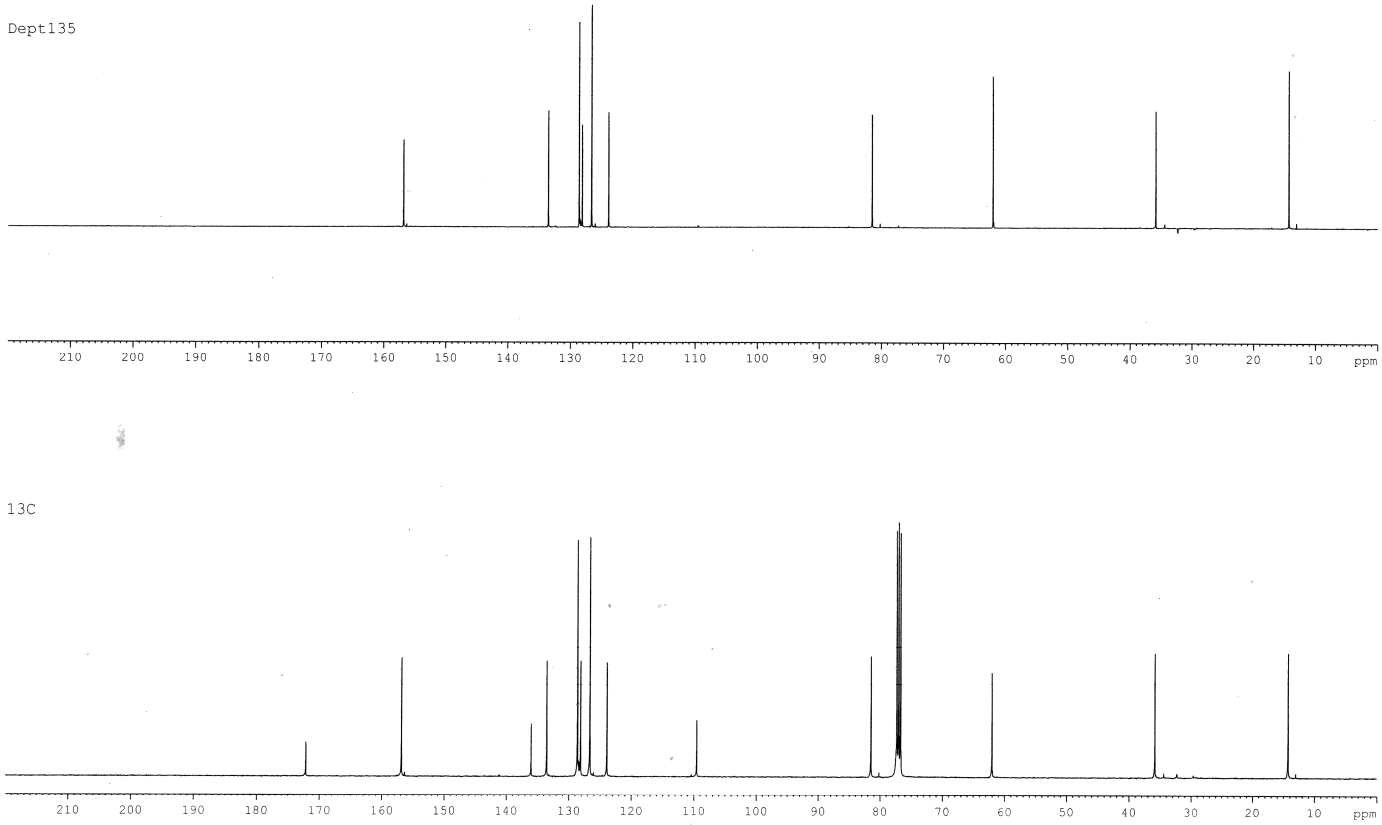

Fig. S45 COSY spectrum of **6** ($CDCl_3$, 400 MHz)

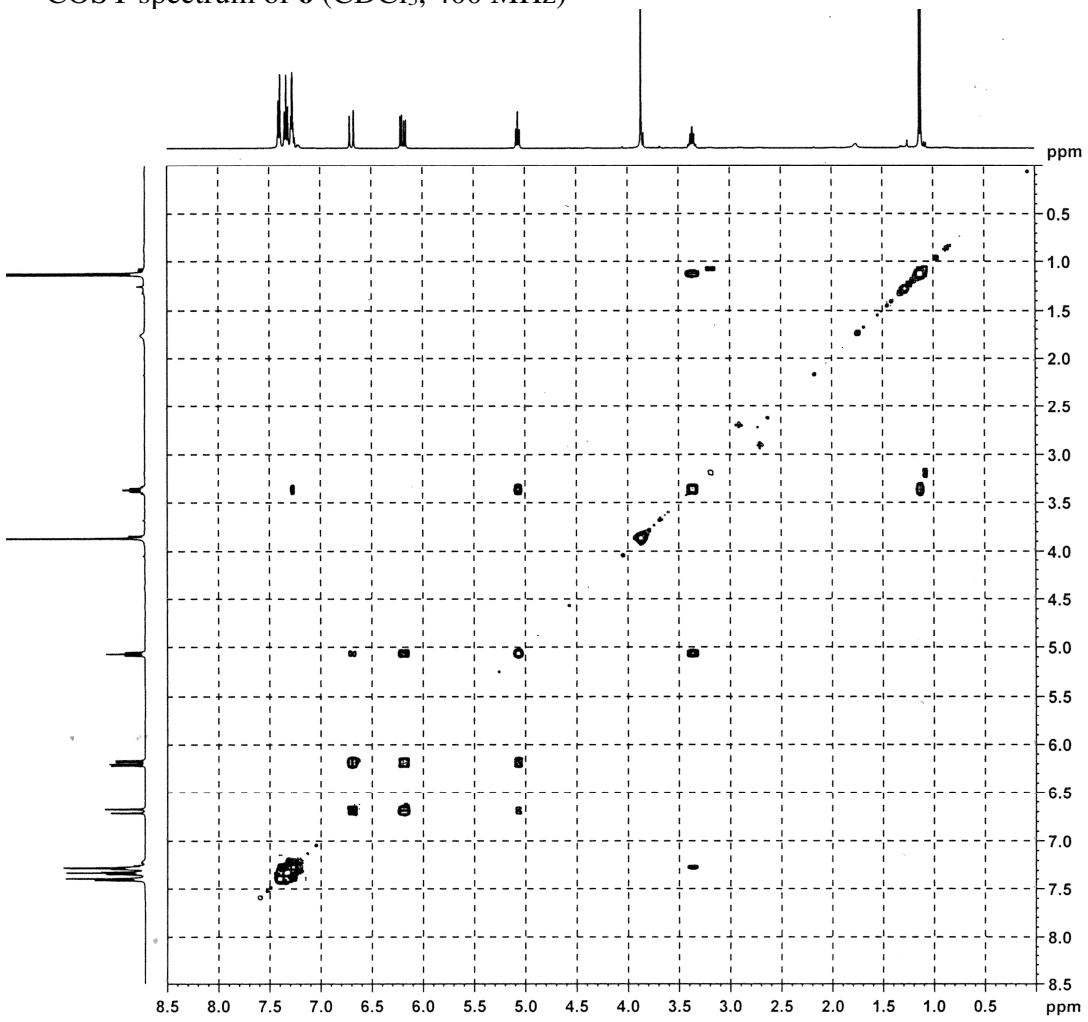

Fig. S46 HMQC spectrum of **6** ($CDCl_3$, 400 MHz)

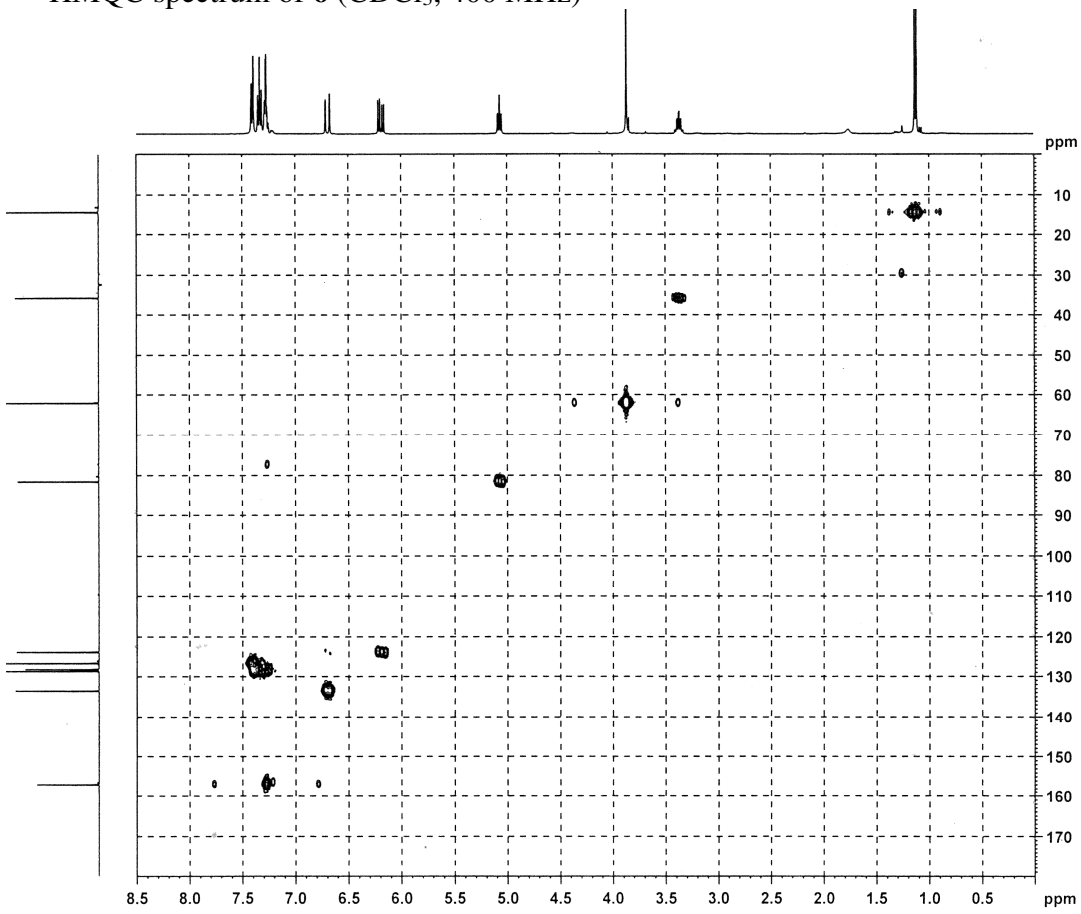

Fig. S47 HMBC spectrum of **6** ($CDCl_3$, 400 MHz)

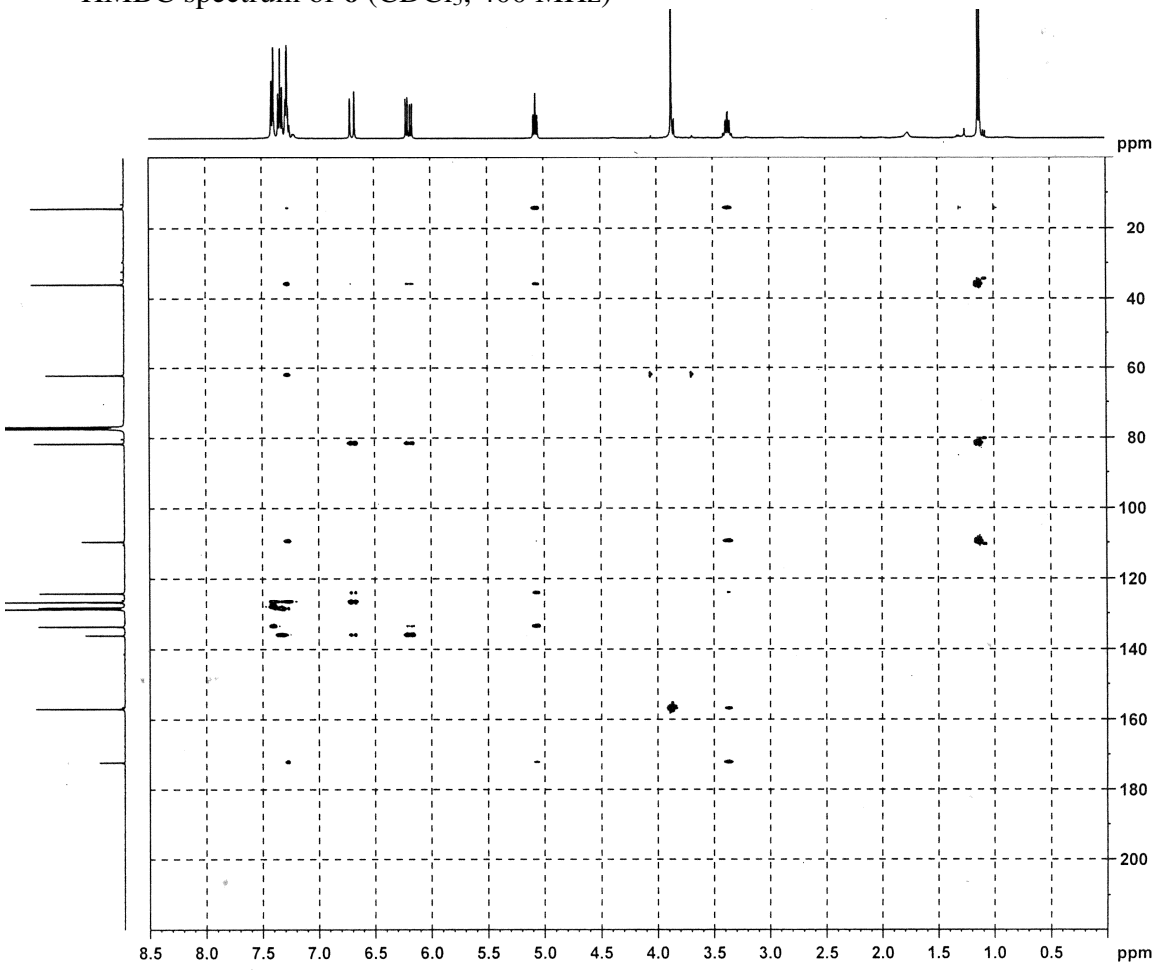

Fig. S48 NOESY spectrum of **6** ($CDCl_3$, 400 MHz)

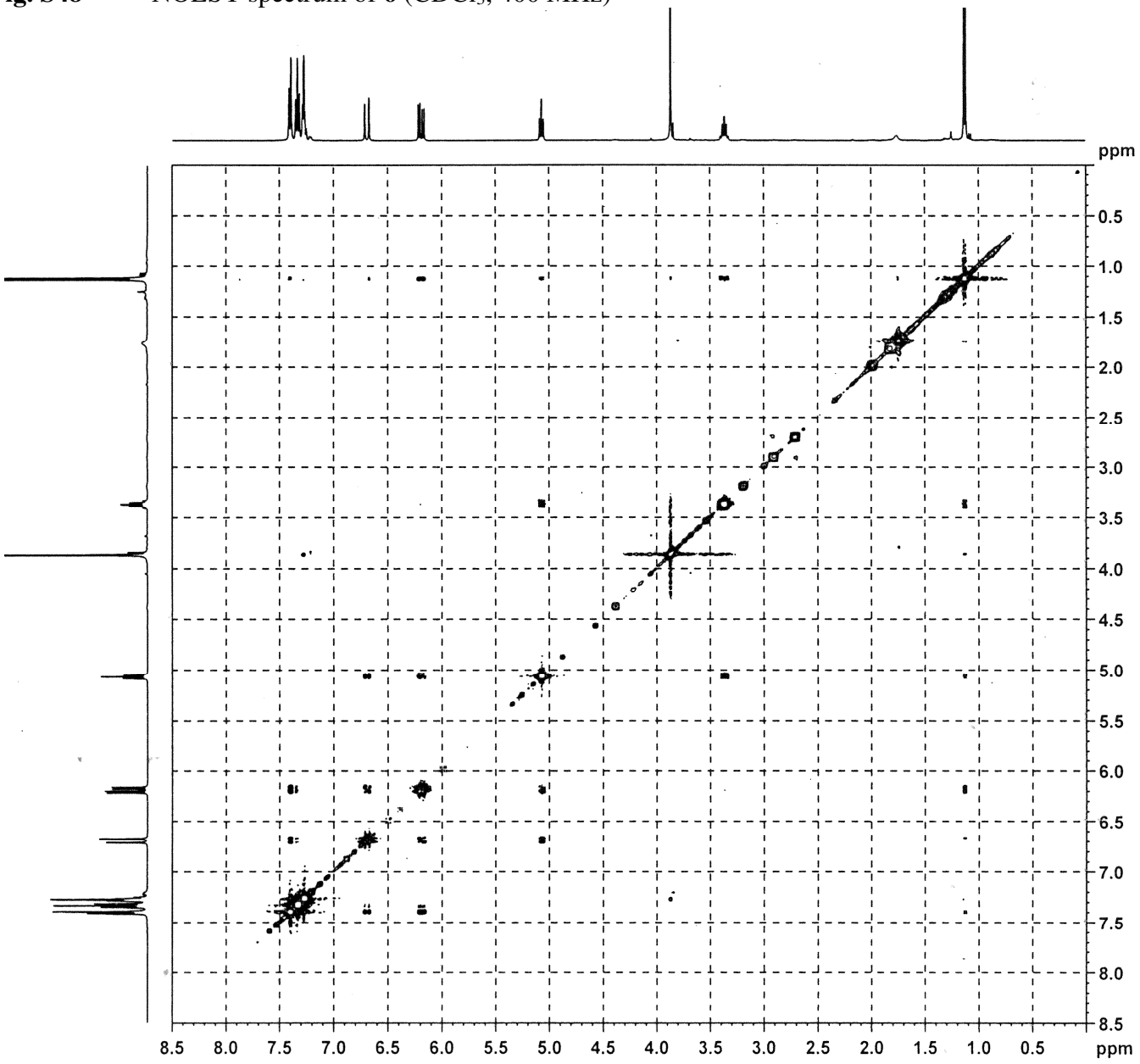

Fig. S49 HRESIMS of **6** (positive ion mode)

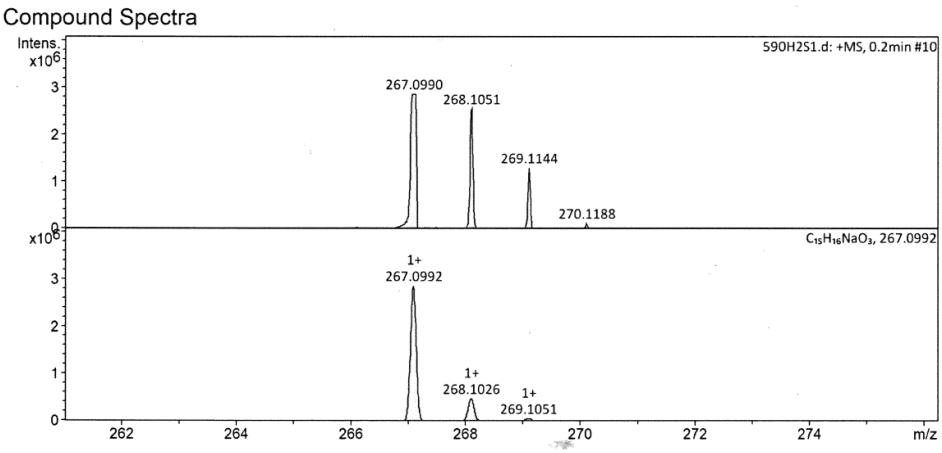

Fig. S50 ^{1}H NMR spectrum of **12** ($CDCl_3$, 400 MHz)

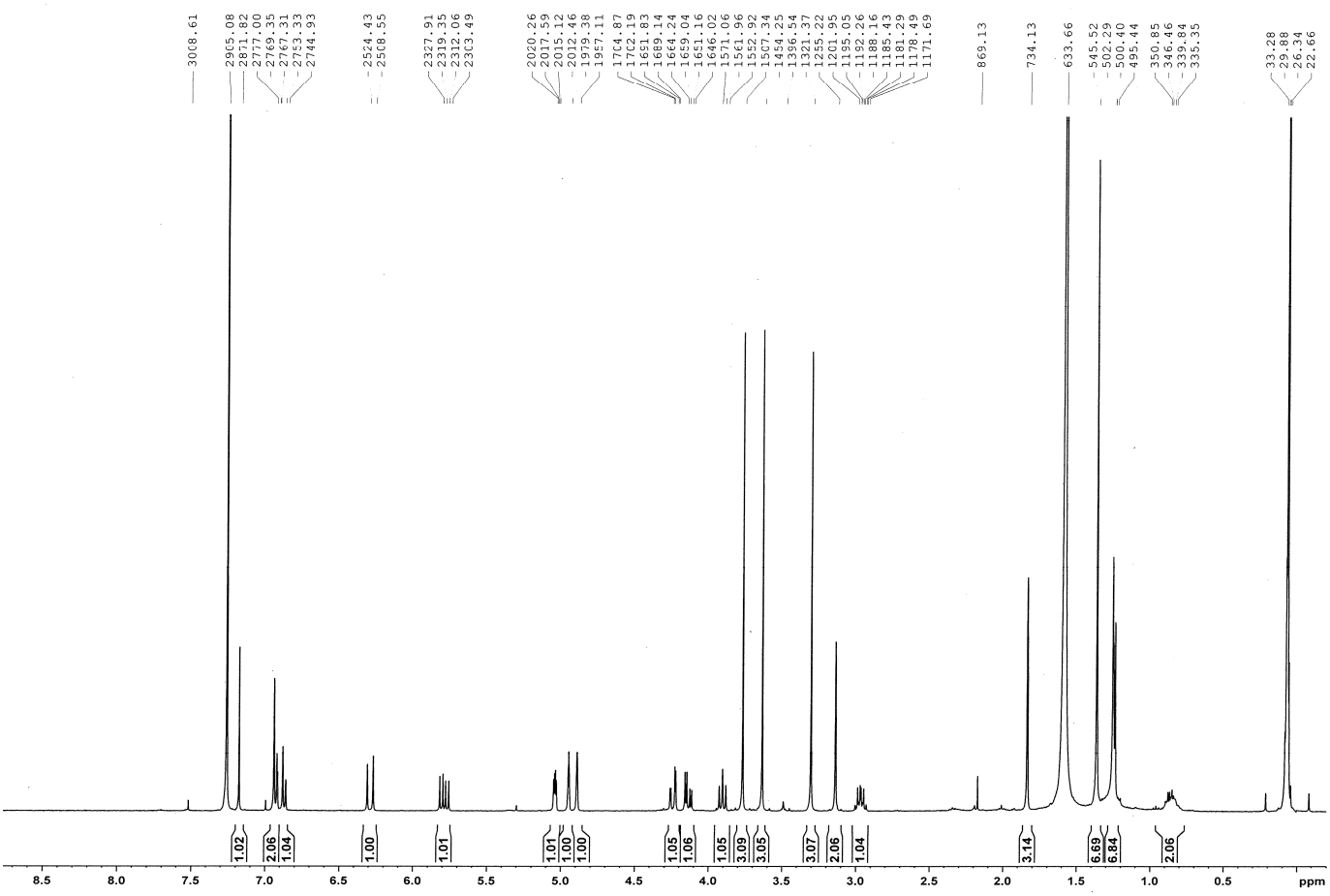

Fig. S51 HRESIMS of **12** (positive ion mode)

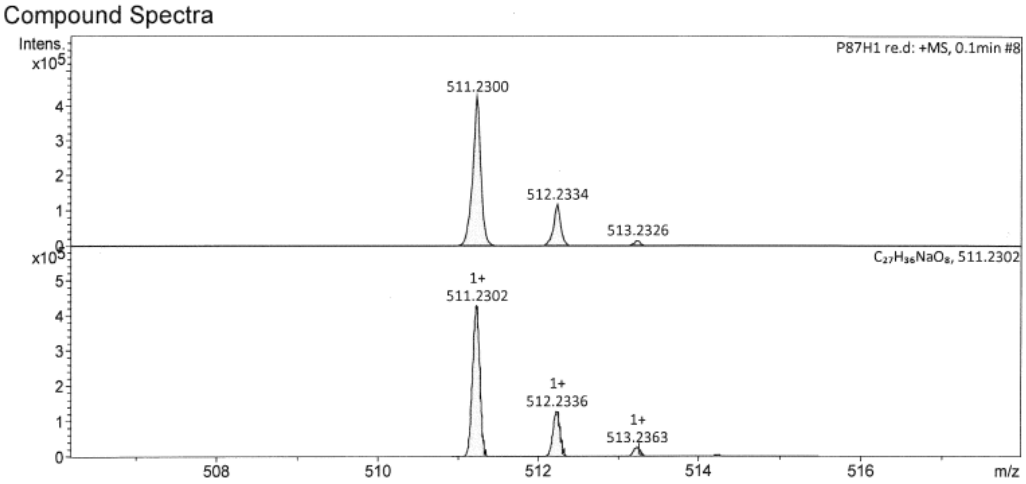

Fig. S52 ^{1}H NMR spectrum of 9-methoxystrobilurin P (**13**) ($CDCl_3$, 500 MHz)

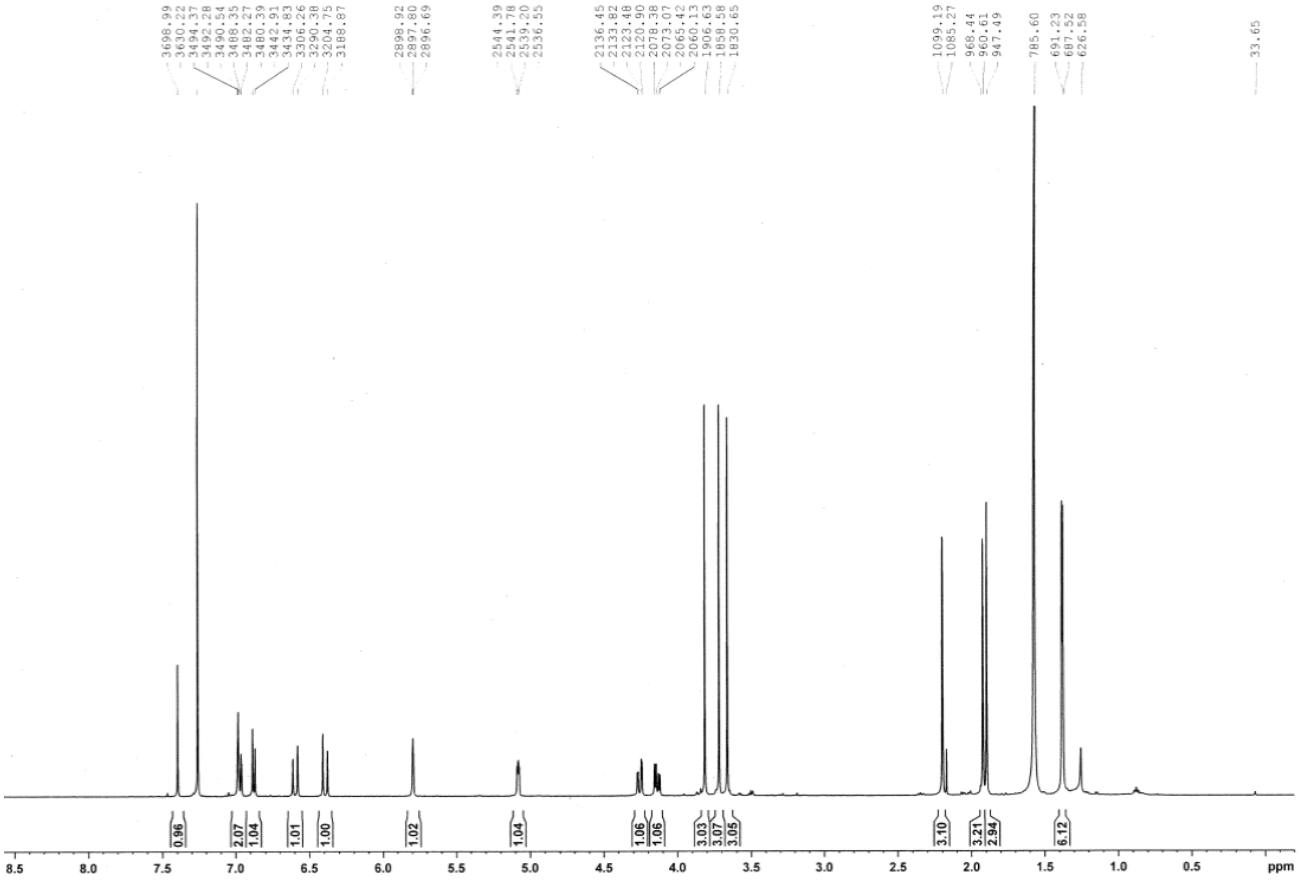

Fig. S53 ^{13}C NMR spectrum of 9-methoxystrobilurin P (**13**) ($CDCl_3$, 125 MHz)

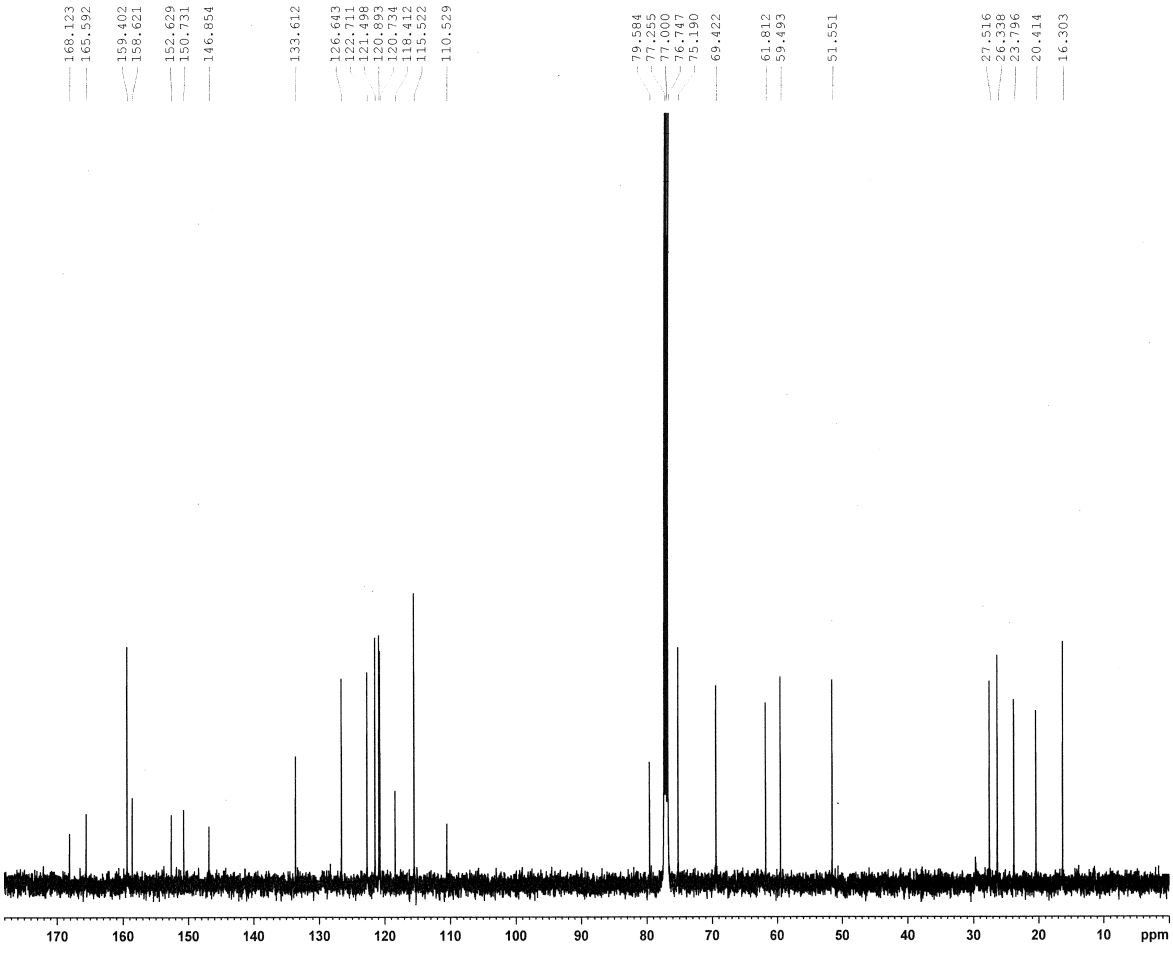

Fig. S54 DEPT-135 spectrum of 9-methoxystrobilurin P (**13**) ($CDCl_3$, 125 MHz)

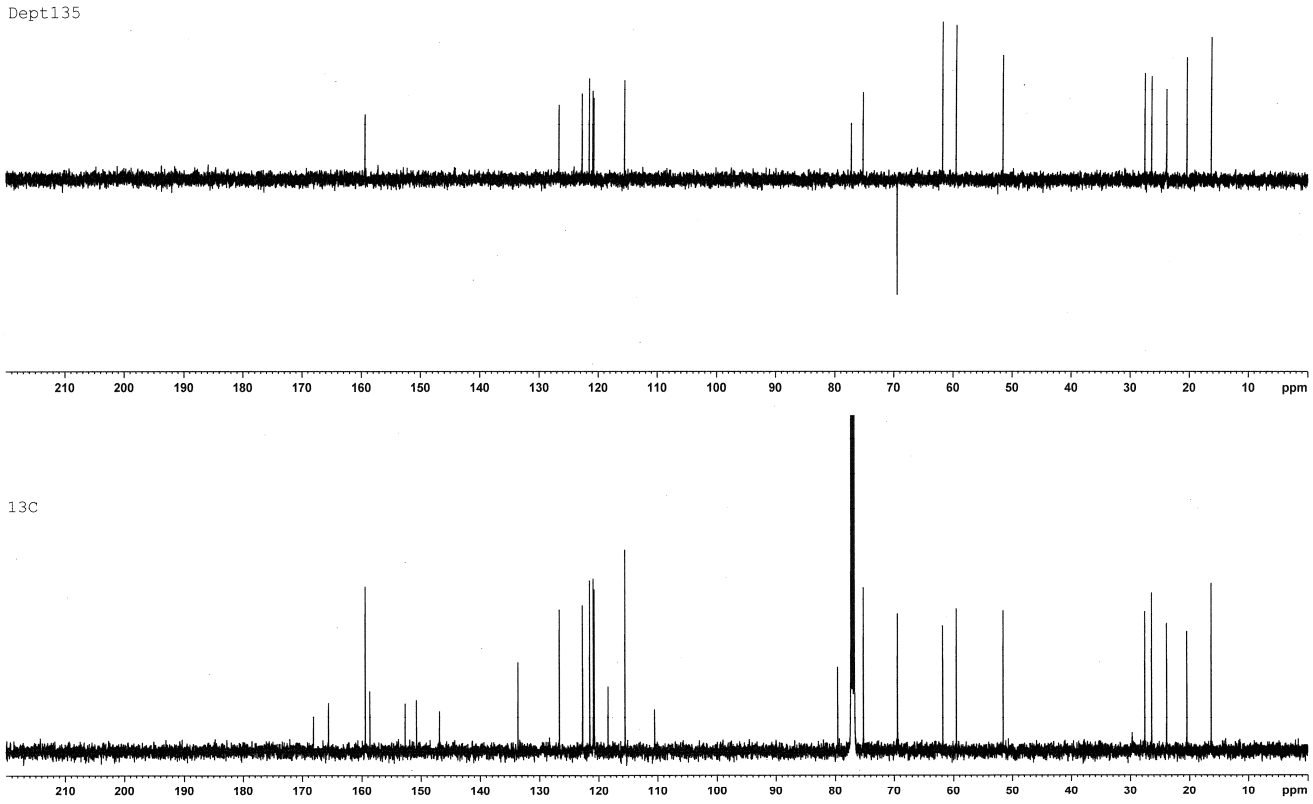

Fig. S55 COSY spectrum of 9-methoxystrobilurin P (**13**) ($CDCl_3$, 500 MHz)

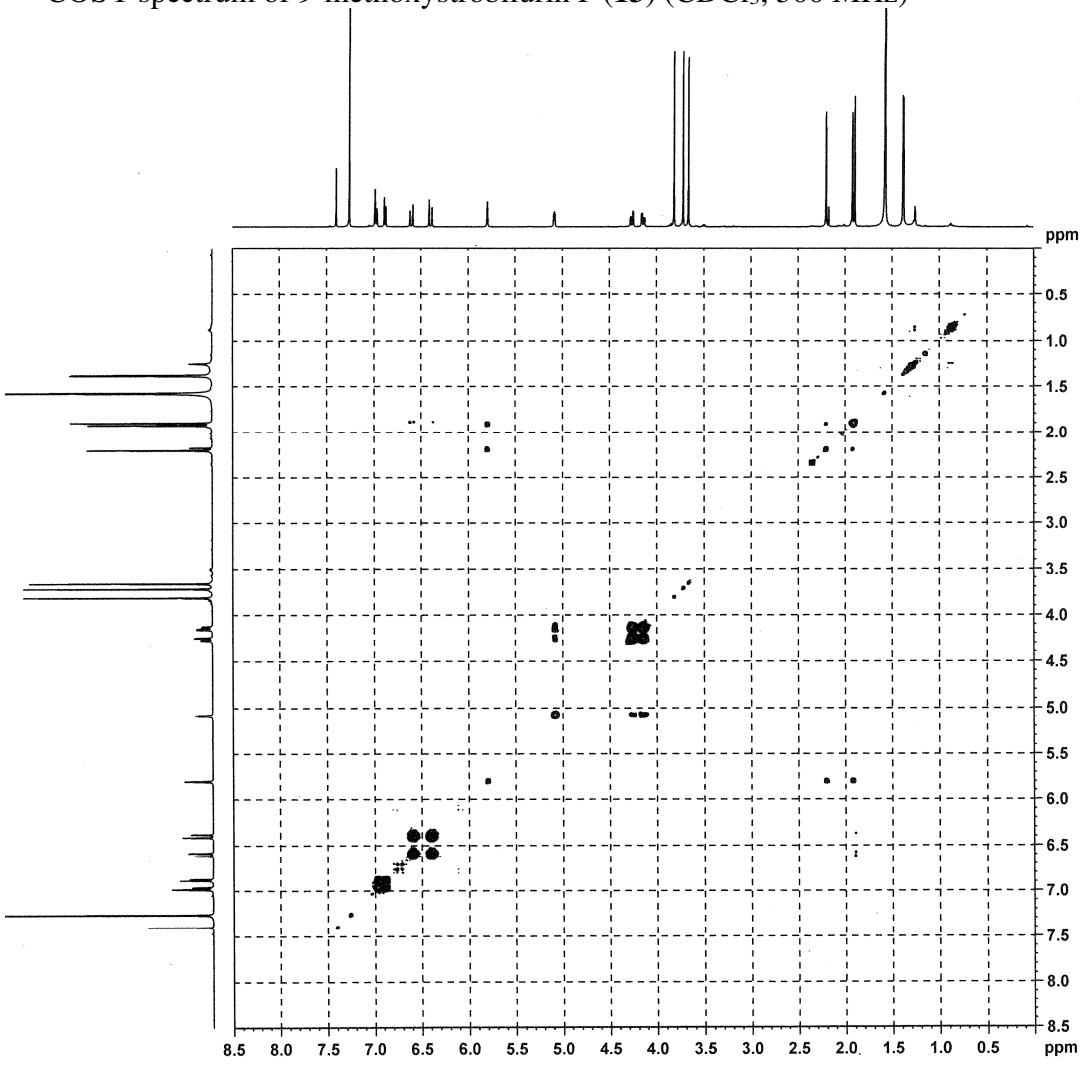

Fig. S56 HSQC spectrum of 9-methoxystrobilurin P (**13**) ($CDCl_3$, 500 MHz)

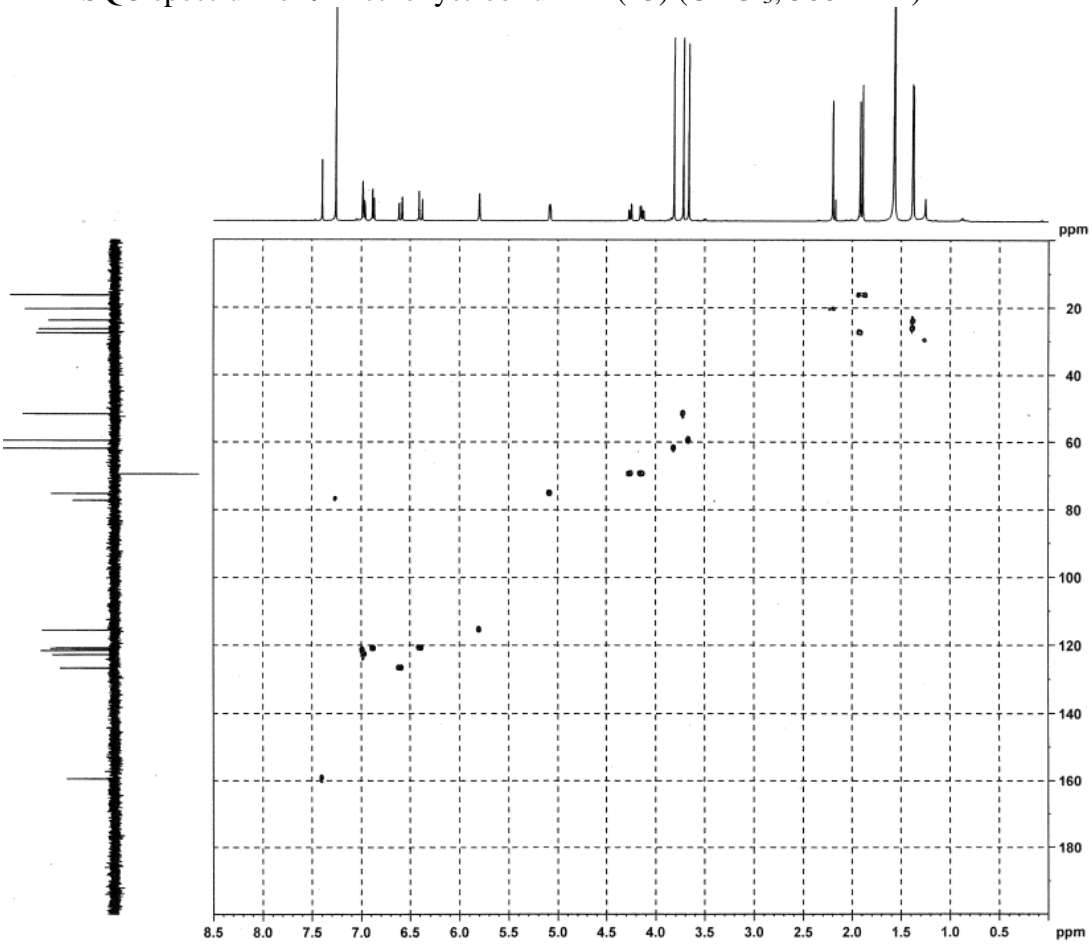

Fig. S57 HMBC spectrum of 9-methoxystrobilurin P (**13**) ($CDCl_3$, 500 MHz)

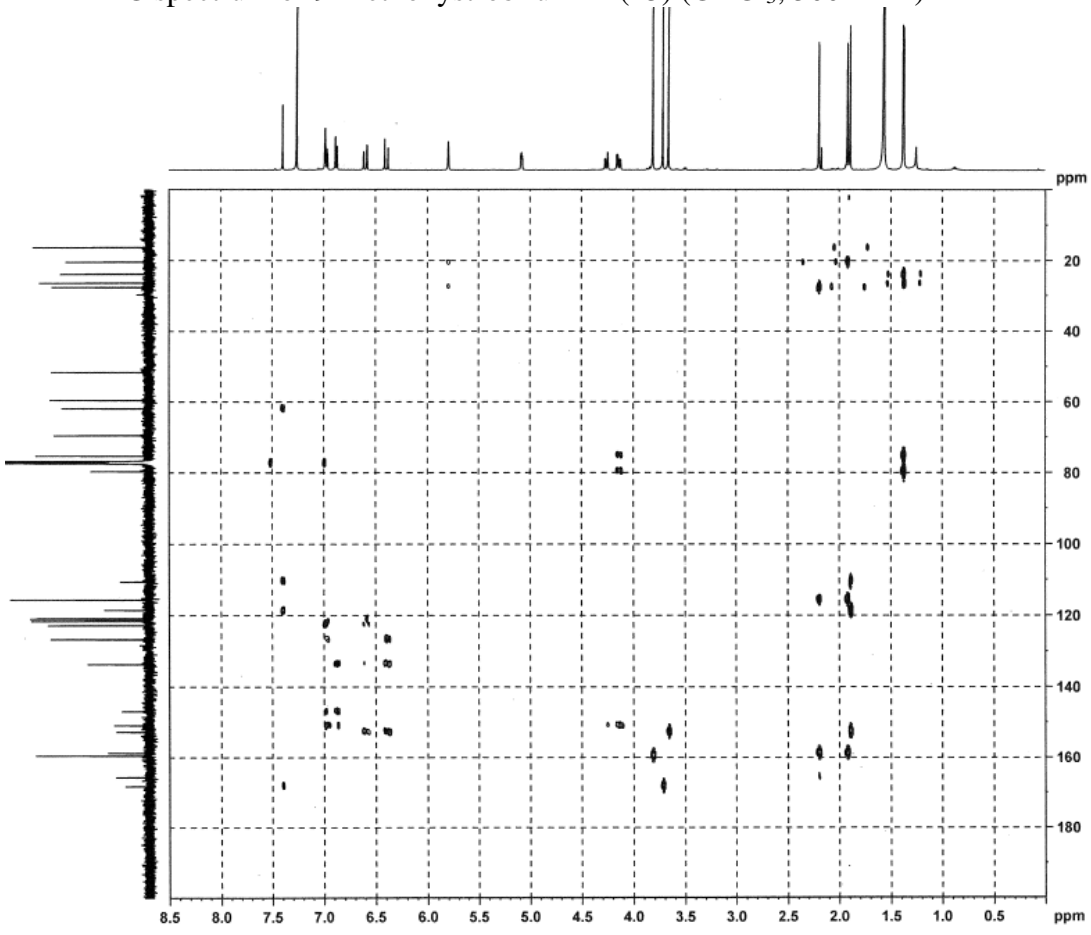

Fig. S58 NOESY spectrum of 9-methoxystrobilurin P (**13**) ($CDCl_3$, 500 MHz)

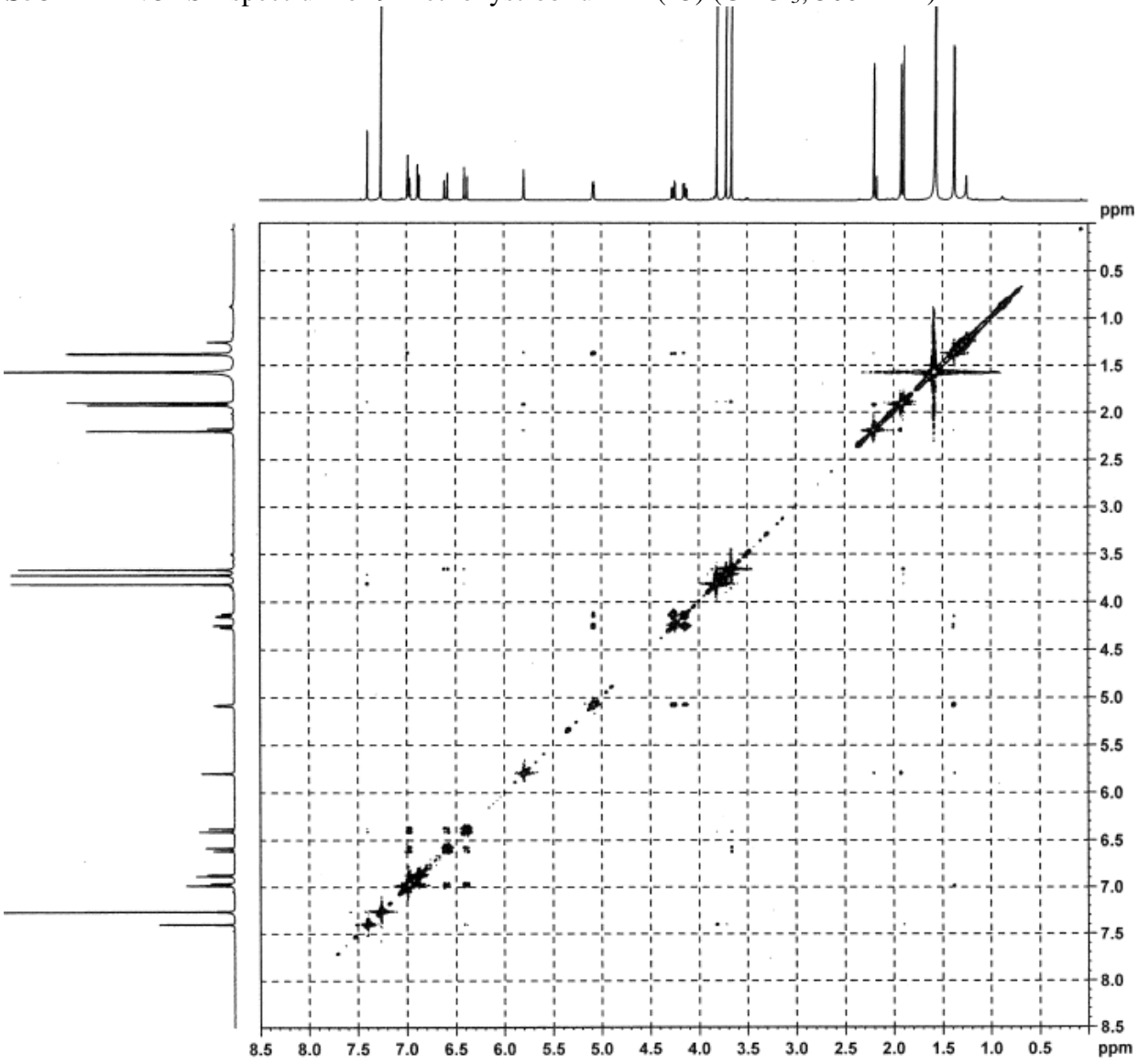

Fig. S59 HRESIMS of 9-methoxystrobilurin P (**13**) (positive ion mode)

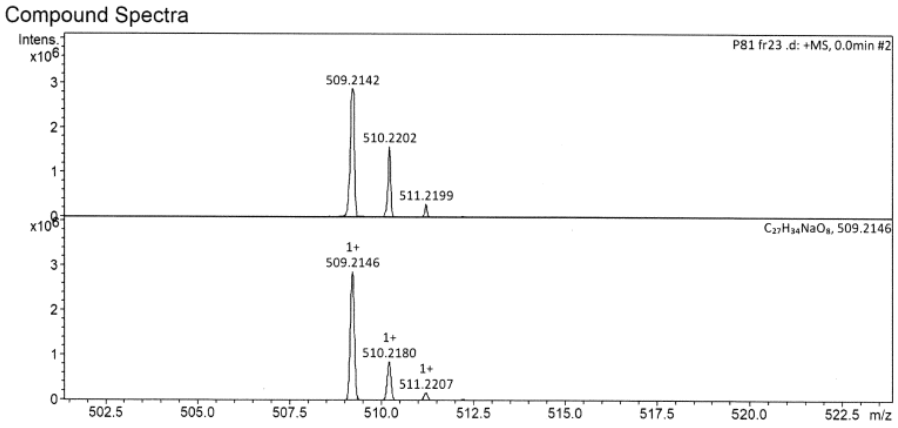

Fig. S60 ^{1}H NMR spectrum of **14** ($CDCl_3$, 500 MHz)

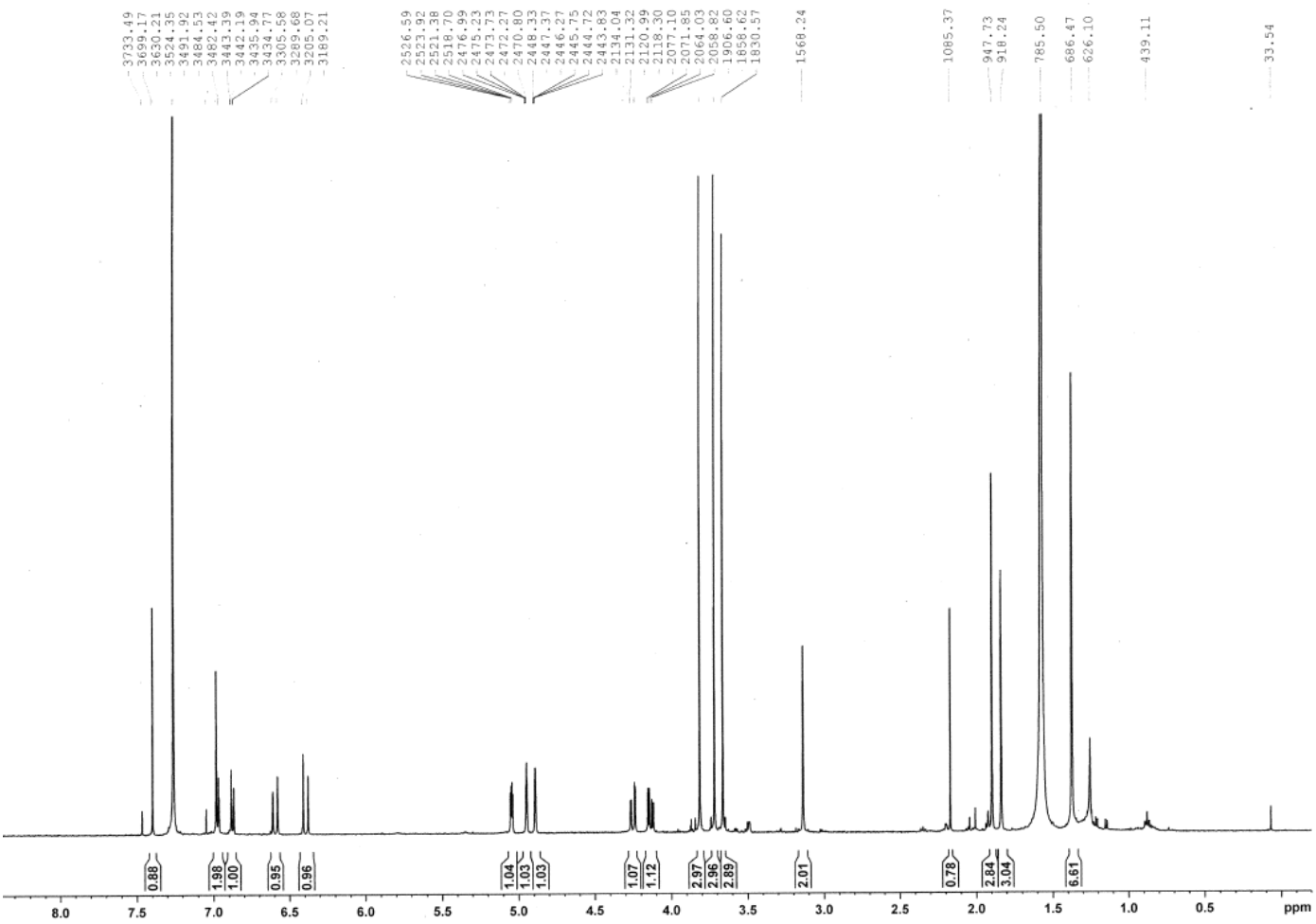

Fig. S61 HRESIMS of **14** (positive ion mode)

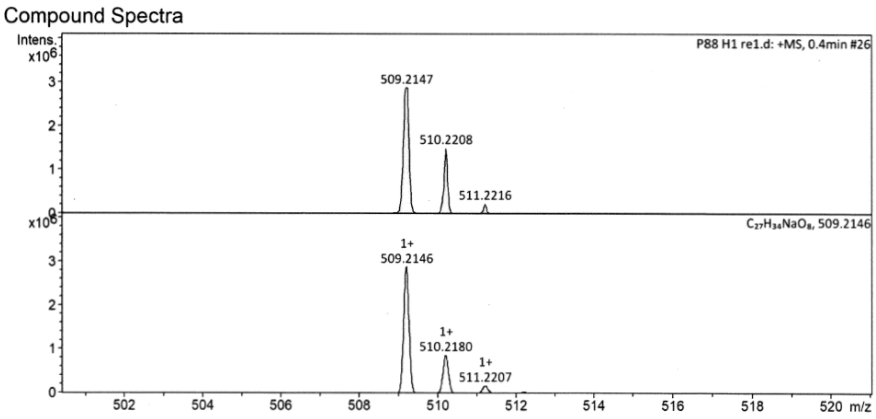

Fig. S62 Experimental ECD spectra of oudemansin E (**1**), oudemansin M (**2**), γ-lactone **6**, oudemansin A (**7**), and 9-methoxystrobilurin E (**9**)

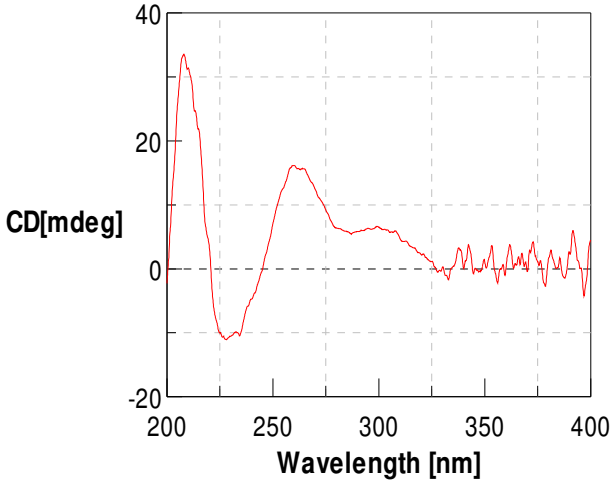

Oudemansin E (**1**) (25 μg/ml in MeCN)

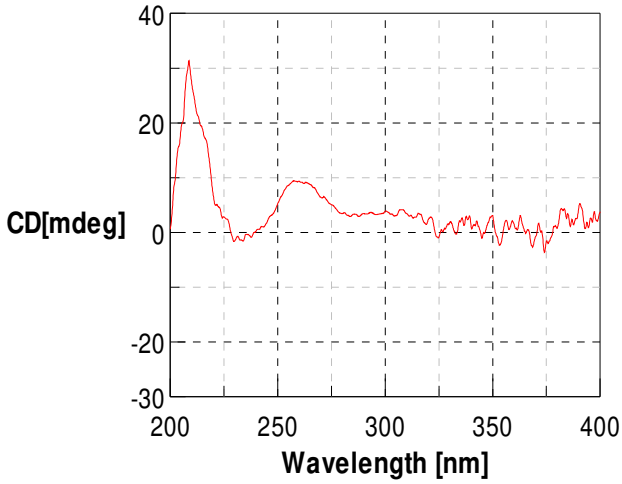

Oudemansin M (**2**) (50 μg/ml in MeCN)

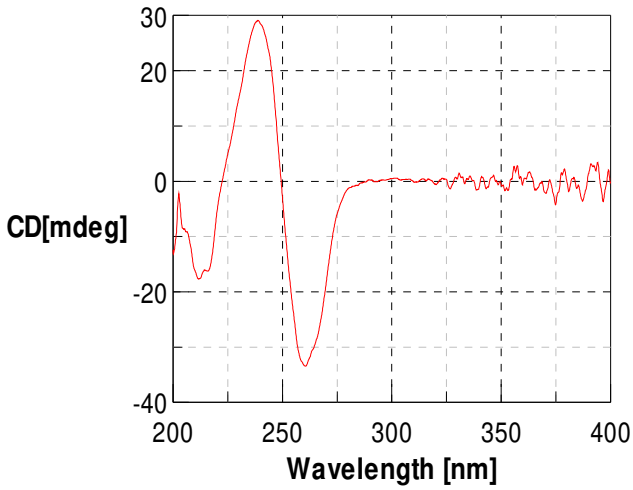

γ-Lactone **6** (10 μg/ml in MeCN)

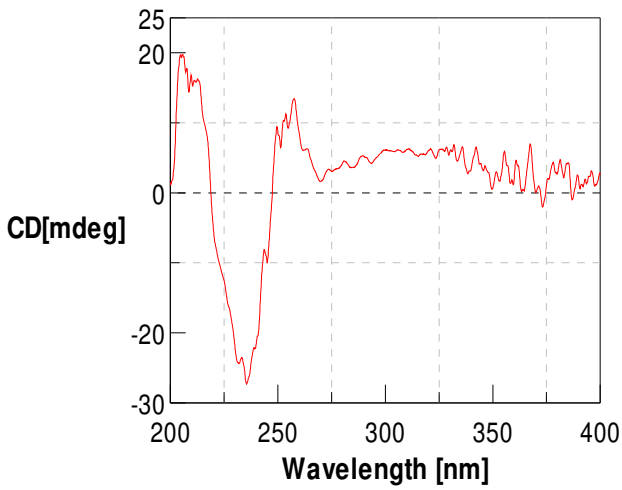

Oudemansin A (**7**) (30 μg/ml in MeCN)

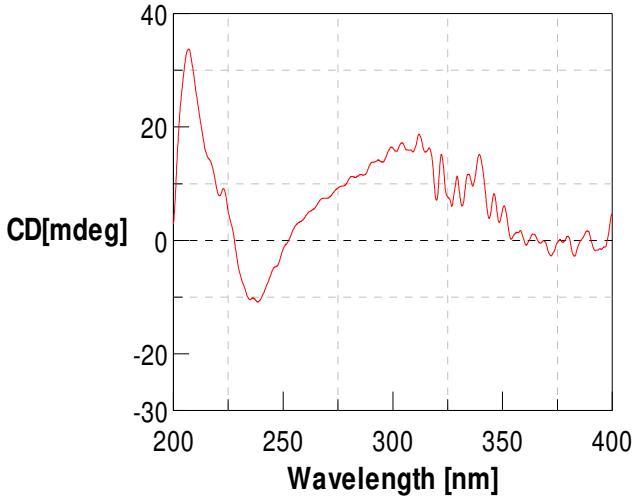

9-Methoxystrobilurin E (**9**) (50 μg/ml in MeCN)

Computational Details for ECD Calculation of 9-Methoxystrobilurin E (9)

The conformational analysis of each enantiomer for compound **9** was perform on Spartan' 18 using MMFF[1] as the molecular mechanics force field. Thirty-seven lowest energy conformers were found contributed to about 90% of the MMFF population. These conformers of **9** were further calculated for geometry optimization in gas phase using B3LYP [2-4] functional and 6-31G(d) [5-7] basis set in Gaussian 16[8]. All calculations of time-dependent density-functional theory (TDDFT) were performed on the gas-phase optimized structures to obtain ECD using CAM-B3LYP[9] functional and 6-311++G(2d,2p) [5-7] basis set with conductor-like polarizable continuum model (CPCM)[10-11] in acetonitrile. Twelve conformers of (2′*S*,6′*R*)-**9** and eleven conformers of (2′*R*,6′*S*)**-9** were found with the relative free energies within ~2 kcal/mol from their most stable conformers (Fig. S63 and Fig. S65). The ECD curve of each enantiomer for **9** was demonstrated by summing of ECD spectra of these conformers based on Boltzmann weighting factors at 298.15 K with a half bandwidth of 0.25 eV using SpecDis v.1.71[12]. Data visualization of the calculated ECD spectra of each enantiomer and experimental CD spectra for 9-methoxystrobilurin E (**9**) were performed using python (version 3.8.13) package[13]. Raw data was imported with pandas (version 1.4.3) library and plotted with matplotlib (version 3.5.1) library.

(1) Computational details for (2′*S*,6′*R*)-9

Table S1. Estimated thermodynamic parameters at 298.15 K and conformational analysis of (2′*S*,6′*R*)-**9** at the CAM-B3LYP/6-311++G(2d,2p) level in acetonitrile solvent, assuming Boltzmann statistics at T = 298.15 K.

Conformers	B3LYP/6-31G(d)	CAM-B3LYP/6-311++G(2d, 2p)					
	E (a.u.)	E* (a.u.)	E_{ZPE} *(a.u.)	H_{298K}*(a.u.)	G_{298K}*(a.u.)	ΔG_{298K}* (kcal/mol)	P_G*
(2′*S*,6′*R*)-**9**_conf 1	-1651.053460	-1650.798558	-1650.226372	-1649.933117	-1650.301598	0.00	17.58
(2′*S*,6′*R*)-**9**_conf 2	-1651.053402	-1650.798531	-1650.226337	-1649.933121	-1650.301375	0.14	13.87
(2′*S*,6′*R*)-**9**_conf 3	-1651.053309	-1650.798432	-1650.226248	-1649.933010	-1650.301350	0.16	13.51
(2′*S*,6′*R*)-**9**_conf 4	-1651.053296	-1650.798436	-1650.226246	-1649.933025	-1650.301292	0.19	12.71
(2′*S*,6′*R*)-**9**_conf 5	-1651.053797	-1650.798497	-1650.226264	-1649.932634	-1650.301231	0.23	11.92
(2′*S*,6′*R*)-**9**_conf 6	-1651.053986	-1650.798501	-1650.226267	-1649.932450	-1650.301161	0.27	11.06
(2′*S*,6′*R*)-**9**_conf 7	-1651.053871	-1650.798391	-1650.226147	-1649.932330	-1650.300942	0.41	8.77
(2′*S*,6′*R*)-**9**_conf 8	-1651.053812	-1650.798395	-1650.226153	-1649.932400	-1650.300870	0.46	8.13
(2′*S*,6′*R*)-**9**_conf 9	-1651.052668	-1650.795962	-1650.223574	-1649.928596	-1650.298511	1.94	0.67
(2′*S*,6′*R*)-**9**_conf 10	-1651.052677	-1650.795935	-1650.223555	-1649.928545	-1650.298454	1.97	0.63
(2′*S*,6′*R*)-**9**_conf 11	-1651.052932	-1650.796067	-1650.223639	-1649.928541	-1650.298375	2.02	0.58
(2′*S*,6′*R*)-**9**_conf 12	-1651.052850	-1650.796075	-1650.223656	-1649.928639	-1650.298350	2.04	0.56

E = gas phase electronic energy; ZPE = gas phase zero-point energy; E_{ZPE} = E+ZPE; H_{298K} = enthalpy; G_{298K} = gas phase Gibbs free energy at the B3LYP/6-31G(d) level in gas phase

E^* = electronic energy in acetonitrile; E_{ZPE}^* = E^*+ZPE; H_{298K}^* = estimated enthalpy in acetonitrile, H_{298K}^* = E^*+(H_{298K}-E); G_{298K}^* = estimated Gibbs free energy in acetonitrile, G_{298K}^* = E^*+(G_{298K}-E); ΔG_{298K}^* = estimated relative Gibbs free energy at the CAM-B3LYP/6-311++G(2d,2p) level in acetonitrile solvent; P_G^* = conformational distribution calculated from relative Gibbs free energy.

Fig. S63. Optimized conformers of (2′*S*,6′*R*)**-9** at the B3LYP/6-31G(d) level in gas phase with the populations calculated from their estimated Gibbs free energies in acetonitrile solvent at the CAM-B3LYP/6-311++G(2d,2p) level

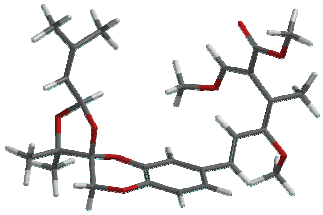

(2′*S*,6′*R*)**-9**_Conf 1 (17.58%)

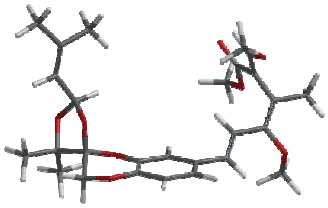

(2′*S*,6′*R*)**-9**_Conf 2 (13.87%)

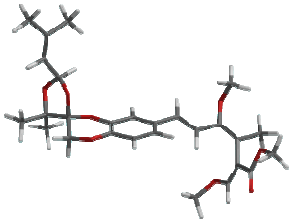

(2′*S*,6′*R*)**-9**_Conf 3 (13.51%)

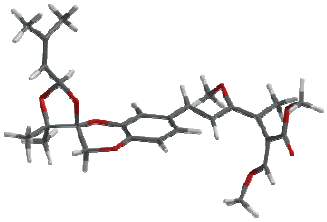

(2′*S*,6′*R*)**-9**_Conf 4 (12.71%)

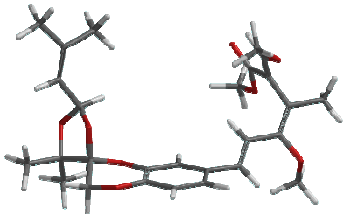

(2′*S*,6′*R*)**-9**_Conf 5 (11.92%)

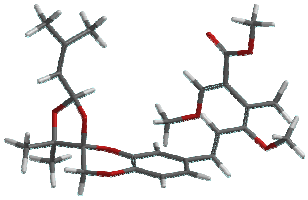

(2′*S*,6′*R*)**-9**_Conf 6 (11.06%)

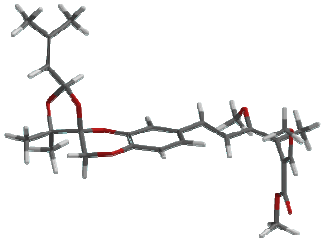

(2′*S*,6′*R*)**-9**_Conf 7 (8.77%)

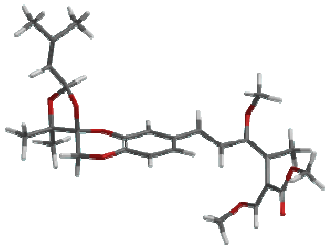

(2′*S*,6′*R*)**-9**_Conf 8 (8.13%)

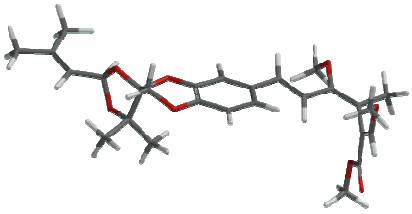

(2′*S*,6′*R*)**-9**_Conf 9 (0.67%)

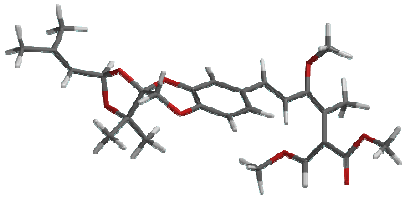

(2′*S*,6′*R*)**-9**_Conf 10 (0.63%)

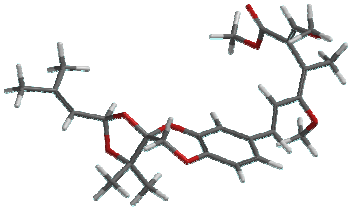

(2′*S*,6′*R*)**-9**_Conf 11 (0.58%)

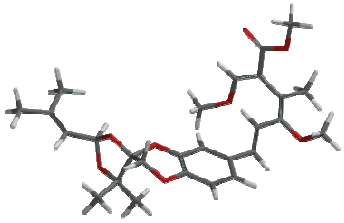

(2′*S*,6′*R*)**-9**_Conf 12 (0.56%)

Fig. S64. Comparison of experimental CD spectrum of 9-methoxystrobilurin E (black) and calculated ECD spectrum of (2′*S*,6′*R*)-**9** (blue)

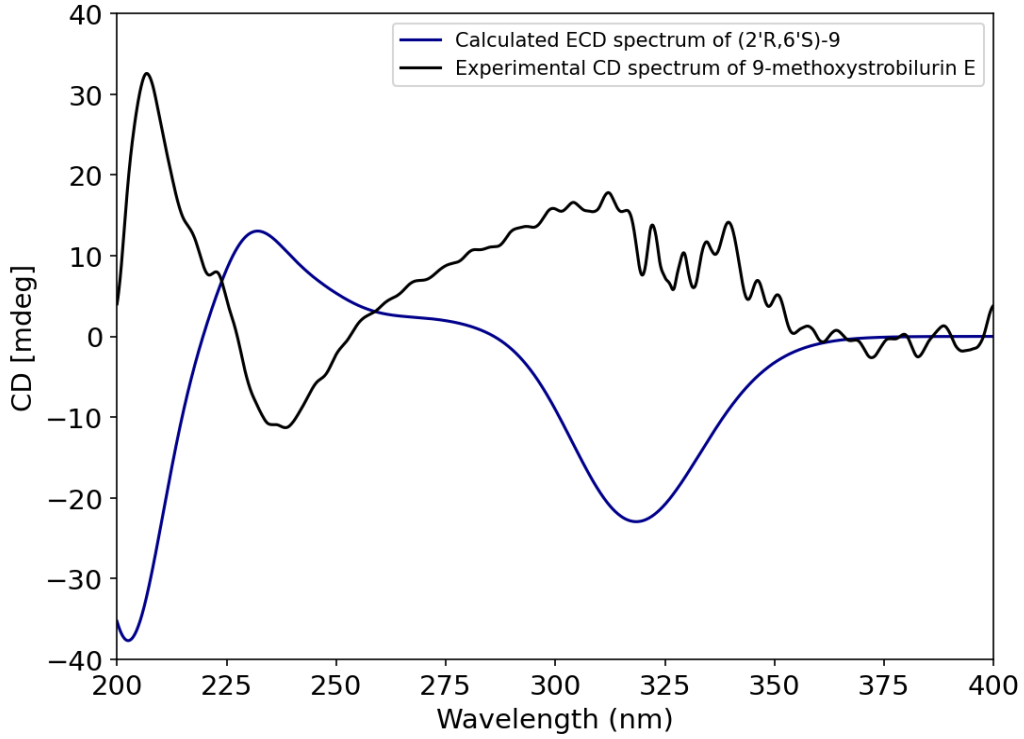

(2) Computational details for (2′*R*,6′*S*)-9

Table S2. Estimated thermodynamic parameters at 298.15 K and conformational analysis of (2′*R*,6′*S*)-**9** at the CAM-B3LYP/6-311++G(2d,2p) level in acetonitrile solvent, assuming Boltzmann statistics at T = 298.15 K

Conformers	B3LYP/6-31G(d)	CAM-B3LYP/6-311++G(2d, 2p)					
	E (a.u.)	E* (a.u.)	E_{ZPE}* (a.u.)	H_{298K}* (a.u.)	G_{298K}* (a.u.)	ΔG_{298K}* (kcal/mol)	P_G*
(2′*R*,6′*S*)-**9**_conf 1	-1651.053460	-1650.798558	-1650.226371	-1649.933115	-1650.301599	0.00	19.28
(2′*R*,6′*S*)-**9**_conf 2	-1651.053402	-1650.798531	-1650.226337	-1649.933121	-1650.301375	0.14	15.21
(2′*R*,6′*S*)-**9**_conf 3	-1651.053309	-1650.798432	-1650.226248	-1649.933010	-1650.301350	0.16	14.81
(2′*R*,6′*S*)-**9**_conf 4	-1651.053296	-1650.798436	-1650.226246	-1649.933025	-1650.301292	0.19	13.92
(2′*R*,6′*S*)-**9**_conf 5	-1651.053797	-1650.798497	-1650.226264	-1649.932634	-1650.301231	0.23	13.07
(2′*R*,6′*S*)-**9**_conf 6	-1651.053986	-1650.798501	-1650.226267	-1649.932450	-1650.301161	0.27	12.13
(2′*R*,6′*S*)-**9**_conf 7	-1651.053812	-1650.798395	-1650.226153	-1649.932400	-1650.300869	0.46	8.91
(2′*R*,6′*S*)-**9**_conf 8	-1651.052668	-1650.795960	-1650.223571	-1649.928593	-1650.298511	1.94	0.73
(2′*R*,6′*S*)-**9**_conf 9	-1651.052677	-1650.795937	-1650.223557	-1649.928549	-1650.298456	1.97	0.69
(2′*R*,6′*S*)-**9**_conf 10	-1651.052932	-1650.796070	-1650.223642	-1649.928546	-1650.298375	2.02	0.63
(2′*R*,6′*S*)-**9**_conf 11	-1651.052850	-1650.796074	-1650.223655	-1649.928637	-1650.298354	2.04	0.62

E = gas phase electronic energy; ZPE = gas phase zero-point energy; E_{ZPE} = E+ZPE; H_{298K} = enthalpy; G_{298K} = gas phase Gibbs free energy at the B3LYP/6-31G(d) level in gas phase

E^* = electronic energy in acetonitrile; E_{ZPE}^* = E^*+ZPE; H_{298K}^* = estimated enthalpy in acetonitrile, H_{298K}^* = E^*+(H_{298K}-E); G_{298K}^* = estimated Gibbs free energy in acetonitrile, G_{298K}^* = E^*+(G_{298K}-E); ΔG_{298K}^* = estimated relative Gibbs free energy at the CAM-B3LYP/6-311++G(2d,2p) level in acetonitrile solvent; P_G^* = conformational distribution calculated from relative Gibbs free energy.

Fig. S65. Optimized conformers of (2′*R*,6′*S*)**-9** at the B3LYP/6-31G(d) level in gas phase with the populations calculated from their estimated Gibbs free energies in acetonitrile solvent at the CAM-B3LYP/6-311++G(2d,2p)

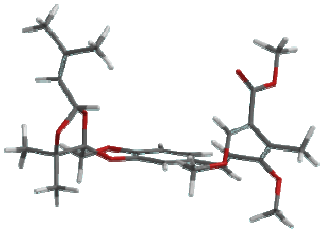

(2′*R*,6′*S*)**-9**_Conf 1 (19.28%)

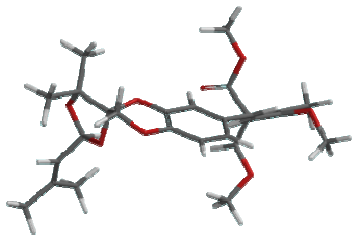

(2′*R*,6′*S*)**-9**_Conf 2 (15.21%)

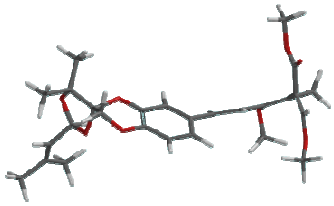

(2′*R*,6′*S*)**-9**_Conf 3 (14.81%)

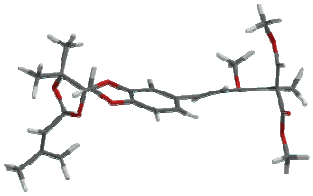

(2′*R*,6′*S*)**-9**_Conf 4 (13.92%)

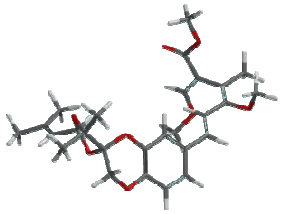

(2′*R*,6′*S*)**-9**_Conf 5 (13.07%)

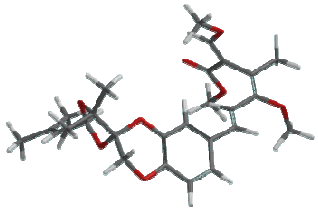

(2′*R*,6′*S*)**-9**_Conf 6 (12.13%)

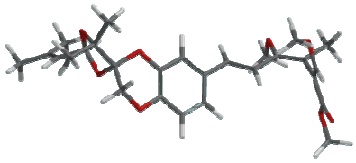

(2′*R*,6′*S*)**-9**_Conf 7 (8.91%)

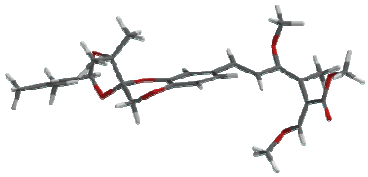

(2′*R*,6′*S*)**-9**_Conf 8 (0.73%)

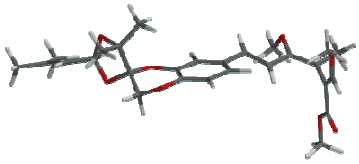

(2′*R*,6′*S*)**-9**_Conf 9 (0.69%)

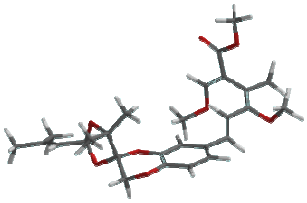

(2′*R*,6′*S*)**-9**_Conf 10 (0.63%)

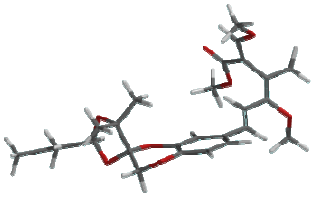

(2′*R*,6′*S*)**-9**_Conf 11 (0.62%)

Fig. S66. Comparison of experimental CD spectrum of 9-methoxystrobilurin E (black) and calculated ECD spectra for (2′*R*,6′*S*)-**9** (red)

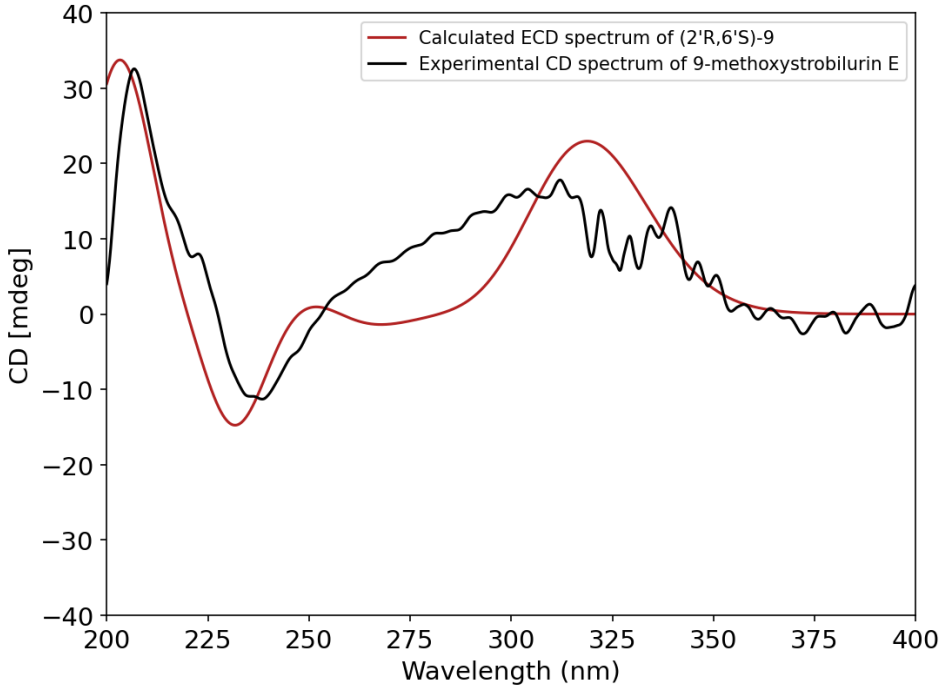

(3) Conclusion

9-Metoxystrobilurin E (**9**) was identified to be the (2′*R*,6′*S*)-isomer.

Fig. 4. (main text). Calculated ECD spectra of (2′*S*,6′*R*)-**9** (blue) and (2′*R*,6′*S*)-**9** (red) and experimental CD spectrum of 9-methoxystrobilurin E (black)

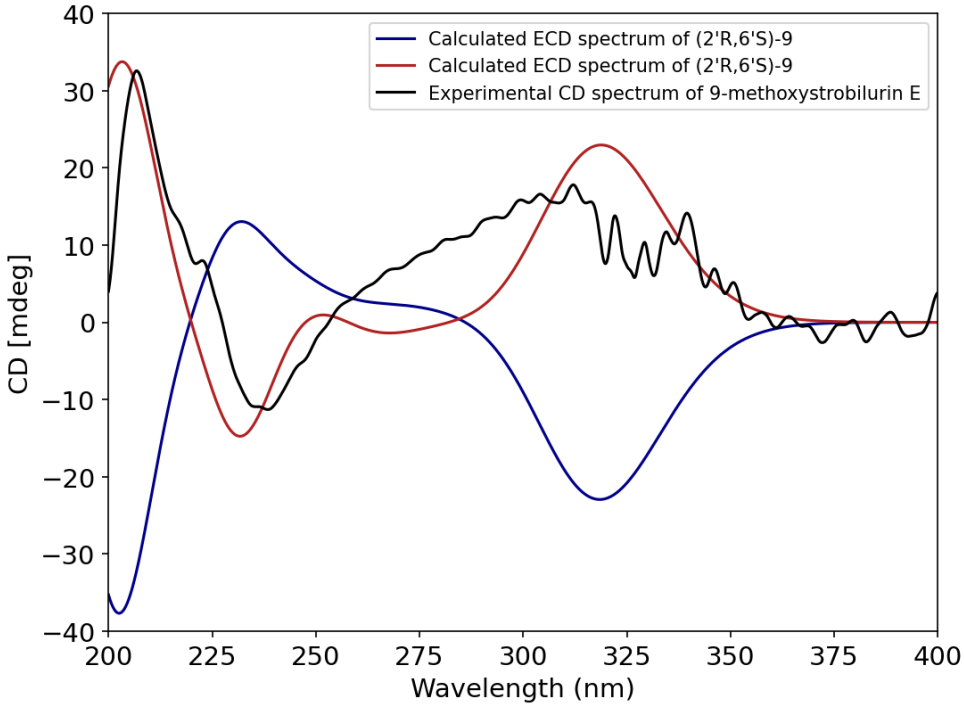

References

1 Halgren, T. A. Merck molecular force field. I. Basis, form, scope, parameterization, and performance of MMFF94. *Journal of Computational Chemistry* **17**, 490-519, doi:https://doi.org/10.1002/(SICI)1096-987X(199604)17:5/6<490::AID-JCC1>3.0.CO;2-P (1996).

2 Becke, A. Density-functional thermochemistry. III. The role of exact exchange (1993) J. *Chem. Phys* **98**, 5648.

3 Lee, C., Yang, W. & Parr, R. G. Development of the Colle-Salvetti correlation-energy formula into a functional of the electron density. *Physical review B* **37**, 785 (1988).

4 Stephens, P. J., Devlin, F. J., Chabalowski, C. F. & Frisch, M. J. Ab Initio Calculation of Vibrational Absorption and Circular Dichroism Spectra Using Density Functional Force Fields. *The Journal of Physical Chemistry* **98**, 11623-11627, doi:10.1021/j100096a001 (1994).

5 Hariharan, P. C. & Pople, J. A. The influence of polarization functions on molecular orbital hydrogenation energies. *Theoretica Chimica Acta* **28**, 213-222, doi:10.1007/BF00533485 (1973).

6 Petersson, a. *et al.* A complete basis set model chemistry. I. The total energies of closed-shell atoms and hydrides of the first-row elements. *The Journal of chemical physics* **89**, 2193-2218 (1988).

7 Petersson, G. A. & Al-Laham, M. A. A complete basis set model chemistry. II. Open-shell systems and the total energies of the first-row atoms. *The Journal of Chemical Physics* **94**, 6081-6090, doi:10.1063/1.460447 (1991).

8 Frisch, M. J.; Trucks, G. W.; Schlegel, H. B.; Scuseria, G. E.; Robb, M. A.; Cheeseman, J. R.; Scalmani, G.; Barone, V.; Petersson, G. A.; Nakatsuji, H.; Li, X.; Caricato, M.; Marenich, A. V.; Bloino, J.; Janesko, B. G.; Gomperts, R.; Mennucci, B.; Hratchian, H. P.; Ortiz, J. V.; Izmaylov, A. F.; Sonnenberg, J. L.; Williams-Young, D.; Ding, F.; Lipparini, F.; Egidi, F.; Goings, J.; Peng, B.; Petrone, A.; Henderson, T.; Ranasinghe, D.; Zakrzewski, V. G.; Gao, J.; Rega, N.; Zheng, G.; Liang, W.; Hada, M.; Ehara, M.; Toyota, K.; Fukuda, R.; Hasegawa, J.; Ishida, M.; Nakajima, T.; Honda, Y.; Kitao, O.; Nakai, H.; Vreven, T.; Throssell, K.; Montgomery, J. A., Jr.; Peralta, J. E.; Ogliaro, F.; Bearpark, M. J.; Heyd, J. J.; Brothers, E. N.; Kudin, K. N.; Staroverov, V. N.; Keith, T. A.; Kobayashi, R.; Normand, J.; Raghavachari, K.; Rendell, A. P.; Burant, J. C.; Iyengar, S. S.; Tomasi, J.; Cossi, M.; Millam, J. M.; Klene, M.; Adamo, C.; Cammi, R.; Ochterski, J. W.; Martin, R. L.; Morokuma, K.; Farkas, O.; Foresman, J. B.; Fox, D. J. Gaussian 16 Rev. C.01; Gaussian. *Inc.:*Wallingford CT (2016).

9 Yanai, T., Tew, D. P. & Handy, N. C. A new hybrid exchange–correlation functional using the Coulomb-attenuating method (CAM-B3LYP). *Chemical Physics Letters* **393**, 51-57, doi:https://doi.org/10.1016/j.cplett.2004.06.011 (2004).

10 Barone, V. & Cossi, M. Quantum calculation of molecular energies and energy gradients in solution by a conductor solvent model. *The Journal of Physical Chemistry A* **102**, 1995-2001 (1998).

11 Cossi, M., Rega, N., Scalmani, G. & Barone, V. Energies, structures, and electronic properties of molecules in solution with the C-PCM solvation model. *Journal of computational chemistry* **24**, 669-681 (2003).

12 Bruhn, T., Schaumlöffel, A., Hemberger, Y. & Bringmann, G. SpecDis: Quantifying the Comparison of Calculated and Experimental Electronic Circular Dichroism Spectra. *Chirality* **25**, 243-249, doi:https://doi.org/10.1002/chir.22138 (2013).

13 Rossum, G. V. & Drake, F. L. *Python 3 Reference Manual*. (CreateSpace, 2009).